Photoejection of molecules from the surface of a liquid microjet

Thesis submitted for the degree of

Doctor of Philosophy

at University of Leicester

by

Veronika Barinkova

Department of Chemistry

University of Leicester

June 2009

Abstract

A new instrument has been constructed for studying the dynamics of photochemical reactions at or near the surface of a liquid. In this apparatus, a liquid microjet is used to deliver a fresh and continuously flowing liquid surface into a high vacuum chamber. This system has been coupled with a laser pump-probe to produce and detect radicals. By using laser-induced fluorescence (LIF) spectroscopy, both the velocity distribution and the population of internal quantum states in the ejected molecules can be determined.

Designing and building the apparatus required considerable attention with several significant adjustments being implemented to allow its operation. For instance, a series of traps were required to attain a vacuum in the low 10^{-5} mbar range. Using Fraunhofer diffraction the stability of the microjet has been demonstrated and the diameter has been confirmed to be 20 μm.

To test the pump-probe procedure, a continuous microjet of a toluene/ethanol mixture has been subjected to laser photo-ejection using nanosecond pulses of 266 nm laser light. The time-of-flight distribution of toluene molecules ejected into the gas phase has been measured using time-resolved LIF spectroscopy. The velocity measurement indicated that the laser phot-ejection process generated two groups of ejected molecules: (i) a collection of hyperthermal toluene molecules, which are assumed to be derived from molecules originally at or near the liquid surface and (ii) a group of slower, hotter molecules that most likely emanate from the liquid interior.

Concise studies of the other liquid system namely aniline, benzene and acetyl acetone has also been made and are discussed in this thesis.

List of figures and tables

List of abbreviations

CCD	Charged-coupled device
DMF	Dimethylformamide
DNA	Deoxyribonucleic acid
ESCA	Electron Spectroscopy for Chemical Analysis
EtOH	Ethanol
EUV	Extreme ultraviolet
EXAFS	Extended X-ray absorption fine structure
FCU	Frequency conversion unit
HPLC	High pressure liquid chromatography
ICN	Iodine cyanide
IR	Infrared
ISO	International Standard Organization
KF	Klein flange
LiCl	Lithium chloride
LIF	Laser induced fluorescence
LILBID	Laser induced liquid beam ion desorption
MALDI	Matrix assisted laser desorption/ionization
NaI	Sodium iodide
Nd:YAG	neodymium-doped yttrium aluminium garnet
NEXAFS	Near edge X-ray absorption fine structure

NMR	Nuclear Magnetic Resonance
PEEK	Polyaryletheretherketone
PES	Photoelectron spectroscopy
PMT	Photomultiplier tube
REMPI	Resonance enhanced multiphoton ionization
SFG	Sum frequency generation
SIMS	Secondary ion mass spectrometry
SSD	Solid state detector
TBAI	Tetrabutylammonium
TEY-XAS	Total electron yield X-ray absorption spectroscopy
TIY- XAS	Total ion yield X-ray absorption spectroscopy
TOF-MS	Time-of-flight mass spectrometry
TTL	Transistor-Transistor Logic
UPS	Ultraviolet photoelectron spectroscopy
UV	Ultraviolet
VI	Virtual instrument
XAS	X-ray absorption spectroscopy
XPS	X-ray photoelectron spectroscopy

Table of content

Chapter 1 - Introduction

Chapter 4 - Conclusions

Chapter 1

Introduction

1.1 Introduction

The nature of the chemical reactions that occur on liquid surfaces constitutes an active area of research that impacts upon many diverse fields such as atmospheric chemistry, catalysis, biology and geology.[1] In spite of a considerable number of studies of reactions taking place at the gas-liquid interface having been undertaken, much remains to be understood. These reactions also play an important role in industrial applications (*e.g.*, bleaching and photography) in biological systems[2] or photochemical reactions at the gas-liquid interface. Many photochemical processes in the atmosphere involve molecules adsorbed on small water droplets with a typical example being the destruction of the ozone layer.[3,4]

The surface region of a liquid may have substantially different properties from the bulk due to the strong asymmetry in the intermolecular forces between the molecules. A lower effective density is expected, and other properties may also differ including the dielectric constant and the extent and strength of hydrogen-bonding. The interfacial region not only provides the initial environment for reaction but also for the other processes such as interface-bulk exchange or solvation.[5] The distribution of energy amongst the gas molecules liberated from the liquid surface provides information about the dynamics of the reaction at the surface. However, fathoming the liquid surface has proven difficult as it is generally partially hidden behind a gas phase. Siegbahn, who was awarded the Nobel prize in 1981, developed different approaches to lower the vapour pressure and to determine the chemical composition of the surface of water.

In the first part of this opening chapter, an introduction of the gas-liquid interface studies will be given (1.2.1). After a brief account of other techniques in section 1.2.2, the discussion will switch to the technique employed in the work that forms the basis for this thesis, the liquid microjet. The different analytical techniques, spectrometric (1.3) and spectroscopic (1.4) combined with liquid microjets will be described. A summary of published works in previous liquid microjet studies will be given in section (1.5). The aims of the current project are described in section 1.6 and summary of all liquid microjet experiments reported to date are provided (1.7). The second part of the chapter is dedicated to the properties of the liquid microjet *i.e.,* formation of the liquid microjet (1.9), parameters specific to certain liquids (1.10), and the design of the liquid microjet sources (1.11).

1.2   From gas-liquid interface studies to liquid microjets

1.2.1   Gas-liquid interface studies

In contrast with solid surfaces, which have been intensely investigated, the surfaces of liquids are relatively unexplored, mainly due to practical difficulties in probing the structure and properties of these surfaces.[6] The main obstacle is that most liquids possess a relatively high vapour pressure at vacuum temperature, which results in a layer of gas directly above the liquid surface and capable of interfering with the analytical techniques employed. Until recently, the vast majority of experimental works on the structure of liquid surfaces has therefore been restricted to studies of non-volatile liquids.[7]

When probing the surface, using some form of particle impact or particle ejection technique, both the incoming particle beam (*e.g.*, an ion beam or an electron beam) and/or the outgoing particles can collide with the vapour molecules. Due to the high vapour pressure often, these collisions are almost inevitable and impede significantly the extraction of any useful information on the liquid surface using many of the standard surface-sensitive analytical techniques. Several technique have been employed to explore the properties and dynamics of gas-liquid interfaces *i.e.,* molecular beam scattering,[5,8] X-ray and electron spectroscopy[9] or non-linear optical spectroscopy technique such as sum frequency generation (SGF).[10,11]

The molecular beam scattering technique allows to access information about the energy transfers and the corresponding elementary steps at gas-liquid interfaces. A molecular beam, directed towards a liquid surface, can result in different processes happening either at the surface or in the bulk of the liquid. Upon the detection of the scattered beam, the adsorbed reaction products or the adsorbed species, several distinct reaction pathways can be distinguished depending on the interaction between the molecules of the beam and that of the liquid (see Figure 1.1). The different reactions (*i.e.*, inelastic scattering, trapping-desorption, desorption after interfacial exchanges and desorption after bulk exchanges) have been identified by Nathanson *et al.*[5] using a molecular beam formed of deuterated and non deuterated hydrochloric acid on liquid glycerol. The initial impact induces inelastic scattering (IS), the short-time interaction where the incoming molecule after a few collisions scatters almost directly away. Molecules leave the surface with a relatively high kinetic energy related to their initial energy. In trapping-desorption (TD), molecules dissipate their excess energy

through at least one bounce and bind momentarily to interfacial molecules. Their trajectories of ejection are solely correlated to the temperature and their interactions with the liquid while all the information before the ejection is lost. They may be propelled back into the gas phase by thermal motions of the surface molecules through desorption. Alternatively, molecules after the trapping (**I**) the molecules can be further solvated in the interfacial region where it can react (**II**) with solvent molecule before being desorbed. An alternative pathway is the migration of the molecule deeper into the bulk of the liquid, where it can react (**III**), migrate back to the interfacial region (**IV**) and be desorbed.[5] Finally, the molecule can undergo reactions with other molecules in the bulk without being desorbed (**V**).
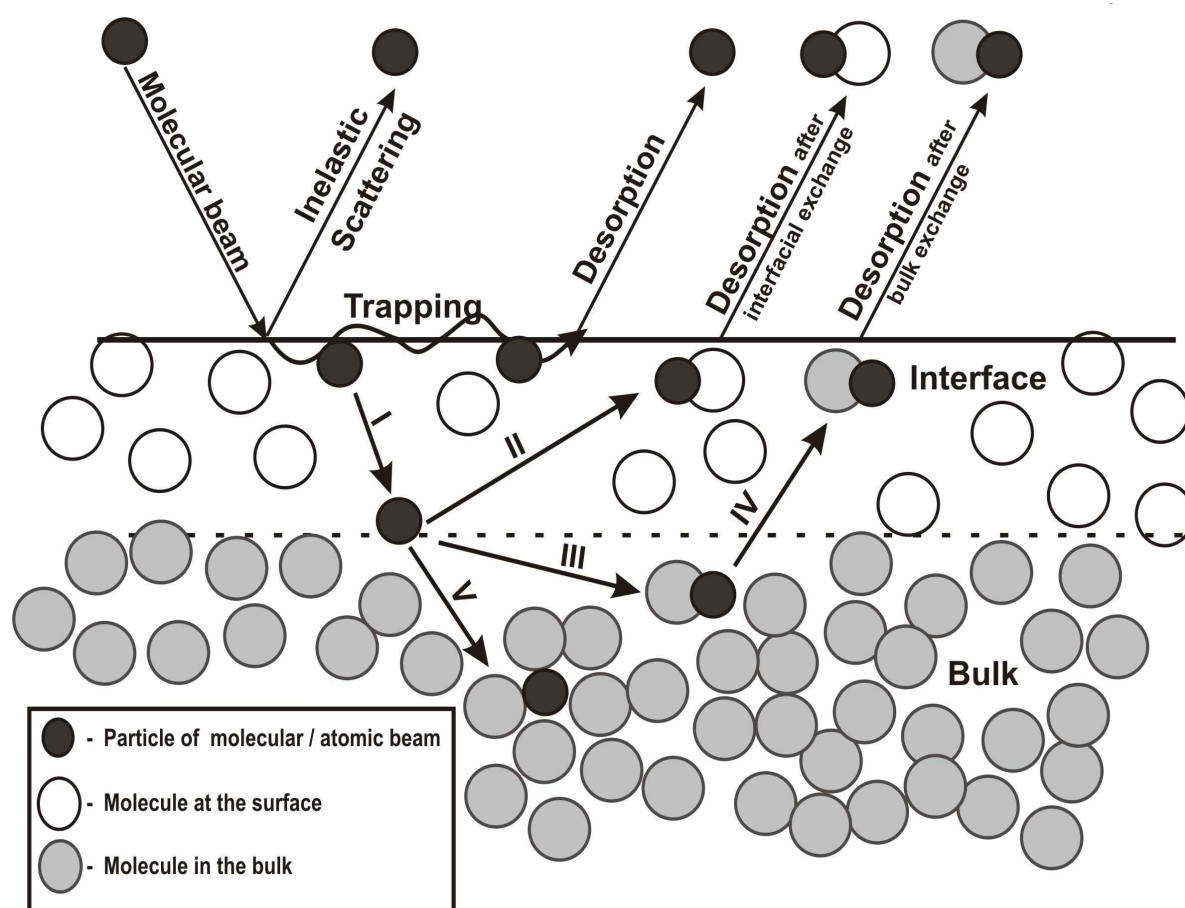
Figure 1.1   Gas-liquid interface interaction (**I** – solvation in the interface, **II**– reaction with interfacial molecule, **III-** reaction with bulk molecules **IV** – migration to interfacial region, **V** – solvation and further reaction). Scheme adapted from Nathanson[5]

Inelastic scattering of noble gases from liquid surfaces has been investigated using atomic and molecular beams combined with time-of-flight (TOF) or laser induced fluorescence (LIF) detection.[12,13] Particular attention have been paid to the influence of the nature of the noble gas employed, the energy and angle of impact and the liquid temperature to access information on the mechanism of the inelastic scattering.

Orientation of the molecules at a liquid surface can be studied by ion scattering and recoiling spectroscopy. The analysis of the kinetic energy of scattered noble gas ions and ejected recoil atoms reveals the identity of the atoms in the topmost atomic surface layer.[14,15]

Another technique employed for studying the details of molecular structure and the dynamics at surfaces and interfaces is sum frequency generation (SFG) spectroscopy. The high surface selectivity of SFG spectroscopy permits the determination of a liquid surface composition, the molecular orientation and conformation, and the surface structure at a microscopic level. This is achieved by performing the measurement with different polarizations of the two incoming beams, and the generated SFG signal beam that can be detected. The advantage of SFG spectroscopy is that it can be applied to all types of liquid interfaces.[10,11]

The elemental composition of liquid surfaces can be characterized by X-ray photoelectron spectroscopy (XPS). The technique is based on energy measurement of electrons emitted from liquid surfaces in order to determine their binding energies. For a long period of time photoelectron spectroscopy was hardly applicable to highly volatile liquids due to the difficulty of transferring electrons from the liquid surface through the vapour phase to an electron detector. However, numerous sampling techniques have been tried and adapted to form suitable conditions for analysis, as will be discussed later in following section. [9,16-18]

Most of the techniques described above require samples to be placed in a vacuum for analysis. Section 1.2.2 gives an overview of these sampling techniques.[16,17]

1.2.2   *Techniques for introducing a liquid into a vacuum chamber*

Among the earliest and most significant studies of the surface of liquids were those reported by Siegbahn *et al.* using the well-known technique of X-ray photoelectron spectroscopy for chemical analysis (XPS also referred to as ESCA) to study the energy levels of atomic core electrons. The core electrons have small chemical shifts depending on the chemical environment of the atom which is ionized, allowing chemical structure to be

determined. For the first time the water O1s binding energy of liquid water was reported (538.0 eV) in 7 M aqueous LiCl.[18] Additives were employed (*e.g.*, LiCl, DMF or ethylene glycol) to lower the freezing point of water thus enabling an acceptable vacuum to be obtained. Siegbahn also provided a number of sampling techniques such as a liquid beam[9], a wetted wire system,[19] and a rotating stainless steel cone[16] to study the properties of the solution (*e.g.*, solute-solute, solute-solvent, solvent-solvent interactions).

A first attempt at generating a liquid beam, so as to introduce liquid samples into a chamber under vacuum conditions, was also reported by Siegbahn. In this arrangement, the liquid is continuously circulated in the system by a centrifugal pump. The aim was to couple the liquid beam with XPS. Partial success was achieved by obtaining an electronic spectrum of formamide, in which the liquid beam was adjusted to achieve a complete separation between the signals from the liquid and the vapour. However, the large size of the beam (a diameter of about 0.2 mm) caused some practical limitations since the residual high vapour pressure of the liquids was found to compromise the XPS studies. Several other limitations were found with this technique; in particular a large volume of liquid was required. There were also difficulties in adjusting and reproducing the liquid beam to a minimum diameter. In addition it was found that the resulting highly viscous samples were less suited for the experiment.

To address the limitations of the previous technique an alternative method, a wetted wire system, was employed to produce a well-defined layer of liquid of suitable dimensions for XPS. This method was developed to explore the kinetics of the reactions at the liquid surface. The technique consisted of a fine wire (0.3 mm diameter) coated with the liquid formed by dipping it first into a reservoir of liquid. By applying reactive constituents onto a wire and changing its rotation speed, liquid surface reactions kinetics were in principle accessible to study.

In addition to the previous sampling techniques, another method in which a rotating cone (Figure 1.2 a) is partially submerged into a cooled tank of the liquid sample was devised. During the rotation of the metal cone, a thin film of the liquid sample covers the metal surface and can be analysed by photoelectron excitation. Under those conditions, the vapor pressure decreased sufficiently to diminish the contribution of the vapour to the photoelectron signal. This allowed Siegbahn and co-workers to record photoelectron spectra of a variety of liquids.

In the mid-1990s an alternative sampling technique was developed by Nathanson[5,8] and co-workers to explore the influence of microscopic surface corrugation on collision dynamics using molecular beams. A rotating disk was employed as a sampling device to form a fresh and continuously renewed liquid film of a non-volatile liquid around 0.2 mm in thickness on the disk. This essentially substitutes the metal cone used by Siegbahn and co-workers by a metal disk. The rotating disk (Figure 1.2 b) technique was further developed by several groups. For example, Furlan has observed the photoejection of molecules into the gas phase from within a few μm of the liquid surface using this approach.[20,21] Watson and co-workers developed a rotating wheel technique (Figure 1.2 c) which exploited the scattering of inert gas ions from liquid surfaces to probe surface composition and the orientation of molecules. The rotating wheel drags a layer of liquid past a knife edge that leaves a fresh liquid film on the wheel of about 0.2 mm in thickness.[14,15]

In all of the cases above a small area of refreshed liquid surface is produced by the movement of some appropriate object, enclosed in a vacuum chamber. These techniques are suitable for the study of involatile liquids such as siloxanes and glycerol.[14] This arrangement (sampling techniques Figure 1.2) minimizes contamination by adsorption and optimizes the sample charging by continuously creating a fresh liquid surface.[14,15] Recently, Nathanson's technique (a rotating stainless steel wheel) has been used by McKendrick and co-workers to investigate the dynamics of collisions at the gas-liquid interface. Their studies have focused on inelastic scattering of OH radicals from reactive (liquid hydrocarbon) and inert (perfluorinated polyether) liquid surfaces. The radicals were detected by laser induced fluorescence (LIF) spectroscopy.[22-24] However, comparable studies of volatile liquids, such as water and light alcohols, require the introduction of new a technique. The breakthrough came with the development of the liquid microjet by Faubel *et al.*[25]
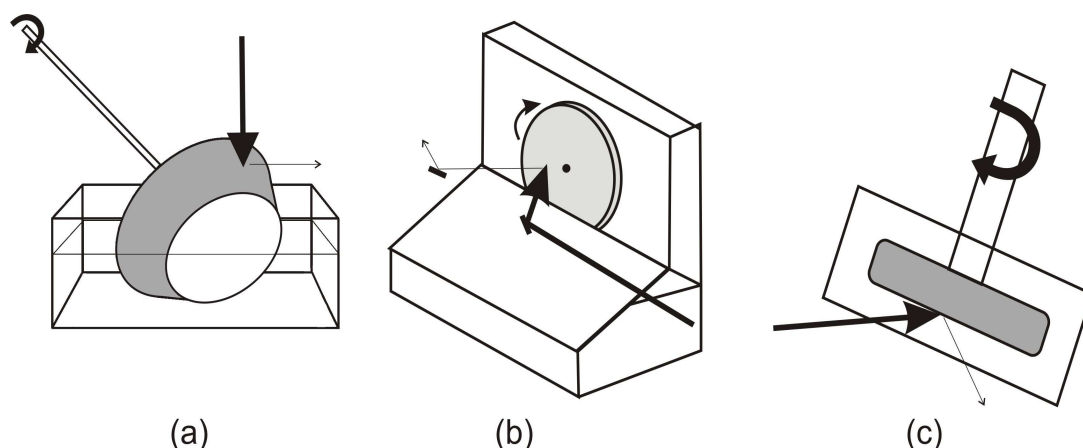
Figure 1.2   Liquid surface sampling techniques based on (a) a rotating cone (b) a rotating disk (c) a rotating wheel (the black thicker arrow shows the direction of the beam (*i.e.,* laser or ion source)

1.2.3   *The introduction of the liquid microjet*

In 1988 Faubel *et al.*[25] showed that it was possible to introduce a continuously refreshed liquid surface in a high vacuum chamber even for relatively volatile liquids. The procedure requires the injection of pressurized liquid through a narrow aperture at relatively high speed into a vacuum (see section 1.8 for full details). The combination of a sufficiently small aperture (generally a few microns) with sufficient pumping allows a good vacuum (~10^{-5} mbar) to be maintained, provided the jet is terminated in a way which does not release large amounts of vapour into the vacuum chamber. This condition is satisfied by using a cold trap or some other liquid collection device. The small jet size (smaller than the free molecular path) results in nearly collisionless evaporation.[26]

The clean and continuously replenished liquid surface available from a microjet is suitable for use with various analytical techniques. It offers many advantages, namely by minimizing contamination and by reducing the interference of vapour with the detecting devices (*e.g.*, optical spectroscopy or by mass spectrometry). Consequently, it has the potential to allow unprecedented insight into the electronic structure of volatile liquids and their molecular dynamics at the gas-liquid interface. Over the past two decades, the methodology of the liquid microjet has been applied to several different liquid substrates and has been coupled with several different probing techniques, as will be detailed shortly.

8

1.2.4   Conceptual outline of the liquid microjet experiment

The conceptual elements involved in the liquid microjet experiment are represented in Figure 1.3. The gas-liquid interface is generated by using pressure to force a liquid beam into a vacuum chamber. A clean surface is always presented because of the continuously flowing liquid sample, as mentioned in the previous section. The liquid surface can then be probed, for example, by laser illumination. If this results in a species being ejected from the liquid surface, such as an ion or a neutral photofragments, these can be potentially monitored by means of a second laser, coupled to either an optical detector or a mass spectrometer. The detection techniques that have actually been used are described in the next two sections.
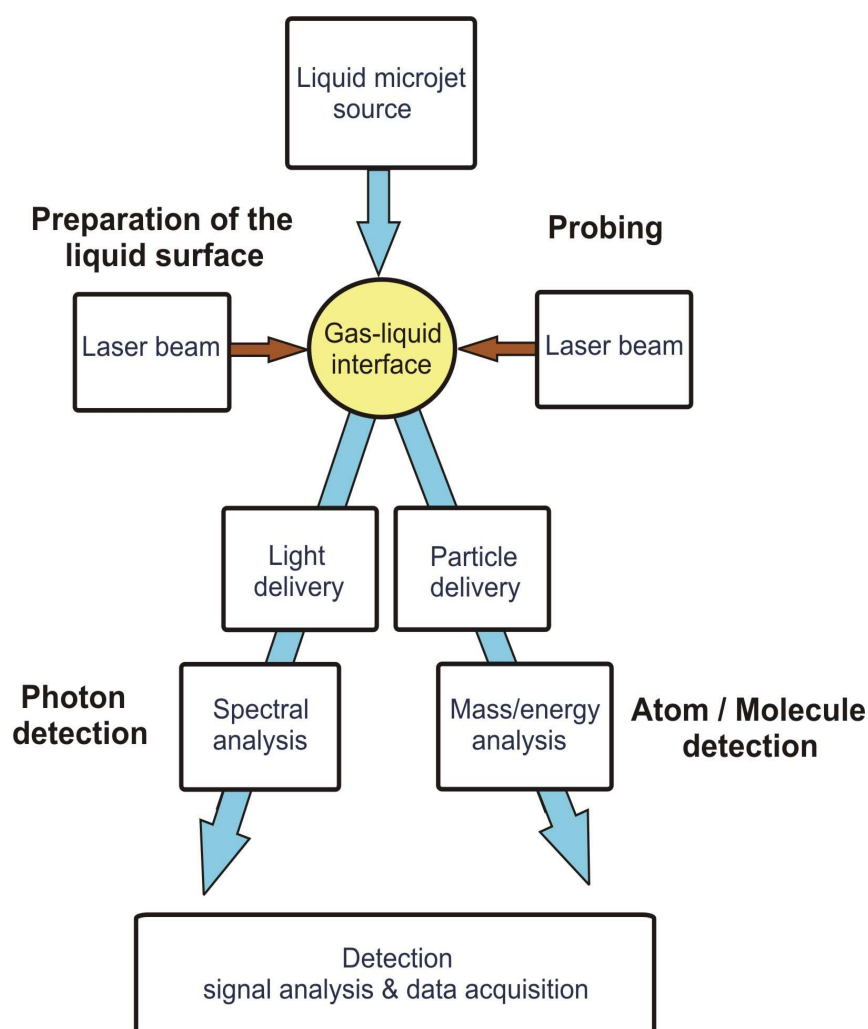
Figure 1.3   Basic elements of a liquid microjet pump-probe experiment

1.3 Mass spectrometric probing

One efficient way of probing species ejected from the surface of a liquid microjet is *via* mass spectrometry. The species ejected from the liquid surface may already be charged or they may be neutral and be subsequently ionized. All such experiments to date on liquid microjets have employed laser photoionization in one form or another, although it is possible in principle, to employ other means of ion generation, *e.g.,* ion bombardment (which would give a liquid version of secondary ion mass spectrometry (SIMS)). The most popular analyzer combined with a liquid microjet is a time-of-flight mass spectrometer (TOF-MS), due in part to its simplicity of use and its high sensitivity to different substrates.[7] A major advantage of a TOF-MS is that it is a multichannel device that collects data in all mass channels simultaneously. In addition it has a fast response time and it is applicable to ionization methods that produce ions in pulses, *e.g.*, pulsed lasers.[27]

The liquid microjet also provides a convenient means of getting ions of large biomolecules (*e.g.*, proteins, peptides or DNA nucleotide fragments) into the gas phase from an aqueous solution. Brutschy and co-workers have developed a method called Laser-induced Liquid Beam Ionization/Desorption (LILBID) that allows mass analysis of large biomolecules. In this method, the ions are desorbed from a liquid microjet by an infrared (IR) laser pulse and then extracted perpendicularly into a mass spectrometer. In Brutschy's group this mass spectrometer is a reflectron TOF-MS.[28-30] To bring about efficient thermal desorption, the IR laser is tuned to a vibrational resonance of the solvent. The laser induces very fast transitions of the irradiated liquid into a supercritical state followed by an explosive expansion of the highly compressed gas. Of all the desorbed species (*i.e.,* neutral molecules and ions) that escape into vacuum only the ions are drawn into the mass analyzer. During the desorption process, non-covalent interactions and some solvation characteristics can be preserved. This approach offers a combination of sensitivity and flexibility and can be used for a range of different substrates including low-charged macro- and bio- molecules. LILBID studies offer the potential to (a) gain insight into ion-ion and ion-solvent interactions in electrolyte solutions, (b) to desorb thermally unstable bio- and macro-molecules without fragmentation and detect them in a low charge state (*cf.* electrospray ionization), and (c) to study non-covalent complexes of ions and molecules present in the liquid phase.[31] LILBID has been shown to exhibit good sensitivity in detecting species in the concentration range 10^{-3}-10^{-5} M.[31]

1.4   Optical spectroscopic probing of molecules in or on a liquid microjet

1.4.1   Photoelectron spectroscopy

In Photoelectron Spectroscopy (PES) a high energy photon source ionizes a molecule and the kinetic energies of recoiling photoelectrons are analyzed, revealing the energy levels of the corresponding ion.[32] PES, when combined with the liquid microjet technique, enables the direct probing of the electronic structure of the surface of a liquid. PES provides information such as electron binding energies, surface states, and adsorbate structure.[33] PES has been proved to be surface sensitive at appropriate photon energies (*e.g.*, 100 eV), which makes it an attractive tool for studying surfaces in detail, including the surface of water.[34,35] Depending on the source of the photons, the application of PES can be adjusted to the requirement of the experiments. When a monochromatic source of soft (low energy) X-rays is used the focus is on core electrons and the technique is often referred to as X-ray-photoelectron spectroscopy (XPS). This technique is particularly useful for chemical analysis. On the other hand, vacuum ultraviolet radiation has sufficient energy to remove only valence electrons, giving rise to ultraviolet photoelectron spectroscopy (UPS).[36] In the case of both XPS and UPS, information is provided mainly on the surface and near-surface layers because electrons are able to escape into the gas phase only from a relatively shallow region (within < 5 nm on the surface) without significant inelastic collisions.

1.4.2   X- ray absorption spectroscopy (XAS)

Recently, X-ray absorption spectroscopy (XAS) has been combined with liquid microjets to investigate volatile liquid surfaces.[1,37] XAS comprises of an array of powerful techniques for probing the electronic and geometric structures of metals, semiconductors, insulators and adsorbents. Related techniques such as near-edge X-ray absorption fine structure NEXAFS and extended X-ray absorption fine structure EXAFS[38] have been used to study liquid surfaces, as detailed in the next section.

1.5   An overview of liquid microjet applications

1.5.1   Water

Water was the first substrate investigated in a liquid microjet and has been essential in the development of the microjet technique. Both mass spectrometric[39-41] and spectroscopic techniques (*e.g.*, XAS,[42,43] Raman spectroscopy[44] and PES[45,46]) have been employed to access information about specific properties such as the solvation of solute ions,[33] hydrogen

bonding,[45] and the electronic structure of the solvent.[42] The aim of this subsection is to give a concise overview of the most significant work done on water *via* the liquid microjet approach.

Faubel and co-workers initiated the first liquid microjet investigations on water; they have contributed to the development of this area by employing both TOF-MS and PES for analysis.[6,25,46] In their earliest studies TOF-MS was used to measure the velocity distribution of H_2O molecules vaporizing from thin jets of pure liquid water, *i.e.,* simple thermal evaporation without any laser excitation. From the measured velocity distribution it was determined that an aqueous liquid microjet is supercooled (*i.e.,* below 210 K) at its surface.[25] In a separate piece of work, a PES study of a microjet of pure water showed an alignment of the dipole moments of the water molecule at the liquid surface.[6] On the basis of this finding it was proposed that the water molecules at the surface are preferentially oriented in such a manner that the H atoms are pointing away from the bulk.[6] Winter and Faubel have also attempted to probe hydrogen bonds in a liquid water microjet using XPS.[45,47,48] By appropriate adjustment of the soft X-ray photon energy (600-1200 eV) the electron probing depth could be altered to access molecules either at the surface or in the bulk. Two distinctive components were seen in the oxygen (O1s) core-electron spectrum, with significantly different binding energies at and below the surface. The dominant contribution, at a vertical binding energy of 538.1 eV, was found in both bulk and surface sensitive spectra. A weaker component at 536.6 eV binding energy appears to be present only in bulk. Consequently, the 538.1 eV peak is attributed to surface water molecules.

Kondow *et al.* have studied the laser excitation of OH stretching vibrational modes of the liquid water with a view to investigating the local structure of liquid water. The Mid-IR laser excitation results in ejection of OH^- $(H_2O)_n$ in the vacuum chamber while ion pair ($H^+...OH^-$) is induced exclusively by a Near-IR laser and their detecting is accomplished by TOF-MS. They concluded that ions are produced in two distinct regions, the surface and the interior of the water beam. The surface and the inside ions are shown to be selectively produced in the gas phase by controlling the delay time between the two lasers.[39-41]

Saykally *et al.* have studied the local electronic structure of water in a microjet using XAS, NEXAFS and EXAFS.[42-44] In their studies they obtained both total ion yield (TIY- XAS) and total electron yield (TEY-XAS) measurements. TEY-XAS is a bulk probe and TIY-XAS is generally thought to provide a measure of the electronic structure of the surface.

Computational predictions indicate that the surface of liquid water should exhibit a TIY-XAS that is fundamentally distinguishable from the bulk liquid XAS. New experimental results however, suggest that the observable TIY-XAS is nearly identical in appearance to the TEY-XAS, which is bulk probe.

1.5.2 Inorganic solutes in water and other solvents

A number of inorganic solutes (*e.g.*, salts, metal clusters) have been characterized by microjet techniques within liquid water or other polar solvent. Aqueous salt solutions have been extensively studied, with particular interest being paid to the distribution of ions, both in the bulk and the near surface region. The existence of ions at the solution surface is important for the physics and chemistry of electrolytes and is likely to have a crucial effect on surface chemistry at liquid-vapour interfaces.

The electronic structure of interfaces of aqueous NaI and surface-active tetrabutylammonium iodine (TBAI) was investigated by Winter and Faubel using extreme ultraviolet (EUV) photoelectron spectroscopy.[33] In their study, the completion of the segregation monolayer at the surface was monitored by following the change of the iodide photoemission signal with salt concentration. In addition, their experimental observations were strongly supported by the results of a molecular dynamics simulation. The simulation also allowed characterization of the thermally averaged geometries of the surface active cations, in particular the orientations of the butyl chains with respect to the water surface.[34,49] Photoemission from aqueous alkali-metal-iodide salt solutions using EUV photoelectron spectroscopy was employed by Winter *et al.* The focus was on the determination of the electron binding energies of solvated anions and cations. The effect of different counter-ions (Li^+, Na^+, K^+ and Cs^+) and salt concentrations was systematically investigated. The electron binding energies of solvated ions were found to differ considerably from those in the gas phase, but the energies did not depend on the salt concentrations.[35]

The structure of NaI on and near the surface of ethanol was investigated by Kondow *et al.* using several techniques (*i.e.,* liquid beam with TOF-MS and also *via* PES).[50,51] In both studies, solutions of NaI in ethanol were introduced into the vacuum chamber as a continuously flowing microjet. The liquid was irradiated with an ultraviolet laser beam to eject ions into the gas phase for analysis by a TOF-MS. The presumption here is that the ions are produced by multiphoton ionization of the liquid near the surface, although other mechanisms

could be in operation here including some thermal ejection of ions. Their first study revealed mass spectra consistent with the presence of two cationic clusters: $Na^+(EtOH)_m$ (m = 0-6) and $Na^+(NaI)_n$-$(EtOH)_m$ (n = 1-7).[50] The cluster formation was explained by unimolecular dissociation of nascent cluster ions present on the surface and composed of Na^+ solvated with ethanol and/or $(NaI)_n$. The dependence of the ion intensities on the NaI concentration suggested the formation of NaI aggregates on the liquid beam surface across the entire NaI concentration range studied. In a subsequent study, the kinetic energies of photoelectrons emitted from the surface were measured as a function of NaI concentration in the solution.[51] The resulting photoelectron spectra exhibit peaks attributed to I^- and $(NaI)_n$, solvated by ethanol. It was concluded that NaI on the surface of the ethanol solution aggregates into clusters, $(NaI)_n$, in agreement with previous photo-ion mass spectrometry studies.[51] Kondow and co-workers have also developed droplet beam laser ablation TOF-MS to study NaI molecules in an aqueous solution after obtaining a beam of droplets of this solution. They reported that the $Na^+(H_2O)_n$ ions, produced by UV laser irradiation of a liquid droplet, were almost identical to those produced from a liquid water beam.[52]

Cluster ions of sodium and calcium solvated in ethanol were characterized by Kondow *et al.*[53] They used multiphoton ionization to form and TOF-MS to detect the ejected cluster ions, $CaOEt^+(EtOH)_m$ (m = 2-9), $CaI^+(EtOH)_m$ (m = 1-7) and $H^+(EtOH)_m$ (m = 3-5) from a liquid beam. The measurement of the velocities of the ions indicated that two types of ejection mechanisms were operating simultaneously. Firstly, ions formed on the liquid surface were ejected with accompanying solvent molecules. Secondly the other ions were generated by Coulomb explosion of a divalent cluster ion, $Ca_2^+(EtOH)_m$. These ions gain a sizable translational energy because of Columbic repulsion.[53-55]

The gas–liquid interface of aqueous sodium halide solutions was examined by Orlando *et al.* using multiphoton ionization combined with TOF-MS.[56] Laser excitation at 193 nm produced cations of the form $H^+(H_2O)_n$ and $Na^+(H_2O)_m$ from a liquid jet containing NaCl, NaBr or NaI. These cations yields, when correlated with concentration, laser power and anion identity, showed that the protonated water cluster yield varied inversely with increasing salt concentration, while the solvated sodium ion cluster yield was proportional to concentration.[56]

The clathrate-like structures of cation, drawn from alkali metal of organic have been investigated with LILBID-MS by Brutschy *et al.* The LILBID process implies desorption of

the ions from a jet of supercooled water using an IR laser beam. The aqueous clusters $M^+(H_2O)_n$ in which $M^+ = K^+$, Cs^+, NH_4^+ and n = 18, 20, 22, 24, 27, 29,… were observed in the cation mass spectra. Predominant cluster sizes for $K^+(H_2O)_n$ are n = 16, 20, 25, 27, and for $Cs^+(H_2O)_n$ n = 18, 20, 22, 24, 27, 29, In both cases, the highest signal intensity was measured for n = 20. This particular size corresponds to a deformed dodecahedral cage structure (*e.g.*, a clathrate) with a cation in the cavity.[57]

1.5.3   *Organic and bioorganic molecules in water*

Various organic substrates such as biomolecules, amino acids, alcohols and aromatic compounds have been characterized using a liquid microjet. The conformation and reactivity of proteins is significantly influenced by non-covalent interaction of the amino acid side chains, such as hydrogen bonding, hydrophobic interactions and ionic interactions. Liquid microjet method in combination with different spectrometry techniques (*e.g.*, LILBID-MS, IR-TOF-MS) offers the possibility of transferring large charged biomolecules into the gas-phase without significant fragmentation.

Brutschy *et al.* have applied LILBID for isolation of biological molecules (*i.e.,* proteins, gramicidin, lysozyme, and synthetic ionophores) from aqueous or alcohol solution into the gas phase for mass-spectrometric investigation. Their work shows mass spectroscopic evidence that IR laser desorption of several different protein solutions preserves the non-covalent interaction within and between the solvent. This method was applied to the detection of non-covalent complexes such as the diglycyl-histidin-complex in and the human hemoglobin complex aqueous solution.[29-31,58,59]

A study of the hydration structure of arginine in aqueous solution by using a liquid microjet in combination with IR laser ablation has been reported by Kondow and co-workers.[60] Hydrated arginine clusters ions ejected from the liquid surface were analyzed by TOF-MS to determine the local composition of the solution. It was assumed that, by IR laser absorption, the removal of a small enough fraction of the solution containing a core ion can be conducted without modifying the composition of the solution. The IR irradiation at (3508 cm^{-1}), which excites an OH stretching vibration, of the water, is a laser ablation process. Their results revealed that arginine aggregates are less hydrated than their monomeric counterparts. The main reasons given by the authors were the smaller dipole moment of the arginine monomer, and the formation of a hydrophobic hydration structure of water around an arginine aggregate

in the solution causing the arginine monomer to be less hydrated in a concentrated arginine solution than the aggregate.[60] Adenine (A) salts in aqueous acidic and alkaline solution were also investigated. Neutral species ejected into vacuum by the IR laser pulse were ionized by a pulsed UV laser and ions were analyzed by TOF-MS. $AH_2^{2+}.2Cl^-$ and $[A-iH]^{i-}.iNa^+$ (where $i =$ 1-3) ions were observed and undergo four-photon ionization involving decomposition and proton transfer of the intermediate species under irradiation of the UV laser.[61]

Further investigation of amino acids (*e.g.*, glycine, lysine) was performed by Saykally *et al.* using total electron yield EXAFS and NEXAFS. The pH of the bulk solution was systematically varied while maintaining a constant amino acid concentration. Spectra were interpreted through comparisons with both previous studies and *ab initio* computed spectra of isolated glycine molecules and hydrated glycine clusters.[62,63] LILBID–MS was used by Charvat *et al.* to study protonated amino acids (ornithine, citrulline, lysine, arginine) and their non-covalent clusters in the gas phase by desorption from water.[64] It was suggested that, the desorption of a biomolecules could be understood as a single step process involving laser heating of the solvent above its supercritical temperature followed by a rapid expansion, the recombination of the ions and finally isolation and desorption of only a small fraction of pre-formed ions and charged aggregates. The aqueous solution concentration and pH-dependence of the laser-induced desorption of protonated species (monomers and dimers) was also studied. It was reported that the desorption process depends critically upon the proton affinity of the molecules, the concentration of other ions, and of the pH of the solution. Crucially, Charvat *et al.* concluded that the ion concentrations measured in the gas phase are very likely to reflect the solution properties (equilibrium concentrations).[28,64] The same technique was used to investigate biomolecules (e.g cytochrome c, bovine serum albumin).[65-67]

1.5.4   Alcohols and others organics liquids

A mixture of alcohols (*e.g.*, ethanol, methanol) and water has been frequently used in liquid microjet studies (see Table 1.1) as a useful solvent in studies of chemical equilibrium as well as in various biological studies. Despite the similar properties of liquid water and methanol (*e.g.*, abnormal heats of vaporization, boiling points, dipole moments, etc.,), experimental results show dramatic differences in the surface hydrogen bond structure, which is shown by the difference in surface tension of these liquids.[37]

Nishi and co-workers have developed a molecular beam technique for generating micro-clusters and liquid droplets a vacuum. Molecular association in ethanol-water solutions with various ethanol concentrations was studied using mass spectrometry by isolating the clusters through adiabatic expansion of liquid jets under the vacuum. The isolation of hydrogen-bonded clusters from the ethanol-water solution through adiabatic expansion of mist particles under vacuum revealed the following characteristic of the ethanol – water and ethanol-ethanol clustering in the solutions: (1) the hydrophobic hydration of the ethanol is so strong that pure water clusters are not detectable at (ethanol mole fraction) $x > 0.04$; (2) ethanol tends to form polymer chains with surrounding water molecules.[68,69]

Saykally *et al.* combined X-ray absorption spectroscopy with a liquid microjet to observe and quantify the intermolecular surface relaxation of liquid water and methanol. Methanol can be considered as the simplest and weakest surfactant, showing positive absorption at the air/water interface of liquid water. Sum-frequency-generation (SFG) studies of methanol/water suggest that methanol accumulates at the liquid interface with evidence of polar ordering of the methyl group about the surface normal.[1,43]

A new analytical and experimental method has been developed by Kaneda *et al.* for measurements of energy losses and the angular distribution of charged particles the trajectory will liquid targets. A liquid microjet of pure ethanol was targeted with an incident beam produced by a Van-de-Graaf accelerator. The energies of the transmitted incident particles were measured by a solid state detector (SSD). This method has the potential to become a reliable measurement technique for charged particles stopping in liquid targets and other collisions interactions (*e.g.*, liquid-ion-collision interaction).[70]

Kondow *et al.* used mutiphoton ionization and TOF-MS to explore ions ejected from liquid surfaces of wide a variety of liquids such as methanol, ethanol, 1-propanol[71] and phenyl-ketones.[72,73] The same technique was used to investigate benzoic acid in alcohol solutions (*i.e.,* ethanol and propanol).[74]

Many papers have been published on liquid microjes and the investigation of aromatic compounds (*e.g.*, phenol[75-79], aniline[80-85], resorcinol[86,87], naphthalene[88], benzene[89] and hydroquinone[90,91]).

1.6 Project description and thesis contents

The original aim of the work was to study photodissociation dynamics at the gas-liquid interface using a liquid microjet. The ability to combine a freshly flowing liquid-gas interface with high vacuum conditions means that fragments can be ejected into the gas phase by laser irradiation without being impeded by collisions with gas molecules. The intention, therefore, was to carry out a series of experiments that were analogous to the many laser pump-probe studies of molecular photodissociation that have already been carried out over the past two decades in the gas phase. An additional motivation stemmed from theoretical predictions of the photodissociation dynamics of molecules at liquid surfaces by Benjamin and co-workers. These theoretical predictions simulated the photodissociation dynamics of ICN at surface of liquid chloroform and could be use to compared with future experimental results.[92,93]

In order to attempt these studies, it was first necessary to design, construct and test a new liquid microjet apparatus. Having completed this task, which was the major part of the work described in this thesis, attention then switched to exploring the combination of the liquid microjet with the laser pump-probe technique. Initial tests were made by attempting to photoeject intact molecules from solutions prior to investigating photodissociation products. This proved to be challenging and it became clear that further improvements in the instrumentation were necessary before the original aim of this work could be met, as will be described later.

1.7 Summary of all liquid microjet experiments

Table 1.1 Summary of all liquid microjet experiments reported to date

Year	Group	Detection [a)]	Liquid medium	Analyte
2008	Kondow [39]	TOF-MS	Water	Ions H$^+$,OH$^-$
2008	Orlando et al.[56]	TOF-MS	Water	NaCl, NaBr, NaI
2008	Saykally et al.[42]	XAS	Water	Water
2008	Winter et al.[94]	X-ray (Synchrotron radiation)	Water	NaOH solutions
2008	Winter et al.[95]	PES	Water	Imidazole
2008	Winter et al.[96]	X-ray (Synchrotron radiation)	Water	NaCl, LiCl
2007	Winter et al.[45]	PES	Water	Water
2007	Charvat et al.[67]	IR- MALDI-MS	Water-alcohol mix	Biomolecules
2007	Winter et al.[47]	Auger-electron spectroscopy	Water	Water
2007	Kaneda et.al.[70]	Solid-State detector	Ethanol	Ethanol
2006	Winter et al.[33]	PES	Water	NaCl, NaBr, NaI, NaF
2006	Kondow et al.[60]	TOF-MS	Water	Arginine solution
2006	Kondow et al.[40]	TOF-MS	Water	Ions H$^+$,OH$^-$
2006	Buntine et al.[89]	TOF-MS	Water	Benzene
2006	Saykally et al.[44]	Raman thermometry	Water	Water
2006	Kondow et al.[52]	TOF-MS	Water	NaI

2006	Charvat et al.[66]	TOF-MS	Water	Biomolecuels
2005	Winter et al.[49]	PES	Water	Tetrabutylammonium iodide
2005	Saykally et al.[62]	NEXAFS	Water	Glycine
2005	Saykally et al.[63]	NEXAFS	Water	Amino acids
2005	Kondow et al.[73]	TOF-MS	Water	Phenyl ketones
2005	Abel et al.[65]	LILBID-MS	Water	Biomolecules
2004	Winter et al.[48]	EUV-PES	Water	Water
2004	Winter et al.[34]	PES	Water	Tetrabutylammonium iodide
2004	Winter et al.[35]	EUV-PES	Water	Alkali Metal (K^+,Li^+, Na^+,Cs^+)
2004	Saykally et al.[1]	XAS	Water	Methanol, Ethanol
2004	Kondow et al.[51]	TOF-MS	Ethanol	NaI
2004	Kondow et al.[79]	TOF-MS	Water	Phenol
2004	Kondow et al.[41]	TOF-MS	Water	OH-stretch vibration of water
2003	Buntine et al.[97]	TOF-MS	Water-ethanol	Hydroquinone
2003	Buntine et al.[91]	TOF-MS	Ethanol	Anisole
2002	Saykally et al.[37]	XAS	Water	Methanol
2002	Kondow et al.[78]	TOF-MS	Water	Phenol
2002	Kondow et al.[61]	TOF-MS	Water	Adenine salt
2002	Charvat et al.[64]	LILBID-TOF-MS	Water	Amino acids

2001	Saykally et al.[43]	XAS	Water	Water
2001	Holstein et al.[90]	1+1 REMPI TOF-MS	Ethanol	Hydroquinone
2001	Kondow et al.[77]	TOF-MS	Water	Phenol
2001	Kondow et al.[55]	TOF-MS	Ethanol	CaI_2
2000	Kondow et al.[84]	TOF-MS	Ethanol and Propanol	Aniline
2000	Brutschy et al.[58]	LILBID_MS	Water	Protein complexes
2000	Kondow et al.[54]	TOF-MS	Ethanol	$CaCl_2$
1999	Kondow et al.[50]	TOF-MS	Ethanol	NaI
1999	Kondow et al.[53]	TOF-MS	Ethanol	CaI_2
1999	Holstein et al.[98]	TOF-MS	Methanol	Methanol
1999	Kondow et al.[83]	TOF-MS	Propanol	Aniline
1999	Kondow et al.[99]	TOF-MS	Alcohol	Benzotrichloride
1999	Kondow et al.[86]	TOF-MS	Water	Resorcinol
1999	Brutschy et al.[59]	LILBID-TOF-MS	Water	Biomolecules
1999	Brutschy et al.[57]	LILBID-MS	Water	Metal ions (K^+,Li^+, Na^+,Cs^+), ammonia
1998	Kondow et al.[85]	TOF-MS	Alcohol	p-haloaniline
1998	Brutschy et al.[31]	LILBID-TOF-MS	Water	Biomolecules complexes
1997	Brutschy et al.[30]	LILBID-TOF-MS	Methanol	Synthetic ionophores
1997	Kondow et al.[76]	TOF-MS	Water/ ammonia	Phenol

1997	Kondow et al.[100]	TOF-MS	Alcohol	Benzotrichloride
1997	Faubel et al.[6]	PES	Water	Benzyl alcohol, formamide
1996	Kondow et al.[74]	TOF-MS	Ethanol/Propanol	Benzoic acid
1996	Kondow et al.[71]	TOF-MS	Alcohols	Methanol,ethanol, propanol
1996	Brutschy et al.[29]	LILBID-MS	Methanol/Ethanol	Gramicidin, lysozyme
1996	Kondow et al.[88]	TOF-MS	Ethanol	Naphthalene
1995	Kondow et al.[101]	TOF-MS	Ethanol	NaI
1995	Kondow et al.[82]	TOF-MS	Propanol	Aniline
1995	Kondow et al.[75]	TOF-MS	Water	Phenol
1995	Kondow et al.[72]	TOF-MS	Alcohol	Phenyl-ketone
1994	Kondow et al.[81]	TOF-MS	Ethanol	Aniline
1994	Kondow et al.[102]	TOF-MS	Anisole	Ethanol
1994	Kondow et al.[103]	TOF-MS	Alcohols	Aceto-phenone
1994	Faubel et al.[46]	PES	Water	Water
1992	Kondow et al.[80]	TOF-MS	Ethanol	Aniline
1990	Nishi et al.[104]	MS	Water	Carboxylic acids
1988	Nishi et al.[69]	MS	Water	Ethanol
1988	Faubel et al.[25]	TOF-MS	Water	Water

1.8   Introduction/ Liquid microjet properties

The focus in this chapter now turns to the proprties of liquid microjets. The formation of a liquid microjet also referred to as a liquid beam is presented in section 1.9. Section 1.10 examines the parameters specific to the liquid with special attention being paid to the choice of the liquid phase (1.10.1) and the conditions in the capillary tube (1.10.2) and in the vacuum chamber (1.10.3). In section 1.11 the designs of various microjet sources, which will be referred to as nozzles, and their use in different experiments are discussed.

1.9   Formation of a liquid microjet

A liquid microjet is formed by forcing a liquid through a small orifice, with a diameter typically in a range of 5-50 μm, at high pressure into a vacuum chamber (Figure 1.4). This technique generates a constantly replenished and clean liquid surface in a vacuum.[25] Through the use of a sufficiently large pump and/or cryopump, it is possible to generate a liquid microjet under high vacuum conditions, *i.e.,* $10^{-5} - 10^{-6}$ mbar. Since the reason for producing the microjet is to probe it in some manner *e.g.*, via a focused laser beam, the stability of the microjet is essential for obtaining usable results. This in turn is dependent on the properties of the liquid (*i.e.,* viscosity, surface tension) and those of the nozzle design and separating conditions (*i.e.,* pressure, flow rate, inner diameter of the aperture).
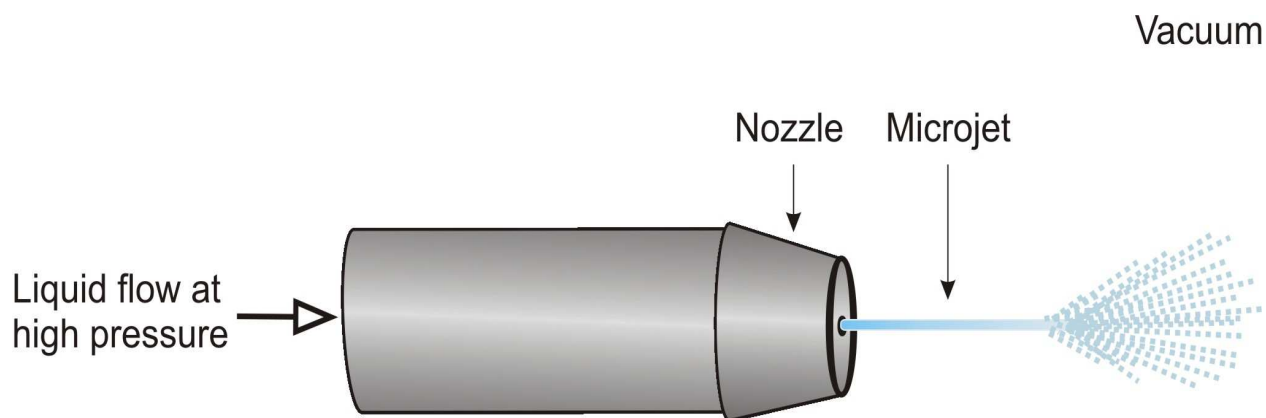
Figure 1.4   General scheme of liquid microjet

1.10 Parameters specific to the liquid

1.10.1 Selection of the liquid

The choice of the solvent used must take into account a variety of demands to make an experiment successful. It must solubilize the substrate of interest, if any, and possess suitable properties for use as a microjet.

Water has been the solvent most commonly employed in liquid microjet experiments,[6,25,33] although other solvents, either pure or mixed with water, such as ethanol, methanol and benzene have also been reported.[1,6,33,90] Both water and liquid alcohols allow access to stable flows and are easy to handle. Water is usually preferred when the substrates of interest (*i.e.,* ionic compounds) are insoluble in alcohol or when the aqueous compounds are specifically targeted. However, due to its high melting point, the formation of solid ice in the chamber can compromise the experiment, as will be discussed later. Two properties of the solvent, its viscosity and its surface tension, are of particular importance.

In general terms, the viscosity can be defined as the resistance of a liquid to flow; higher viscosity results in a lower flow rate for a given applied pressure. This resistance acts between molecules of the fluid that are traveling at different velocities. The viscosity of a liquid is strongly dependent on its temperature. Its influence is important while the fluid is flowing in the capillary and upon going through the nozzle aperture.

Surface tension is the cohesive tension between liquid molecules that is responsible for the elasticity of its surface. Surface tension plays an important role in the stability of the jet and on the formation of droplets[105] and will be discussed in the following subsection. Table 1.2 lists the viscosities and surface tensions of commonly used solvents.[106]

Table 1.2 Values of the surface tension and viscosity

Liquid	Ethanol	Methanol	Benzene	Water
Surface tension (σ) / N m^{-1}	0.0226	0.0227	0.028	0.0728
Viscosity $\times 10^{-4}$ (η) / kg m^{-1} s^{-1}	10.74	5.44	6.04	8.91

1.10.2 Parameters specific to the liquid within the capillary tube

As mentioned earlier it is essential to keep the microjet as stable as possible. Consequently, turbulence needs to be avoided and so the flow of the liquid should be maintained in the laminar flow regime to allow coupling with analytical techniques. Turbulent and laminar regimes can be defined in terms of the so-called Reynolds number (*R*). The Reynolds number is a measure of the ratio of inertial forces to the viscous forces as a fluid flows through a tube of diameter *d*:[107]

$$R = \frac{\rho v d}{\eta} \tag{1}$$

where ρ, v, *d* and η are the density, the flow velocity, the beam diameter and the viscosity of the liquid, respectively. For a microjet of a diameter *d* we have essentially a wall-less tube but equation (1) still applies.

Laminar flow occurs for Reynolds numbers between 250 and 2000;[107] under these conditions the viscous forces within the liquid are dominant over inertial forces. Lower values (*i.e., R* < 250) indicate that the flow rate is insufficient to form a beam and would result in single droplets. For *R* > 2000, turbulence appears and disintegrates the beam to form a spray. It is noteworthy that other parameters such as (*e.g.*, fluctuation in pressure or velocity, air bubbles in fluid) can also favour turbulence.[107]

Figure 1.5 shows the differences in the velocity distribution between turbulent and laminar flows. Laminar flow occurs when the velocity of the liquid gradually increases and reaches a maximum near the centre of the tube, with a roughly parabolic velocity distribution. Conversely, in a turbulent flow, the slower solvent molecules adjacent to the capillary wall mix with the high-speed molecules in the middle of the stream, creating a velocity distribution that is more uniform radially while following a logarithmic character on the side.
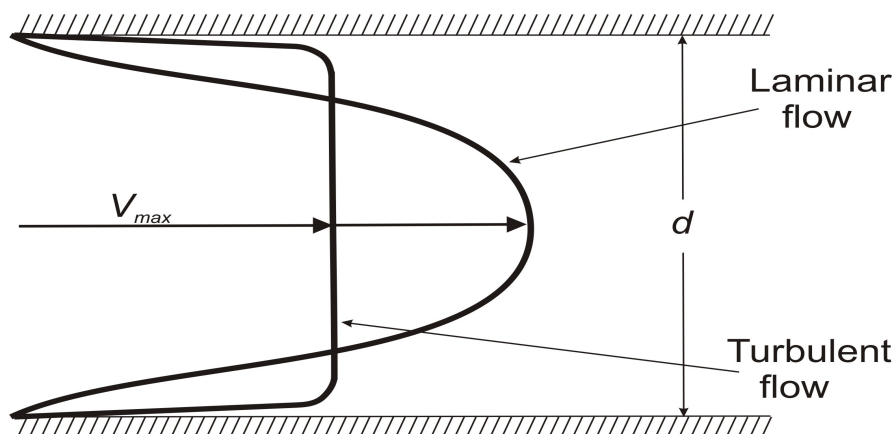
Figure 1.5   Velocity profiles of laminar and turbulent flow in cylindrical capillaries

The flow velocity (ν) of the microjet depends on the flow rate of the liquid and microjet diameter (see Table 1.3). The flow velocity can be determined from equation 2:[25,108]

$$\nu = \sqrt{\frac{2P}{\rho}}$$

(2)

where P is the pressure (bars) acting behind the nozzle. Table 1.3 summarizes typical values of the flow rates, velocities and inner diameters of the nozzles from various experiments.

Table 1.3 Flow rates and velocities of liquid microjets reported in the literature

Microjet diameter/ μm	Flow rate / ml min^{-1}	Velocity / m s^{-1}	Group
5	-	45	Faubel[25]
6	-	120	Winter-Faubel[33]
10	0.4	30	Charvat[28]
10	0.5	38	Saykally[1]
10	-	50-150	Brutchy[30]
20	0.2	10.6	Kondow[7]
25	0.2-1.2	-	Holstein[98]

1.10.3 Parameters specific to the liquid in the vacuum chamber

Once the liquid enters the vacuum chamber, the laminar flow can only be maintained for a relatively small distance and the liquid beam eventually disintegrates to form droplets. If the aim is to probe the liquid microjet rather than droplets, then the length of the intact microjet is important since, if it is too short, it will make it more challenging to probe this portion of the liquid flow.

1.10.3.1 *Influence of surface tension on the microjet breakdown*

The process of liquid jet instability has been studied by Furlani[105] and also by Mashayek and Ashgriz.[109] Figure 1.6 illustrates the process of a microjet breaking into droplets. The thermal energy imparted to the jet is carried downstream by its velocity. Since the surface tension of the jet is temperature-dependent, the advection of the thermal energy gives rise to a time-dependent spatially periodic variation (or gradient) of surface tension along the free surface. This surface tension gradient gives rise to a shear stress at the free surface, which is balanced by inertial forces in the fluid. Consequently, a so-called Marangoni flow, the mass transfer of the liquid layer due to the surface tension differences, is induced towards regions of higher surface tension. This, in turn, produces a deformation of the free surface that ultimately leads to instability and droplet formation. In Figure 1.6 λ_j represents the period between microjet breakage and *d* represents the microjet diameter. Consequently, the surface of tension is critical in determining the length of a liquid microjet.

1.10.3.2 The distance to droplet formation

Regardless of the conditions, the liquid microjet is only stable for a finite distance, after which it fragments into droplets. The intact length of the microjet, *L*, can be calculated using the following equation 3:[110]

$$L = C_d\, v \left(\sqrt{\frac{\rho d^3}{\sigma} + \frac{3\eta d}{\sigma}} \right)$$

(3)

where σ is the surface tension and C_d is a constant on the order of 10. Table 1.4 contains the parameters used in equation (2) to obtain the velocity (v) and equation (3) to calculate the droplet formation distance (L) for water and ethanol. As can be seen from the table, the

breakdown distance is significantly longer in the case of ethanol compared to water due to the difference in surface tensions.

Table 1.4 Calculated breakdown distances (L)

Liquid	σ / N m^{-1}	$10^{-4}\eta$ / kg m^{-1} s^{-1}	ρ / kg m^{-3}	d / μm	v / m s^{-1}	L /mm *
Water	0.0728	8.91	1000	25	14.4	2.1
Ethanol	0.0226	10.74	789	25	16.2	4.2

* Based on a flow rate of 0.25 ml/min through a 25 μm aperture

1.10.3.3 *Evaporative cooling*

Once the liquid beam is in the vacuum chamber, molecules will evaporate from its surface. As the heat of vapourization is transported away from the liquid core, the liquid jet will cool significantly. Furthermore, this cooling increases with the distance from the nozzle aperture.

Various studies have been carried out with the aim of determining the surface temperature of liquid beams. In the earliest report by Faubel *et al*.,[7] the surface temperature for different liquid jet diameters was estimated by measuring the velocity distributions of molecules evaporating from the surface and fitting them to a floating Maxwellian distribution. A 5 μm diameter jet was reported to have a surface temperature as low as 210 K with an approximate cooling rate of $\sim 1.7 \; x \; 10^5$ K s^{-1}.[25]

For larger diameter jets the vapour density at the jet surface increases, indicating that evaporating molecules undergo many collisions and expand from the liquid surface. In order to obtain reliable surface temperatures for larger diameter jets, a skimmer was placed perpendicular to the liquid jet to reduce collisions in the expanding vapour;[25] this allowed freezing of the translational degrees of freedom. For diameters between 20 and 50 μm only moderate evaporative cooling was reported, giving surface temperatures between 275 and 300 K.

Kondow *et al*.[7] reported a cooling rate of 5 K mm^{-1} for the surface temperature of ethanol as the distance of the liquid jet from the nozzle exit was varied. A reduction in the cooling rate was observed when the distance from the nozzle exit was reduced due to a reduction in the vapour pressure as the surface temperature decreases.[7]
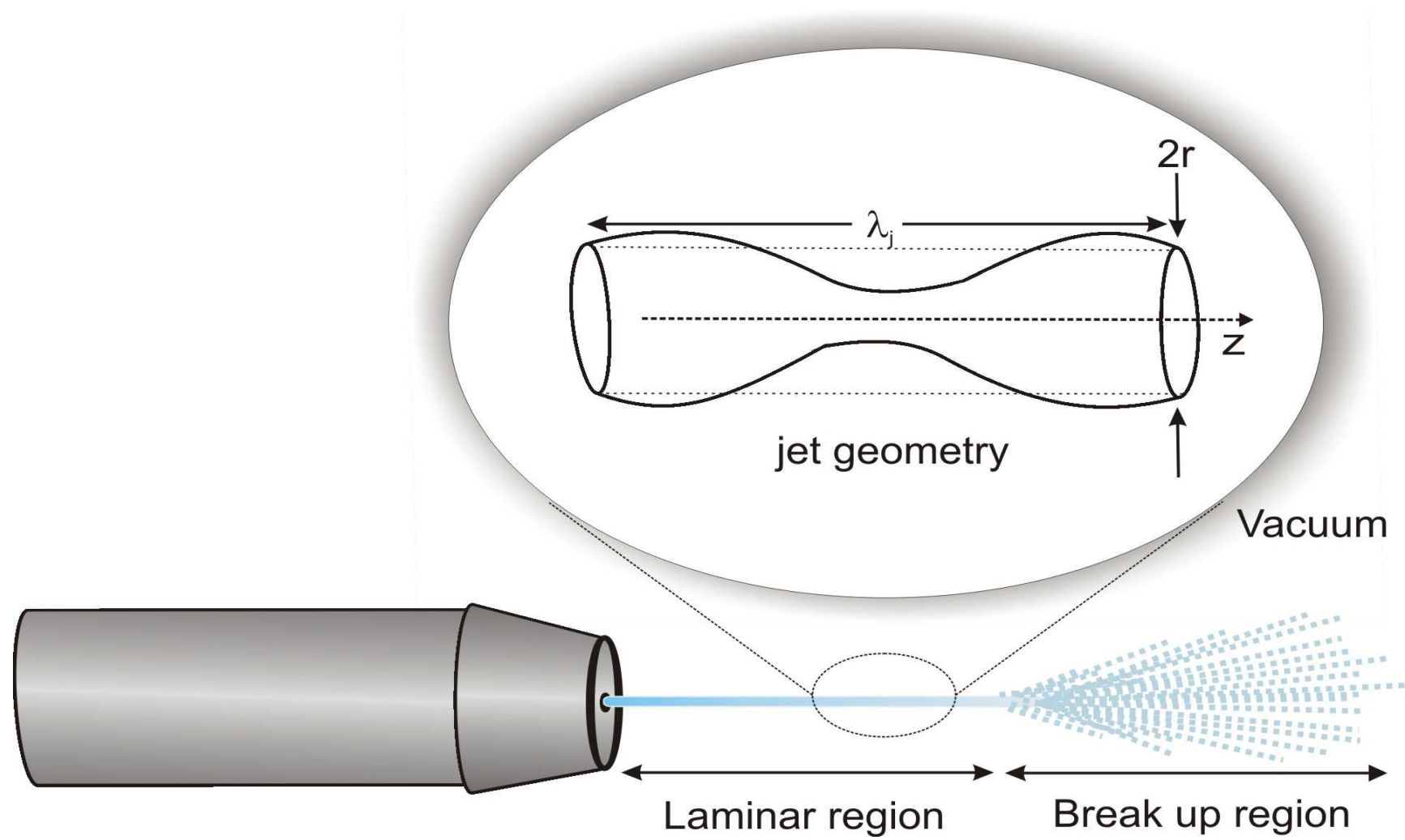
Figure 1.6   Schematic diagram of microjet stability and droplet formation

The cross-section of a liquid beam and its environment is shown in Figure 1.7. It consists of three separate regions. The first region comprises of the liquid core, the second region is a vapour-phase layer (atomic layer), and the third region is the free molecular flow field.[25]
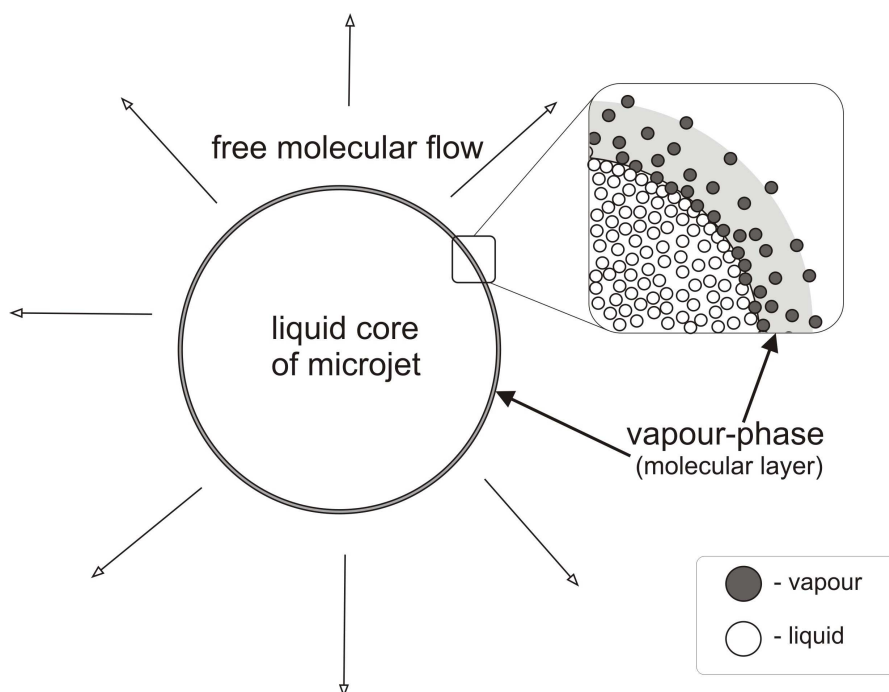
Figure 1.7   The structure of the microjet

One of the main problems presented by evaporative cooling during operation of the microjet is freezing of the liquid jet. Ice formation can lead to nozzle damage and cause permanent distortion to the beam direction. Faubel *et al*. reported that frost deposits on the liquid trap and freezing of out flowing water can be avoided by running the liquid jet while the main chamber is being evacuated.[25]

1.10.3.4 *Gas atmosphere over the liquid microjet surface*

One of the main disturbances occurring on the early liquid sampling models was due to the presence of a layer of gas around the liquid beam as molecules evaporating from the liquid surface were forming a vapour layer. In spite of the density of this gas decreasing rapidly away from the surface, it could compromise the spectroscopic results.[7] A schematic representation of the gas atmosphere over a typical liquid jet is shown in Figure 1.8. A dense liquid jet is surrounded by a collisional atmosphere, the size of which depends on the diameter of the liquid jet, and beyond which the number density of evaporating molecules drops by $1/r$, where r is radial distance from the source aperture in a collision-free zone.[1]

Radial vapour density ~ 1/r

Molecular flow

Vacuum

Collisional vapour layer

Laminar region   Break up region
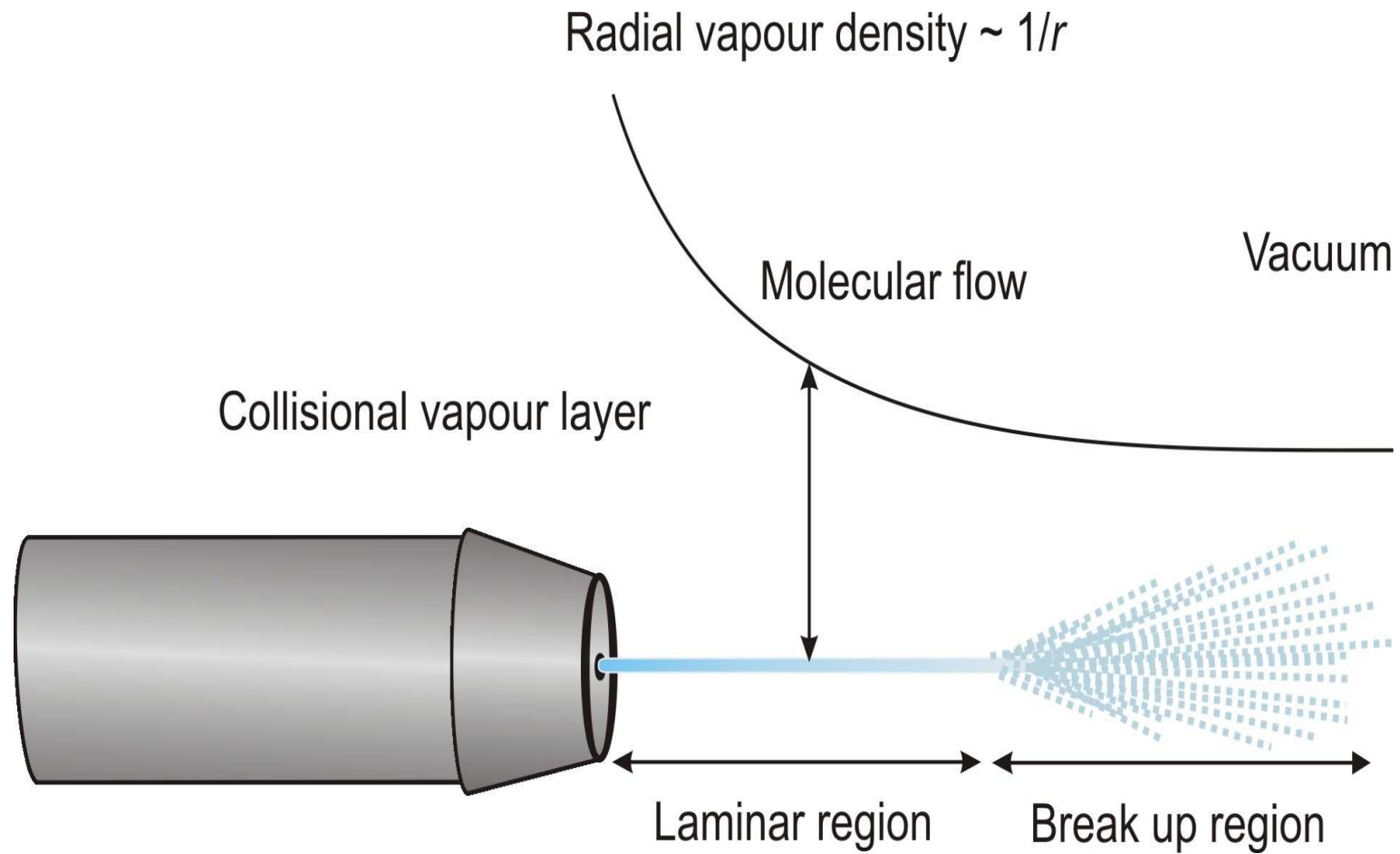
Figure 1.8   Schematic diagram of the gas atmosphere forming over the liquid microjet (The quantity of the r refers to the distance of the microjet from the source aperture)

Faubel *et al*. reported that by decreasing the diameter of a water liquid jet until it was smaller than or comparable to the mean free path in the equilibrium vapour, it is possible to satisfy the Knudsen condition, $\lambda > d$, for effusive flow, where λ is the mean free path and d is the diameter of the liquid jet.

The mean free path in the vapour is given by:

$$\lambda = \frac{C}{P_v} \tag{4}$$

where C is a constant (5.3×10^{-3} torr cm for water), and P_v is the vapour pressure of the liquid. With the use of this equation, Faubel *et al*. calculated the mean free path for water to be 11.5 μm at a temperature of 273 K, under an equilibrium vapour pressure of 4.58 torr. For liquid jets with diameters smaller than 11.5 μm, it was found that the surface temperature of the liquid jet was much less than larger diameter beams, as reported in an earlier section. As such, evaporating molecules from smaller diameter beams move directly from the liquid beam to the vacuum region with minimal collisions in the gas atmosphere.

For larger diameter beams, $d > \lambda$, Faubel *et al*. observed a supersonic expansion of evaporated solvent, which indicated the existence of a collisional atmosphere above the liquid surface. The collisional atmosphere was shown to limit the evaporation of molecules from the liquid beam by requiring gas phase diffusion to occur. This was supported by observed lower evaporation rates and warmer temperatures of the liquid surface. For example, Saykally *et al*.[1] calculated the diameter of the gas atmosphere surrounding a 20 μm water liquid jet to be 5d. Molecules in this region make around six collisions with other molecules as they traverse through the vapour layer, beyond which the vapour density decreases as a reciprocal of the distance from the liquid jet. As the liquid beam diameter increases relative to the mean free path, the evaporation rate becomes limited by diffusion through the vapour layer and approaches an asymptotic value of steady-state evaporation comparable to that under atmospheric conditions.[1]

Various methods have been employed to reduce the effect of collisions in the gas atmosphere such as higher vacuum conditions (better pumping speed), reduction of the distance the liquid beam travels from the nozzle exit, introducing a skimmer into the gas

atmosphere and reducing the size of the liquid beam diameter. Minimizing the size of the gas atmosphere is important for obtaining reliable information about the surface of the liquid beam, as it reduces the disturbing interference of the gas atmosphere with probe particles.

1.11 Nozzle designs

Regardless of the flow rate and the physical properties of the liquid employed, the quality of the liquid microjet depends strongly on the nozzle design. Several designs of microjet nozzles, with different shapes and materials, have been reported.[1,7,25,28,91] Generally, the nozzle aperture diameter controls the diameter of the beam. Table 1.5 lists the various materials for the nozzle assembly construction used by different research groups. As indicated in Table 1.5 two main materials are used in microjet nozzle assembly: (i) metal nozzles fabricated from electron microscopy apertures and (ii) glass capillaries. Compared to metal nozzles the glass capillaries offer more advantages (as discussed below). Several groups have reported improved stability of liquid microjets when a glass or silica capillary is employed.

Table 1.5 Summary of the types of microjet nozzles

Orifice diameter /μm	Material	Group
6	Glass capillary	Winter - Faubel[33]
10	Platinum-Iridium	Brutchy[30]
10-15	Quartz glass	Charvat[28]
20	Stainless steel	Kondow[7]
25	Fused silica capillary	Buntine[98]
0.5 - 50	Fused silica capillary	Saykally[1]
5-50	Platinum-Iridium	Faubel[25]

The first experiment was carried out by Faubel *et al.* in 1988 using a series of platinum-iridium nozzles (electron microscopy plates) of 5 to 50 μm in diameter.[25] Kondow and co-workers employed a platinum nozzle (i.d. of 20 μm),[7,111]while Saykally *et al.* followed Faubel's approach and used Pt-Ir electron microscope apertures.[1] Holstein *et al.* in their first

configuration used stainless steel apertures with a nozzle diameter between 5-40 μm.[98] A stainless steel nozzle has a number of disadvantages such as electrochemical corrosion and degradation of the material over time and so most groups have now replaced metal nozzles with less corrosive materials such as glass or fused silica.

Buntine and co-workers also employed a silica capillary for their liquid microjet assembly. The typical inner diameter of the capillary used was 25 μm, although in their most recent experiment a capillary with a 15 μm diameter has been reported. The significant point about the capillary used by Buntine and co-workers is that it makes use of off-the-shelf HPLC components, which can be easily replaced or repaired and are relatively cheap. The liquid microjet assembly described later in this thesis is an adaptation of the Buntine system.

More recently fused silica capillaries, due to their inexpensiveness and readily availability, have been increasingly used with various inner diameters.[90,91] Saykally *et al.* have reported standard fused silica capillaries (i.d. 100 μm) pulled to the desired final nozzle diameter (500 nm- 50 μm) with a commercial CO_2 laser micropipette puller.[1]

In 2004, Charvat *et al.* reported a new type of quartz nozzle capable of improving the long time stability of the liquid beam. A convergent quartz glass nozzle was fabricated from a quartz capillary tube. The tube is pulled-out over an oxygen-hydrogen flame, and is then cut at the thinnest part and polished. Apertures range between 10 and 15 μm.[28]

1.11 References

(1) Wilson, K. R.; Rude, B. S.; Smith, J.; Cappa, C.; Co, D. T.; Schaller, R. D.; Larsson, M.; Catalano, T.; Saykally, R. J. *Rev. Sci. Instrum.* **2004**, *75*, 725.

(2) Qvist, J.; Persson, E.; Mattea, C.; Halle, B. *Faraday Discuss* **2009**, *141*, 134.

(3) Knipping, E. M.; Lakin, M. J.; Foster, K. L.; Jungwirth, P.; Tobias, D. J.; Gerber, R. B.; Dabdub, D.; J., F.-P. B. *Science* **2000**, *288*, 301

(4) Ravishankara, A. R. *Science* **1997**, *276*, 1058

(5) Nathanson, G. M. *Annu. Rew. Phys. Chem.* **2004**, *55*, 231.

(6) Faubel, M.; Steiner, B.; Toennies, J. P. *J. Chem. Phys* **1997**, *106*, 9013.

(7) Kondow, T.; Mafune, F. *Annu. Rew. Phys. Chem.* **2000**, *51*, 731.

(8) Nathanson, G. M. *J. Phys. Chem.* **1996**, *100*, 13007.

(9) Siegbahn, H.; Siegbahn, K. *J. Electron. Spectrosc. Relat. Phenom* **1973**, *2*, 319.

(10) Miranda, P. B.; Shen, Y. R. *J. Phys. Chem. B* **1999**, *103*, 3292.

(11) Tian, C.; Ji, N.; Waychunas, G. A.; Shen, Y. R. *J. Am. Chem. Soc.* **2008**, *130*, 13033.

(12) Nathanson, G. M.; Davidovits, P.; Worsnop, D. R.; Kolb, C. E. *J. Phys. Chem.* **1996**, *100*, 13007.

(13) King, M. E.; Fiehrer, K. M.; Nathanson, G. M. *J. Phys. Chem. A* **1997**, *101*, 6556.

(14) Tassotto, M.; Gannon, T. J.; Watson, P. R. *J. Chem. Phys* **1997**, *107*, 8899.

(15) Gannon, T.; Tassotto, M.; Watson, P. *Chem. Phys. Lett.* **1999**, *300*, 163.

(16) Siegbahn, H.; Svensson, S.; Lundholm, M. *J. Electron. Spectrosc. Relat. Phenom* **1981**, *24*, 205.

(17) Siegbahn, H. *J. Phys. Chem.* **1985**, *89*, 897.

(18) Siegbahn, H.; Lundholm, M.; Holmberg, S.; Arbman, M. *J. Electron. Spectrosc. Relat. Phenom* **1986**, *40*.

(19) Fellner-Feldegg, H.; Siegbahn, H.; Asplund, L.; Kelfve, P.; Siegbahn, K. *J. Electron. Spectrosc. Relat. Phenom* **1975**, *7*, 421.

(20) Furlan, A. *Chem. Phys. Lett.* **1997**, *275*, 239.

(21) Furlan, A. *Chem. Phys. Lett.* **1999**, *309*, 157.

(22) Bagot, P. A. J.; Waring, C.; Costen, M. L.; McKendrick, K. G. *J. Phys. Chem. C* **2008**, *112*, 10868.

(23) Allan, M.; Bagot, P. A. J.; Westacott, R. E.; Costen, M. L.; McKendrick, K. G. *J. Phys. Chem. C* **2008**, *112*, 1524.

(24) Köhler, S. P. K.; Allan, M.; Kelso, H.; Henderson, D. A.; McKendrick, K. G. *J. Chem. Phys* **2005**, *112*, 024712

(25) Faubel, M.; Schlemmer, S.; Toennies, J. P. *Z Phys D Atom Mol Cl* **1988**, *10*, 269.

(26) Faubel, M.; Kisters, T. *Nature* **1989**, *339*, 527.

(27) Herbert , C. G.; Johnstone, R. A. W. *Mass Spectrometry Basics*, 1 edition ed.; CRC, 2002.

(28) Charvat, A.; Lugovoj, E.; Faubel, M.; Abel, B. *Rev. Sci. Instrum.* **2004**, *75*, 1209.

(29) Kleinekofort, W.; Avdiev, J.; Brutschy, B. *Int. J. Mass Spectrom. Ion Processes* **1996**, *152*, 135.

(30) Sobott, F.; Kleinekofort, W.; Brutschy, B. *Anal. Chem.* **1997**, *69*, 3587.

(31) Sobott, F.; Wattenberg, A.; Kleinekofort, W.; Pfenninger, A.; Brutschy, B. *Fresnius J. Anal. Chem.* **1998**, *360*, 745.

(32) Telle, H. H.; Urena, A. G.; Donovan, R. J. *Laser Chemistry: spectroscopy, dynamics and applications*; John Wiley & Sons Ltd, 2007.

(33) Winter, B.; Faubel, M. *Chem. Rev.* **2006**, *106*, 1176.

(34) Winter, B.; Weber, R.; Schmidt, P. M.; Hertel, I. V.; Faubel, M.; Vrbka, L.; Jungwirth, P. *J. Phys. Chem. B* **2004**, *108*, 14558.

(35) Weber, R.; Winter, B.; Schmidt, P. M.; Widdra, W.; Hertel, I. V.; Dittmar, M.; Faubel, M. *J. Phys. Chem. B* **2004**, *108*, 4729.

(36) Hollas, J. M. *Modern spectroscopy*, 3rd edition ed.; John Wiley & Sons, 1996.

(37) Wilson, K. R.; Schaller, R. D.; Co, D. T.; Saykally, R. J.; Rude, B. S.; Catalano, T.; Bozek, J. D. *J. Chem. Phys* **2002**, *117*, 7738.

(38) Wilson, K. R.; Tobin, J. G.; Ankudinov, A. L.; Rehr, J. J.; Saykally, R. J. *Phys. Rev. Lett* **2000**, *85*, 4289

(39) Toyama, N.; Kohno, J. Y.; Kondow, T. *Chem. Phys. Lett.* **2008**, *459*, 194.

(40) Toyama, N.; Kohno, J. Y.; Kondow, T. *Chem. Lett.* **2006**, *35*, 966.

(41) Kohno, J.; Mafune, F.; Kondow, T. *J. Phys. Chem. A* **2004**, *108*, 971.

(42) Cappa, C. D.; Smith, J. D.; Wilson, K. R.; Saykally, R. J. *Journal of Physics: Condensed Matter* **2008**, *20*, 205105/1.

(43) Wilson, K. R.; Rude, B. S.; Catalano, T.; Schaller, R. D.; Tobin, J. G.; Co, D. T.; Saykally, R. J. *J. Phys. Chem. B* **2001**, *105*, 3346.

(44) Smith, J. D.; Cappa, C. D.; Drisdell, W. S.; Cohen, R. C.; Saykally, R. J. *J. Am. Chem. Soc.* **2006**, *128*, 12892.

(45) Winter, B.; Aziz, E. F.; Hergenhahn, U.; Faubel, M.; Hertel, I. V. *J. Chem. Phys* **2007**, *126*.

(46) Faubel, M.; Steiner, B. *Linking the Gaseous and Condensed Phases of Matter* **1994**, *326*, 517.

(47) Winter, B.; Hergenhahn, U.; Faubel, M.; Bjorneholm, O.; Hertel, I. V. *J. Chem. Phys* **2007**, *127*.

(48) Winter, B.; Weber, R.; Widdra, W.; Dittmar, M.; Faubel, M.; Hertel, I. V. *J. Phys. Chem. A* **2004**, *108*, 2625.

(49) Winter, B.; Weber, R.; Hertel, I. V.; Faubel, M.; Vrbka, L.; Jungwirth, P. *Chem. Phys. Lett.* **2005**, *410*, 222.

(50) Matsumura, H.; Mafune, F.; Kondow, T. *J. Phys. Chem. B* **1999**, *103*, 838.

(51) Mafune, F.; Kondow, T. *Aust. J. Chem.* **2004**, *57*, 1165.

(52) Kohno, J.; Toyama, N.; Kondow, T. *Chem. Phys. Lett.* **2006**, *420*, 146.

(53) Kohno, J.; Mafune, F.; Kondow, T. *J. Phys. Chem. A* **1999**, *103*, 1518.

(54) Kohno, J.; Mafune, F.; Kondow, T. *J. Phys. Chem. A* **2000**, *104*, 1079.

(55) Kohno, J.; Mafune, F.; Kondow, T. *J. Phys. Chem. A* **2001**, *105*, 5990.

(56) Grieves, G. A.; Petrik, N.; Herring-Captain, J.; Olanrewaju, B.; Aleksandrov, A.; Tonkyn, R. G.; Barlow, S. A.; Kimmel, G. A.; Orlando, T. M. *J. Phys. Chem. C* **2008**, *112*, 8359.

(57) Sobott, F.; Wattenberg, A.; Barth, H. D.; Brutschy, B. *Int. J. Mass spectrom.* **1999**, *187*, 271.

(58) Wattenberga, A.; Sobotta, F.; Bartha, H. D.; Brutschy, B. *Int. J. Mass spectrom.* **2000**, *203*, 47.

(59) Wattenberg, A.; Sobott, F.; Barth, H. D.; Brutschy, B. *Eur. Mass Spectrom.* **1999**, *5*, 71.

(60) Toyama, N.; Kohno, J. Y.; Mafune, F.; Kondow, T. *Chem. Phys. Lett.* **2006**, *419*, 369.

(61) Kohno, J. Y.; Mafune, F.; Kondow, T. *Eur. Phys. J. D* **2002**, *20*, 339.

(62) Messer, B. M.; Cappa, C. D.; Smith, J. D.; Wilson, K. R.; Gilles, M. K.; Cohen, R. C.; Saykally, R. J. *J. Phys. Chem. B* **2005**, *109*, 5375.

(63) Messer, B. M.; Cappa, C. D.; Smith, J. D.; Drisdell, W. S.; Schwartz, C. P.; Cohen, R. C.; Saykally, R. J. *J. Phys. Chem. B* **2005**, *109*, 21640.

(64) Charvat, A.; Lugovoj, E.; Faubel, M.; Abel, B. *Eur. Phys. J. D* **2002**, *20*, 573.

(65) Abel, B.; Charvat, A.; Diederichsen, U.; Faubel, M.; Girmannc, B.; Niemeyer, J.; Zeeck, A. *Int. J. Mass spectrom.* **2005**, *243*, 177.

(66) Charvat, A.; Bogehold, A.; Abel, B. *Aust. J. Chem.* **2006**, *59*, 81.

(67) Charvat, A.; Abel, B. *Phys. Chem. Chem. Phys* **2007**, *9*, 3335

(68) Yamamoto, K.; Nishi, N. *J. Am. Chem. Soc.* **1990**, *112*, 549.

(69) Nishi, N.; Koga, K.; Ohshima, C.; Yamamoto, K.; Nagashima, U.; Nagami, K. *J. Am. Chem. Soc.* **1988**, *110*, 5246.

(70) Kaneda, M.; Sato, S.; Shimizu, M.; He, Z.; Ishii, K.; Tsuchida, H.; Itoh, A. *Nucl. Instrum. Methods Phys. Res., Sect. B* **2007**, *256*, 97.

(71) Mafune, F.; Kohno, J. Y.; Kondow, T. *J. Phys. Chem.* **1996**, *100*, 10041.

(72) Kohno, J.; Horimoto, N.; Mafune, F.; Kondow, T. *J. Phys. Chem.* **1995**, *99*, 15627.

(73) Kohno, J.; Mafune, F.; Kondow, T. *Bull. Chem. Soc. Jpn.* **2005**, *78*, 957.

(74) Mafune, F.; Kohno, J. Y.; Kondow, T. *J. Phys. Chem.* **1996**, *100*, 4476.

(75) Mafune, F.; Hashimoto, Y.; Hashimoto, M.; Kondow, T. *J. Phys. Chem.* **1995**, *99*, 13814.

(76) Mafune, F.; Hashimoto, Y.; Kondow, T. *Chem. Phys. Lett.* **1997**, *274*, 127.

(77) Kohno, J. Y.; Mafune, F.; Kondow, T. *J. Phys. Chem. A* **2001**, *105*, 8939.

(78) Kohno, J. Y.; Mafune, F.; Kondow, T. *Chem. Phys. Lett.* **2002**, *366*, 531.

(79) Kohno, J. Y.; Toyama, N.; Mafune, F.; Kondow, T. *Isr. J. Chem* **2004**, *44*, 215.

(80) Mafune, F.; Takeda, Y.; Nagata, T.; Kondow, T. *Chem. Phys. Lett.* **1992**, *199*, 615.

(81) Mafune, F.; Takeda, Y.; Nagata, T.; Kondow, T. *Chem. Phys. Lett.* **1994**, *218*, 234.

(82) Mafune, F.; Kohno, J. Y.; Kondow, T. *J. Chin. Chem. Soc.* **1995**, *42*, 449.

(83) Horimoto, N.; Mafune, F.; Kondow, T. *J. Phys. Chem. B* **1999**, *103*, 9540.

(84) Kohno, J. Y.; Mafune, F.; Kondow, T. *J. Phys. Chem. A* **2000**, *104*, 243.

(85) Hashimoto, Y.; Mafune, F.; Kondow, T. *J. Phys. Chem. B* **1998**, *102*, 4295.

(86) Horimoto, N.; Kohno, J.; Mafune, F.; Kondow, T. *J. Phys. Chem. A* **1999**, *103*, 9569.

(87) Horimoto, N.; Kohno, J.; Mafune, F.; Kondow, T. *Chem. Phys. Lett.* **2000**, *318*, 536.

(88) Horimoto, N.; Mafune, F.; Kondow, T. *J. Phys. Chem.* **1996**, *100*, 10046.

(89) Maselli, O. J.; Gascooke, J. R.; Kobelt, S. L.; Metha, G. F.; Buntine, M. A. *Aust. J. Chem.* **2006**, *59*, 104.

(90) Holstein, W. L.; Hammer, M. R.; Metha, G. F.; Buntine, M. A. *Int. J. Mass spectrom.* **2001**, *207*, 1.

(91) Holstein, W. L.; Dobeck, L. M.; Otten, D. E.; Metha, G. F.; Buntine, M. A. *Aust. J. Chem.* **2003**, *56*, 481.

(92) Winter, N.; Benjamin, I. *J. Chem. Phys* **2004**, *121*, 2253.

(93) Chorny, I.; Vieceli, J.; Benjamin, I. *J. Chem. Phys* **2002**, *116*, 8930

(94) Aziz, E. F.; Ottosson, N.; Faubel, M.; Hertel, I. V.; Winter, B. *Nature* **2008**, *455*, 89.

(95) Jagoda-Cwiklik, B.; Slavicek, P.; Cwiklik, L.; Nolting, D.; Winter, B.; Jungwirth, P. *J. Phys. Chem. A* **2008**, *112*, 3499.

(96) Winter, B.; Aziz, E. F.; Ottosson, N.; Faubel, M.; Kosugi, N.; Hertel, I. V. *J. Am. Chem. Soc.* **2008**, *130*, 7130.

(97) Otten, D. E.; Trevitt, A. J.; Nichols, B. D.; Metha, G. F.; Buntine, M. A. *J. Phys. Chem. A* **2003**, *107*, 6130.

(98) Holstein, W. L.; Hayes, L. J.; Robinson, E. M. C.; Laurence, G. S.; Buntine, M. A. *J. Phys. Chem. B* **1999**, *103*, 3035.

(99) Horimoto, N.; Mafune, F.; Kondow, T. *J. Phys. Chem. B* **1999**, *103*, 1900.

(100) Horimoto, N.; Mafune, F.; Kondow, T. *Chem. Lett.* **1997**, 159.

(101) Matsumura, H.; Mafune, F.; Kondow, T. *J. Phys. Chem.* **1995**, *99*, 5861.

(102) Mafune, F.; Kohno, J.; Nagata, T.; Kondow, T. *Chem. Phys. Lett.* **1994**, *218*, 7.

(103) Kohno, J. Y.; Mafune, F.; Kondow, T. *J. Am. Chem. Soc.* **1994**, *116*, 9801.

(104) Nishi, N. *Z Phys D Atom Mol Cl* **1990**, *15*, 239.

(105) Furlani, E. P. *J. Phys. A: Math. Gen.* **2005**, *38*, 263.

(106) Patnaik; Pradyot. *Dean's Analytical Chemistry Handbook*; Mc Graw Hill, 2004.

(107) Hwang, N. H. C.; Houghalten, R. J. *Fundamentals of Hydraulic Engineering Systems*; Prentice Hall, 1996.

(108) Hirschfelder, J. O.; Curtiss, C. F.; Bird, R. B. *Molecular theory of gases and liquids*; John Wiley & Sons, Inc., New York, 1954.

(109) Ashgriz, N.; Mashayek, F. *J Fluid Mech.* **1995**, *291*, 163.

(110) de Groot, J.; Johansson, G. A.; Hertz, H. M. *Rev. Sci. Instrum.* **2003**, *74*, 3881.

(111) Kondow, T.; Mafune, F.; Kohno, J. Y. *Aust. J. Chem.* **2006**, *59*, 79.

Chapter 2

Experimental

2.1 General overview

This chapter guides the reader through the overall experimental setup in detail by starting to discuss the ideas necessary to devise the instrument and by finishing with the optimization of the experiment. First section (2.2) is dedicated to the instrument design by explaining the stepwise process followed to reach the final configuration. Second section (2.3) is concerned with the optimization of the microjet instrument and the characterization of liquid generated (i.e., determination of the liquid microjet). To the best of our knowledge the construction of such an instrument is previously unreported in UK.

2.2 Design history and configuration of the liquid microjet instrument

The construction of the experimental apparatus progressed stepwise by setting up and assembling the five main components (i.e., Vacuum system (1), Liquid microjet assembly (2), Liquid trap (3), Light collection assembly (4) and Data acquisition unit (5) as shown in Figure 2.1. and described in the following subsections. The particular detail, in regard of each component, will be discussed in separate subsections.

The system has been constructed to allow laser pump-probe experiments on a continuously flowing liquid microjet using pulsed lasers. In particular, the pump laser pulse is intended to bring about the ejection of molecules into the gas phase and the probe laser pulse subsequently detects those ejected molecules. The delay between the pump and probe laser pulses provides a means of determining the speed of the ejected molecules; therefore by varying this delay it is possible to elucidate the distribution of speeds. This is achieved using an electronic delay system, as detailed later.

The microjet is directed downwards and is aimed at the inlet of a liquid trap, which will be described later. The liquid microjet can be exposed to laser light, which enters the chamber *via* a window at the far end of the secondary vacuum chamber. Any molecules ejected into the gas phase by this laser, whether by photodissociation or by laser ablation, are then interrogated by a second laser beam using laser-induced fluorescence (LIF) spectroscopy. To determine the kinetic energies of the ejected molecules, it is necessary to define the direction of motion. Consequently, only those molecules passing through an aperture are subjected to LIF probing.
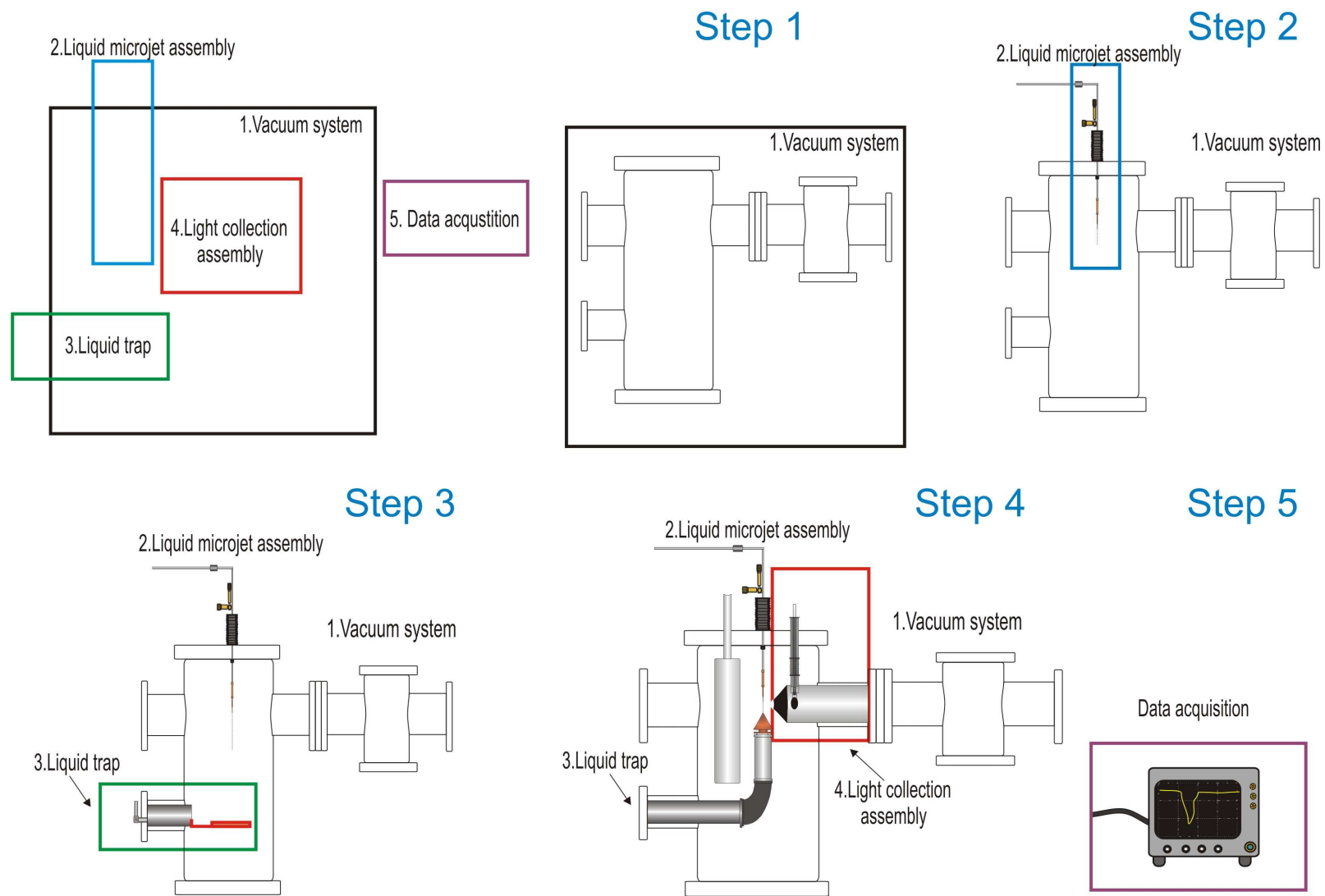
Figure 2.1   Diagram of the history design of the experimental apparatus

2.2.1   Vacuum chambers and pumping

The vacuum system used for the experiment comprises of two vacuum chambers constructed from stainless steel. Both of them have been designed by the author with assistance from Dr. A. M. Ellis and were fabricated in the mechanical workshop of the Department of Chemistry (University of Leicester). Both of them possess multiple access ports (seven in the main chamber, three in the secondary chamber) based on standard ISO flange sizes. Each chamber is also equipped with a Penning gauge for pressure measurement. Figure 2.2 shows a schematic diagram of the vacuum chambers with some specific dimensions that have been originally design for this project. The secondary vacuum chamber was designed to potentially accommodate new elements to the apparatus, e.g., to couple with a mass spectrometer.

Both vacuum chambers are positioned on metal frame that is located next to the optic table. In addition, secondary vacuum chamber was placed on rail support that allows chamber to be mobile and detachable from main chamber (see Figure 2.3). Each chamber is evacuated by a diffusion pump; a Varian VHS-6 (2400 l s^{-1}) for the main chamber and a VHS-4 (1200 l s^{-1}) for the secondary chamber, each backed by a Varian DS 602 rotary pump. The vacuum chambers can be isolated from the diffusion pumps by a pair of gate valves.

With the liquid microjet in operation and originally designed liquid trap, the pumping speed from the diffusion pumps alone was insufficient to cope with the amount of liquid vapour released into the main chamber. Indeed, without additional measures the pressure in the main chamber would have exceeded the maximum operating pressure ($\sim 10^{-3}$ mbar) of the diffusion pump.

Two steps were taken to try and improve the pressure to the desired level of $\sim 10^{-5}$ mbar or better. The first step was to modified liquid trap from original design. The resulting pressure in the main chamber was still higher than desired ($\sim 10^{-4}$ mbar). The second step was to include a liquid nitrogen tank inside the main vacuum chamber in order to condense as much of the liquid vapour as possible. Consequently, further improvement of the vacuum pressure will be discussed in subsection 2.2.2.3.

Side view

Main vacuum chamber

Secondary vacuum chamber

ISO 80K

Viewing port - 50 mm

ISO 200F

ISO 160K

ISO 80K

Baffle window

Overall height 404 mm

Overall height 180 mm

ISO 160K

ISO 80K

ISO 63K

ISO 160F

ID 154 mm

ISO 63K

ID 213 mm

ISO 200F

UV silica window 50mm diameter

Top view

Baffle arm

Flange size	Flange OD in mm
ISO 200	285
ISO 160	180
ISO 80	110
ISO 63	95

Note: K or F denote whether flange uses clamps or bolts for securing

UV silica window
50 mm diameter

UV silica window
50 mm diameter

Baffle arm

Viewing port - 50 mm
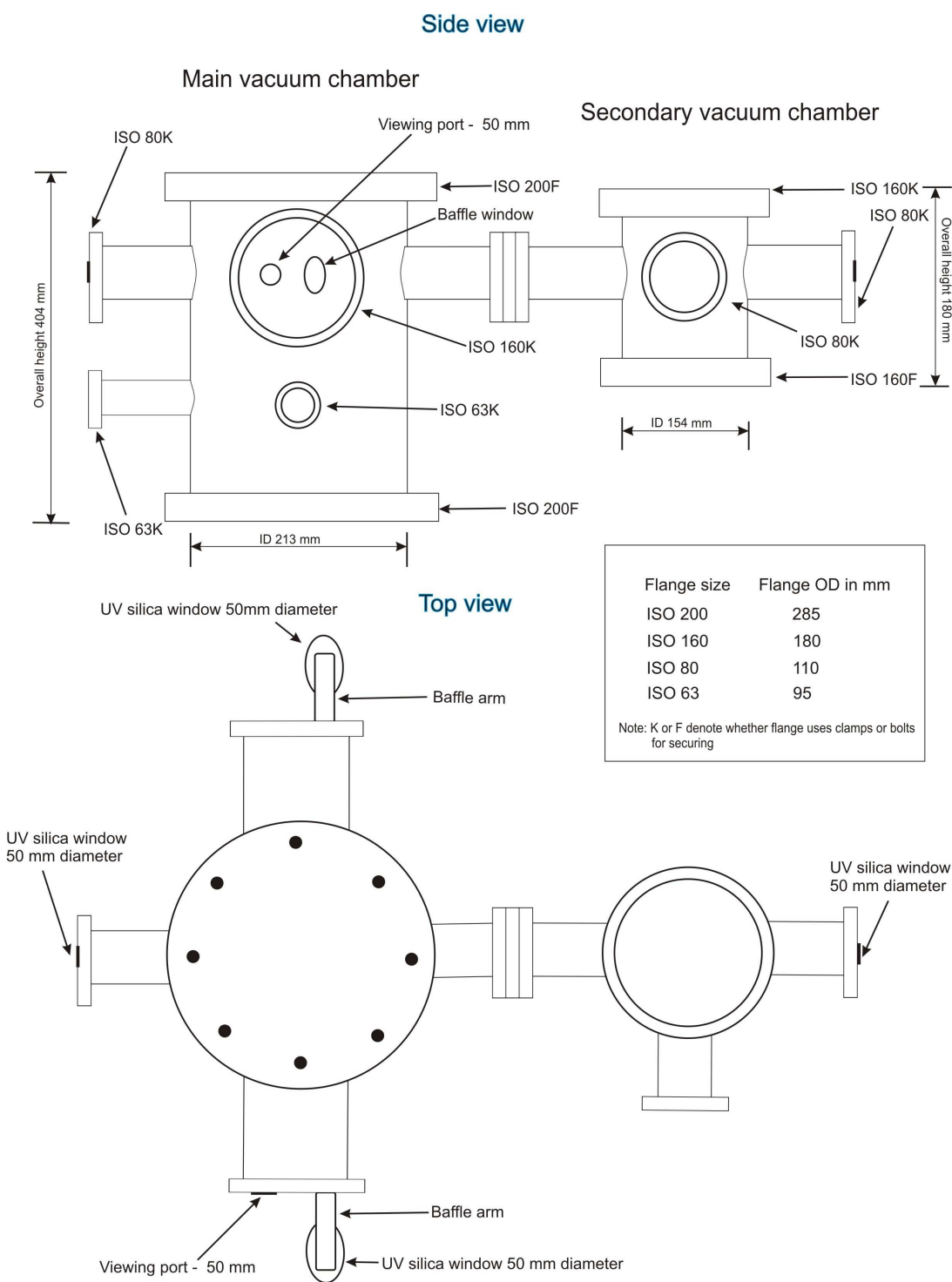
UV silica window 50 mm diameter

Figure 2.2 Schematic drawing of the vacuum chambers showing the various ports and attachments
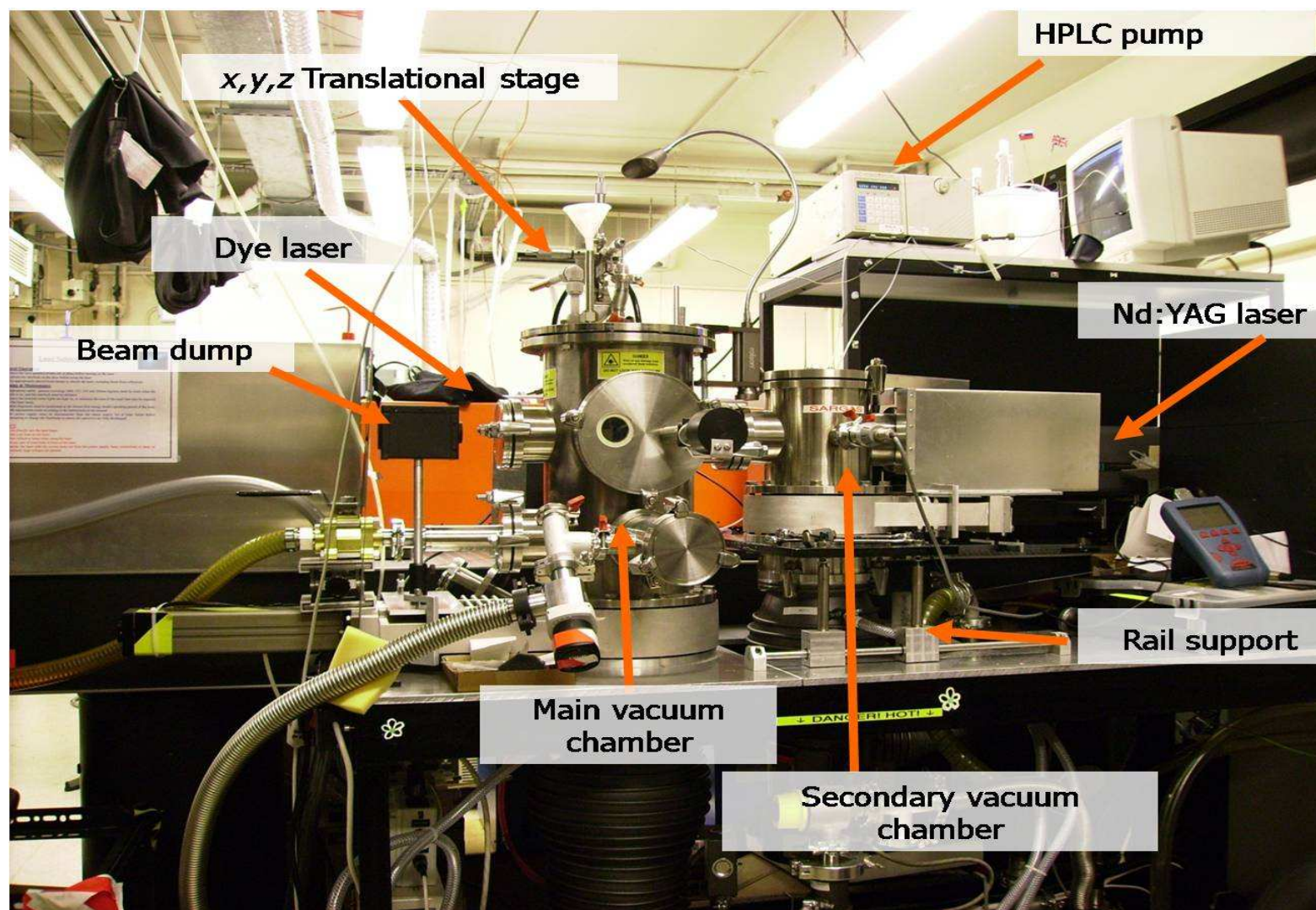
Figure 2.3   Photo of the experimental setup

2.2.2 *Liquid microjet source*

This subsection outlines the components employed to generate and maintain the liquid microjet. The first part is focused on the microjet assembly while the second one explains the details of different designs of the liquid traps and drain system.

2.2.2.1 Microjet assembly

As explained in Chapter 1, generation of a liquid microjet requires a high pressure liquid source coupled with a small pinhole leading through to a vacuum chamber. The source employed in this work is adapted from a design by Holstein *et al*. in which the pinhole is provided by a chromatography tube with a narrow internal diameter.[1] This was chosen in preference to a source based on a micron-sized pinhole in a metal plate (e.g., electron microscope plates) because of the ready availability and the relatively low cost of the desired chromatography tubing. The liquid of choice is forced through this tubing *via* a liquid chromatography pump and eventually exits into the main vacuum chamber.

Figure 2.4 shows the components of the liquid microjet assembly. The liquid is fed into the inlet of the liquid chromatography pump (Shimadzu LC 1000) *via* nylon chromatography tubing from a liquid container. At the output of the pump the pressurized liquid exits *via* 0.0625" of outer diameter stainless steel chromatography tubing, which is labeled as B in Figure 2.4. This tubing, which is approximately 1 m in length, provides the means of directing the liquid into the vacuum chamber. Before entering the vacuum chamber, a 2 μm porous in-line particle filter (A) (purchased from VWR) is inserted within the chromatography tube to prevent clogging of the narrow fused silica capillary by particulates. A vacuum seal to the chromatography tubing is provided by a Swagelok fitting (D). The portion of the tubing inside the vacuum chamber inserts into a polyaryl-ether-ether-ketone (PEEK) microtight adaptor (purchased from Upchurch Scientific). The microtight adaptor (F) includes a female nut (E) and a ferrule (G) and provides a means of joining together the final part of the liquid microjet assembly, a fused silica capillary, to the standard 0.0625" stainless steel tubing. The adaptor, combined with an appropriate size of the microtight sleeve (H), permits connection to the fused silica capillary. The microtight sleeve slides into the ferrule and holds the fused silica capillary in place, as shown in Figure 2.5.

In-line particle filter (A)

Chromatography tubing (B)

x,y,z Translational stage

Air

Vacuum

Flexible bellow (C)

Swagelok screw (D)

Chromatography tubing (B)

Female nut (E)

Microtight adaptor (F)

Ferrule (G)

Nozzle

Microtight sleeve (H)

Fused silica capillary (I)
ID: 0.025mm
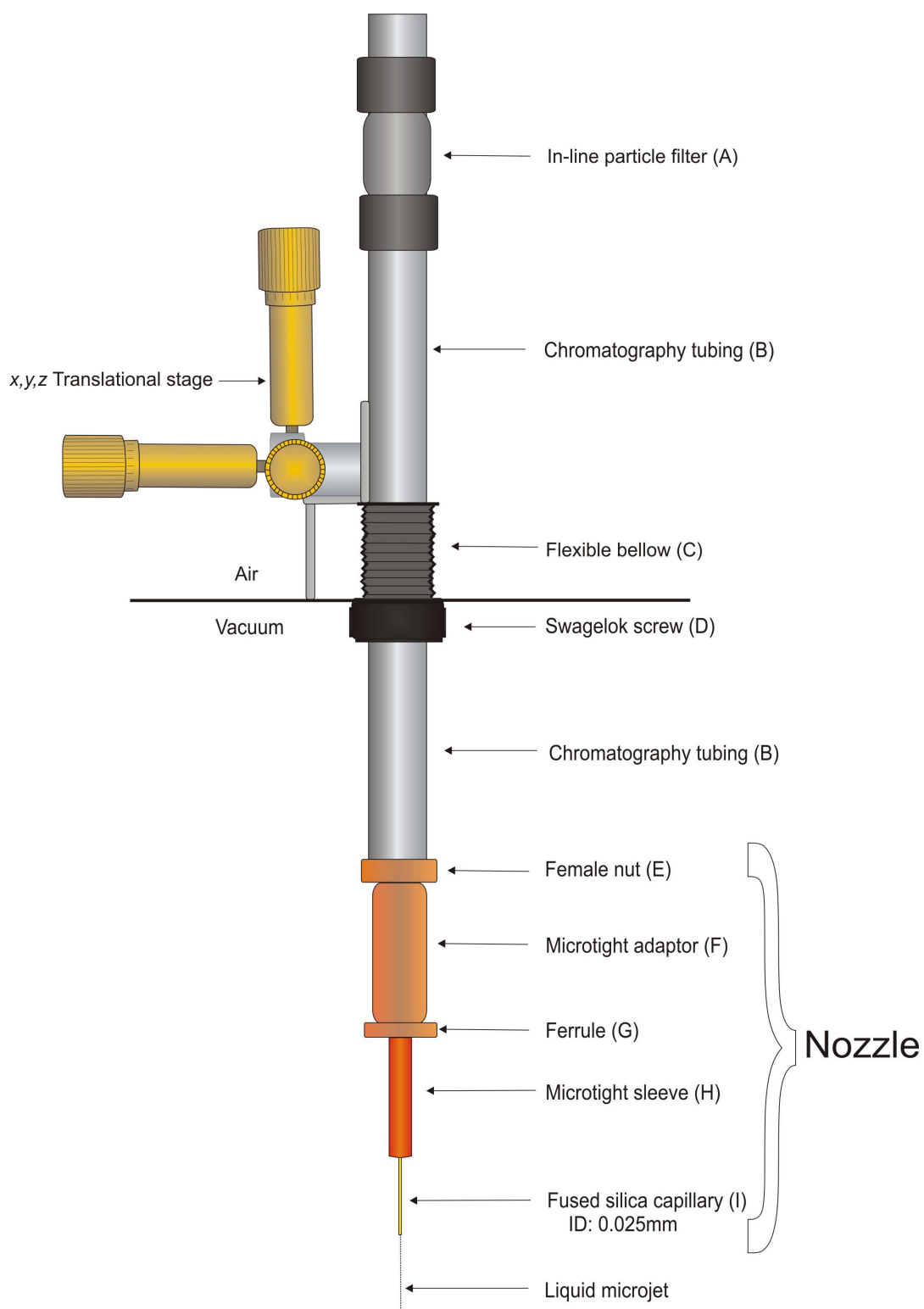
Liquid microjet

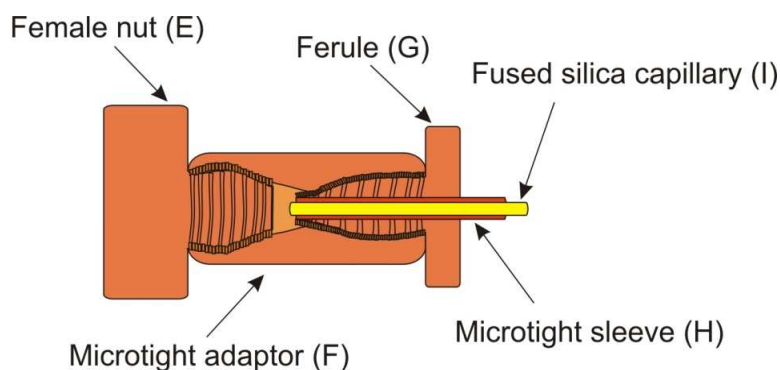**Figure 2.4**   Liquid microjet assembly

Figure 2.5   Cross-sectional view of the microtight adaptor

The fused silica capillary (I) (purchased from SGE analytical science) has internal and external diameters of 0.025 mm and 0.285 mm, respectively. An approximately 2.5 cm length of capillary was cut using a ceramic capillary cutter and used as the liquid microjet 'nozzle'. The cut piece is then placed into the microtight sleeve (H) and positioned in the ferule (G). All parts are then screwed into the microtight adaptor. Before installing the cut piece of the capillary into a microjet sleeve, both ends must be cut as square as possible to ensure good quality and stability of the liquid microjet. If the cut is not square the performance of the experiment can be affected and can result in possible deviation in the direction and the stability of the microjet.

The fused silica capillary was frequently damaged during the experiment and needed to be replaced after each experiment. Several processes are believed to cause this damage, with laser burns from misdirected laser beams and ice deposits from supercooled liquids being the two likely causes.

The flow of the liquid phase is controlled by the HPLC pump. The pump can operate in two modes: constant flow (ml / min) or constant pressure (kgf / cm^2) mode. In our experiment the pump is operated in the constant flow mode, typically at 0.25 ml/min. The flow rate of the liquid phase has been optimized to obtain a laminar regime of the liquid microjet (see Chapter two). In addition, it has been experimentally found that a higher flow rate caused the displacement of the fused silica tubing from the microtight adaptor.

The *x,y,z* translation stage, mounted on the top of the main vacuum chamber, was designed and fabricated in the Department of Chemistry. The translation stage allows micrometric alignment of the liquid microjet relative to the liquid trap entrance aperture (see later). The

ability to move the microjet assembly is allowed by the bellows connection (C) on the top flange of the main vacuum chamber (see Figure 2.4). After each venting and evacuation cycle of the vacuum chambers, the alignment and the distance of the microjet with respect to the liquid trap needed to be adjusted both before and, if necessary, during the course of the experiment.

2.2.2.2 Original design of the liquid microjet trap

In order to trap the liquid injected into the main vacuum chamber, a copper plate was originally attached to the liquid nitrogen tank (see Figure 2.6). The whole assembly slides in through the lower side port of the main vacuum chamber. The liquid nitrogen tank was continuously refilled to cool the cooper plate at the lowest temperature. As the microjet travels downward and reaches the surface of the copper plate an ice deposit formed. The ice deposit grew rapidly towards the liquid microjet source and eventually blocked the nozzle. Unfortunately, the combination of a diffusion pump with a liquid nitrogen cooled trap proved to be insufficient to achieve the intended vacuum of $\sim 10^{-5}$ mbar when operating the liquid microjet.
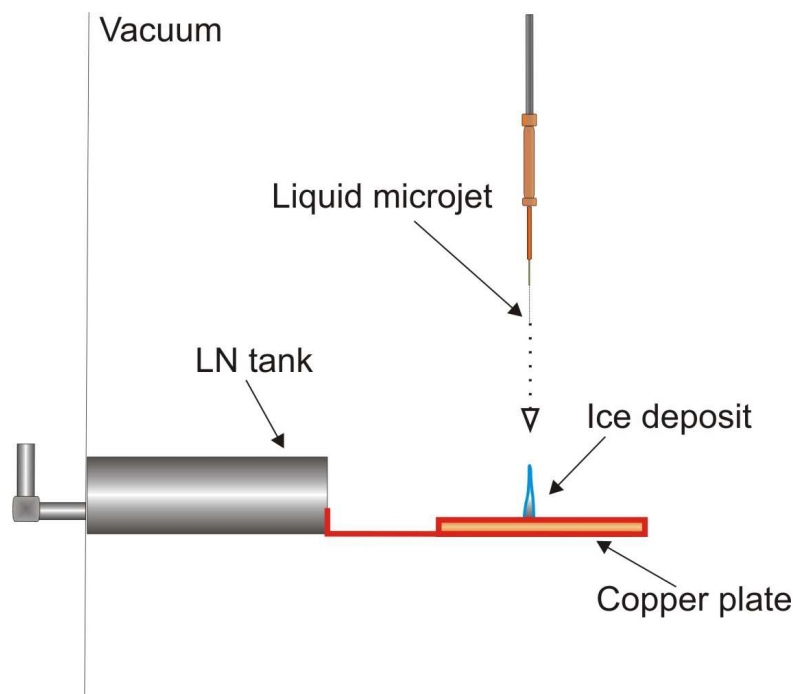

Figure 2.6   Copper plate trap

2.2.2.3 Final design of the liquid microjet trap

Consequently an additional specially designed trap was developed to try and lower the chamber pressure to an acceptable level and the prevent the formation of an ice column. The process involved a considerable amount of trial and error in the design and the operational procedure and the final version is detailed below.

The design of this trap is a modification of the trap recently described by Charvat *et al*.[2] Their idea is that, with properly chosen dimensions, the vapour stream out of the microjet trap can be minimized, and a stable liquid jet can be operated without applying a second vacuum system or any cooling to the beam trap. The trap operation depends crucially on the hydrodynamic interaction between the incoming jet and the outward streaming vapour in the entrance channel of the liquid trap. Charvat *et al*. calculated the ideal diameter (d) and length (l) of the entrance channel for generation of a stable liquid microjet for maintaining a good vacuum.

The results of these calculations are strongly affected by the diameter of the liquid microjet. For example, with a microjet of 10 μm diameter, the parameters of the entrance orifice of the trap should be in the range of $0.1 < l < 0.5$ mm and $0.05 < d < 0.1$ mm. Their model of the trap consists of two parts: a cone attached to stainless steel tubing, which is then connected to a glass reservoir equipped with a standard vacuum flange and placed outside the vacuum system.

In our experiment, a similar trap to that reported by Charvat *et al*. was constructed. The smallest diameter of the aperture of the copper cone achieved was 0.2 mm. This diameter of the entrance channel did not minimize backstream gas flow in main vacuum chamber. In addition, small the diameter of the aperture causes problems with alignment of the liquid microjet into the cone. To facilitate the alignment process, the diameter of the entrance orifice was enlarged from the original 0.2 mm to 0.5 mm. Unfortunately, once this change was made backstreaming of vapour proved to be a serious problem (see Figure 2.7). In order to resolve this dilemma with the flow, the drain assembly was required (discussed later in subsection 2.2.2.4).
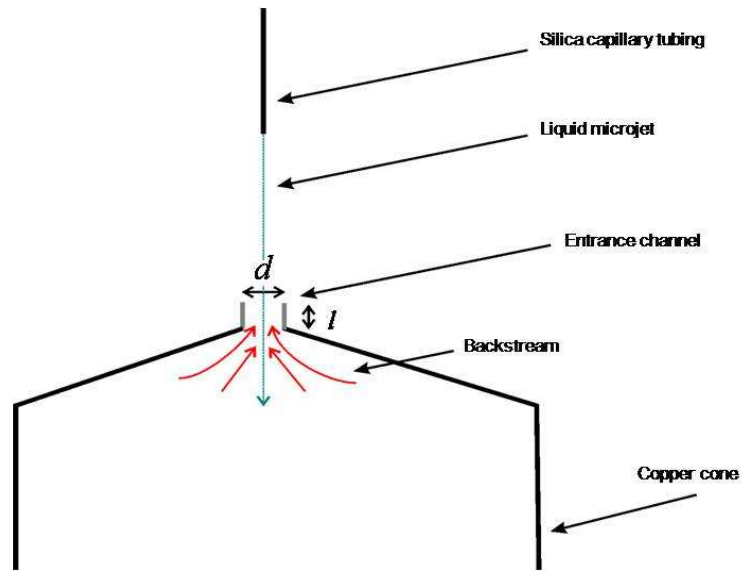
Figure 2.7   Cross-section of the copper cone

The final model of the liquid microjet trap employed consists of a copper cone and a series of tubes to collect and remove as much liquid as possible from the chamber (see Figure 2.10).
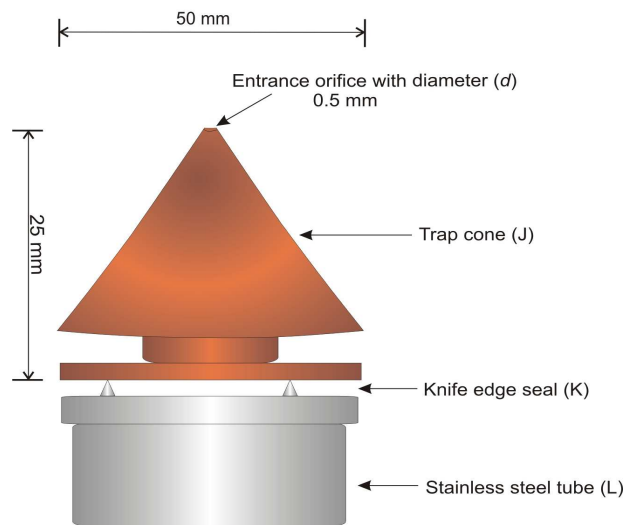
Figure 2.8   Expanded view of the copper cone

The trap cone (J) is made of copper and is positioned in the main vacuum chamber directly under the microjet assembly. It has a height of 25 mm, a base diameter of 50 mm, a conical profile with an angle of vertex of 90° and an entrance orifice with a diameter (d) of 0.5 mm (see Figure 2.8). Such a profile helps to prevent the formation of icicles when the supercooled

liquid microjet in vacuum touches the trap cone surface during initial adjustments. The cone can potentially be equipped with a heating element; thick walls of the upper part provide a good heat transfer to the tip of the cone. Initially, a heating element was employed but, after a modification of the microjet trap assembly, it was found to be unnecessary to use the heating element for the experiments. The trap cone (J) is connected to the stainless steel tube (L). Both parts are screwed together and a vacuum seal is provided by a knife edge surface (K). The liquid can flow from L through an elbow (M), a horizontal stainless steel tube (N) and a vacuum flange that connects to the drain assembly (see 2.2.2.4).

The stainless steel tube (N) is welded to a vacuum flange on the side of the main vacuum chamber. The flange seals the vacuum chamber thought an O-ring and holds the whole microjet trap in position.

All parts of the microjet trap were made in the workshop in the Department of Chemistry (University of Leicester) and were designed by the author.
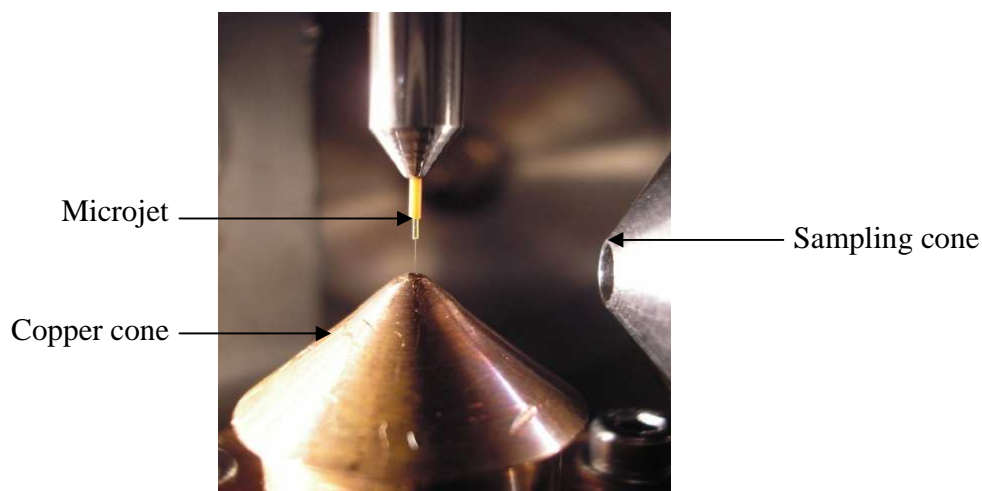
Figure 2.9   Detail of the liquid microjet in operation. The liquid passes through a hole in the copper cone, which acts as an entrance to the liquid trap

Figure 2.9 shows a photograph of the actual liquid microjet emanating from the fused silica capillary. This microjet flows downwards and is directed through an aperture in a copper cone, which is the entrance point to the liquid trap and drain assembly. The purpose and components of the liquid microjet trap and drain are described in some detail in the next subsection.
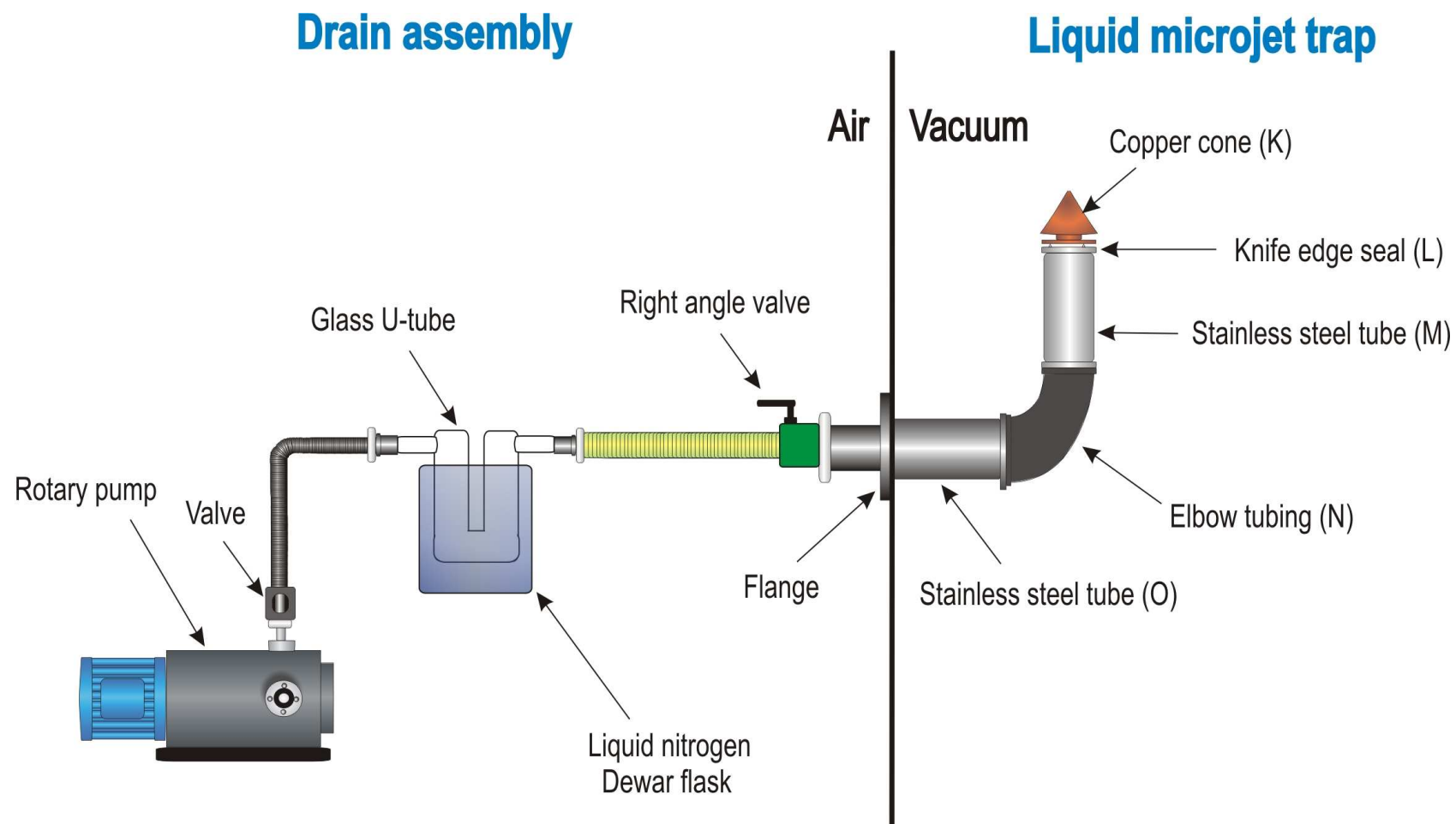
Figure 2.10   Schematic of the liquid trap and drain assembly

2.2.2.4 Drain assembly

   The second part of the evacuation system is the drain assembly, whose purpose is to put any collected liquid beyond the reach of the main vacuum chamber. The assembly is made of several parts (see Figure 2.10) including a glass U-tube placed in a liquid nitrogen cooled Dewar and a rotary pump (Edwards 5). The rotary pump is intended to remove any traces of liquid that enters the drain assembly. However, there are two problems with using a rotary pump alone for this task. First, the quantity of liquid to remove is large while the pump is not designed to handle such volumes of condensable vapours and damage is expected if operated under such extreme conditions. Secondly, the pump proved ineffective at lowering the pressure in the main vacuum chamber. Consequently, a wide-bore U-tube cooled by liquid nitrogen was placed upstream of the rotary pump to act as the primary liquid remover. This U-tube/rotary pump combination increased the performance of the system significantly making it possible to maintain a sufficiently low pressure in the main chamber. In particular, any gas not fully condensing within the U-tube is pumped away by the rotary pump, thus minimizing backstreaming to the main chamber.

   To facilitate the cleaning of the assembly, several valves with appropriate lengths of tubing joined the different parts of draining system, thus allowing the isolation of selected portions when needed. A high throughput in-line isolation valve is placed upstream of the Dewar between the vacuum chambers to allow the separation of the trap from the evacuation system.

   The liquid removed from the instrument is trapped in a glass U-tube (40 mm external diameter) maintained at -196 ^{o}C by liquid nitrogen in a Dewar flask of internal diameter 135 mm and internal depth of 220 mm. The Dewar is placed on a trolley next to the vacuum system. The glass U-tube was made in the glassblowing workshop in the Department of the Chemistry (University of Leicester) so as to maximize its volume while fitting the dimensions of the Dewar. Figure 2.11 shows photo of the drain system.

   The main limitation of the drain system is the quantity of liquid the glass U-tube can potentially trap without losing its efficiency. It has been found that experiments lasting over five hours result in the glass tube being obstructed by frozen liquid and the pressure rise in the main chamber then becomes severe. At this point the experiment has to be stopped. Once the liquid nitrogen is evaporated from the Dewar the U-tube has to be removed and cleaned before re-use.

The liquid trap/drain system employed here made it possible to achieve a main chamber pressure of ~10^{-5} mbar when the liquid microjet was in operation.
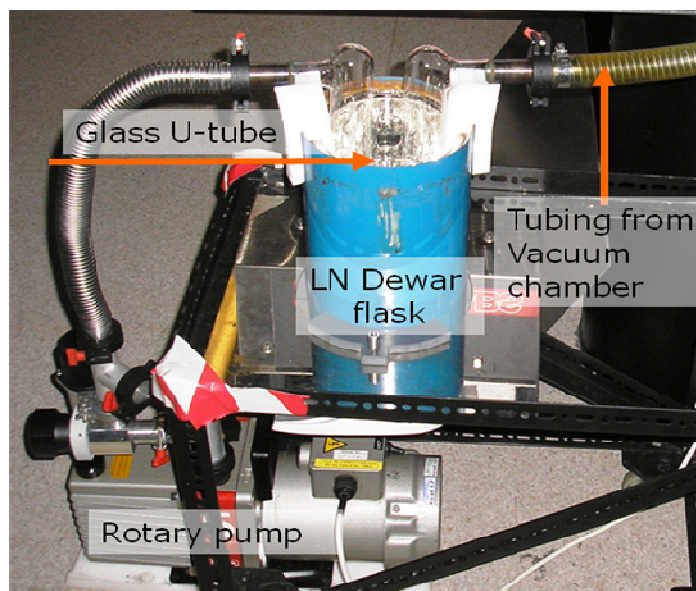
Figure 2.11   Photo of the drain system

2.2.3 *Laser systems and optical arrangement*

For the laser pump-probe experiments, two different lasers were required. One laser a (Nd:YAG laser) was employed to initiate a photoejection or photoablation process on the molecules at or near surface of the liquid beam. The function of the other laser system (a dye laser pumped by a Nd:YAG laser) was to provide a means of detecting the release of specific molecules from the liquid. Both lasers are pulsed and were operated at a 10 Hz repetition rate. Figure 2.15 illustrates the optical arrangement of the lasers relative to the vacuum chamber.

2.2.3.1 Photoejection laser

Photoejection was achieved using a Continuum Surelite II-10 Nd:YAG laser. The fundamental output wavelength is 1064 nm, which is too long for electronic exitation (and thus photodissociation). However with harmonic generation this laser can produce intense radiation at the second (532 nm), third (355 nm) and fourth (266 nm) harmonics. In our experiment, the Nd:YAG laser was operated mainly at the fourth harmonic output wavelength (266 nm).

The Nd:YAG laser beam was aligned into the vacuum system using two dichroic mirrors, coated for optimum performance at 266 nm. The laser beam enters the vacuum system *via* a UV silica window on the exposed end of the secondary chamber. It passes through the sampling cone and intersects with the liquid microjet. A residual beam exits from the vacuum system *via* another window and it is stopped in a beam dump.

2.2.3.2 Probe laser

A dye laser pumped by a Nd:YAG laser provides a tunable excitation source for the LIF detection of photo-ejected molecules. Principles of LIF detection is briefly described in following subsection. The laser system used in this case consists of a combination of a Continuum Surelite I-10 Nd:YAG pump laser and a Lambda Physik Scanmate dye laser. The Scanmate is equipped with a frequency conversion unit (FCU), which allows access to the near UV (~220-440 nm) by frequency doubling of visible or near IR radiation from the dye laser. The dye laser wavelength scanning is controlled by a specially written computer program, as detailed later.

The dye laser beam is aligned into the vacuum system using three prisms mounted on adjustable stages. The beam enters *via* a UV silica window on the end of a baffle arm on the side of the main vacuum chamber. It passes through a hole in the side of the sampling cone to reach the desired set of molecules and exits the vacuum system into a beam dump on the far side of the main chamber.

2.2.3.3 Laser induced fluorescence (LIF)

LIF spectroscopy was the technique used in the current work to detect molecules ejected into the gas phase. LIF is one of the most suitable techniques for studying electronic transitions of both neutral molecules and molecular ions due to its high sensitivity and potentially good resolution. In LIF spectroscopy, an electronic transition of the molecule is excited, typically using a tunable laser, and any fluorescence generated is monitored.[3] As presented in Figure 2.12, following the initial absorption, fluorescence can be observed *via* the emission of a photon with a less energetic wavelength. The energy difference between the absorbed and emitted photon ends up as internal energy of the molecule (rotation and/or vibration). For many decades LIF has been one of the dominant laser spectroscopic techniques due to its extreme sensitivity for probing chemical reactions. Fluorescence signals can be detected in all directions and have very low background signal.[4]
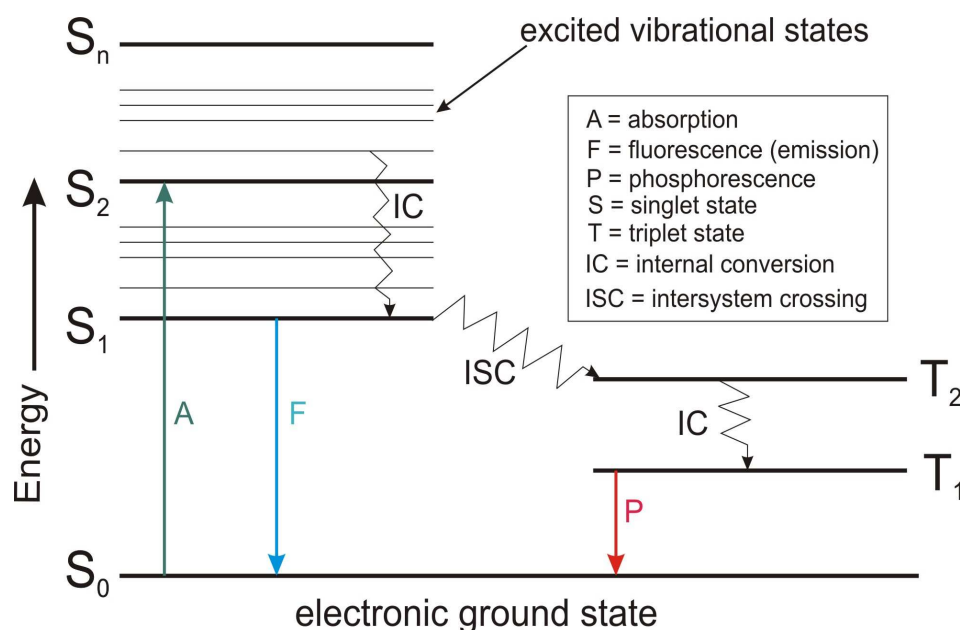
Figure 2.12   Energy level diagram and summary of photochemical processes

2.2.4   Light collection assembly

Since ejected molecules are detected *via* laser induced fluorescence (LIF), some means of light collection and detection was required. A specific light assembly was therefore designed for this purpose. In the light collection assembly, a sampling cone separates the two vacuum chambers (see Figure 2.18). The sampling cone has an aperture with a diameter of 4 mm. The distance between the aperture of the cone and the liquid microjet is 15 mm. The cone serves two purposes: its main purpose is to ensure that only a small subset of the molecules ejected from the liquid microjet can actually be probed by the probe laser. This is necessary for measuring the translation energy distribution, since we have to define a sub-set of the molecules travelling roughly in the same direction.

An additional purpose of the cone is to ensure that the two laser beams (i.e., pump and probe) are correctly aligned into the vacuum system. The laser beam from the pump laser is focused by a fused silica lens (50 cm focal length) and enters the vacuum system through a UV silica window in the end port of the secondary chamber (see Figure 2.15). It passes through the stainless steel cone aperture and ideally will intersect with the liquid microjet in the main chamber. One of the challenges in the experiment is to make sure that the liquid

microjet and the focused pump laser beam do actually intersect. Fortunately, it was found that, when correct alignment was achieved, a clear diffraction pattern could be observed on a card outside of the vacuum system (see chapter 4 for further details). The initial alignment of the laser beam into the vacuum system is always performed at low power for safety purposes.

The probe beam enters the vacuum system through a fused silica window. The window is on the end of baffle arm and is orientated at Brewster's angle. The baffle consists of two metal disks with holes in the centres, which are placed inside the baffle arm. The purpose of the baffle is to minimize the amount of scattered light reaching the light detector, i.e., any stray laser light should bounce around in the baffle arms and dissipate. After travelling through the main vacuum chamber, the laser beam enters the sampling cone *via* a hole on the side and exits from a similar hole on the other side. The holes, of 4 mm diameter, for entrance and exit of the probe laser beam were drilled on both sides directly into the cone and are not covered by windows (see Figure 2.13). The probe beam intersects with photo-ejected molecules inside the cone region and the distance between the liquid microjet and probe laser beam as it crosses the cone is 25 mm.
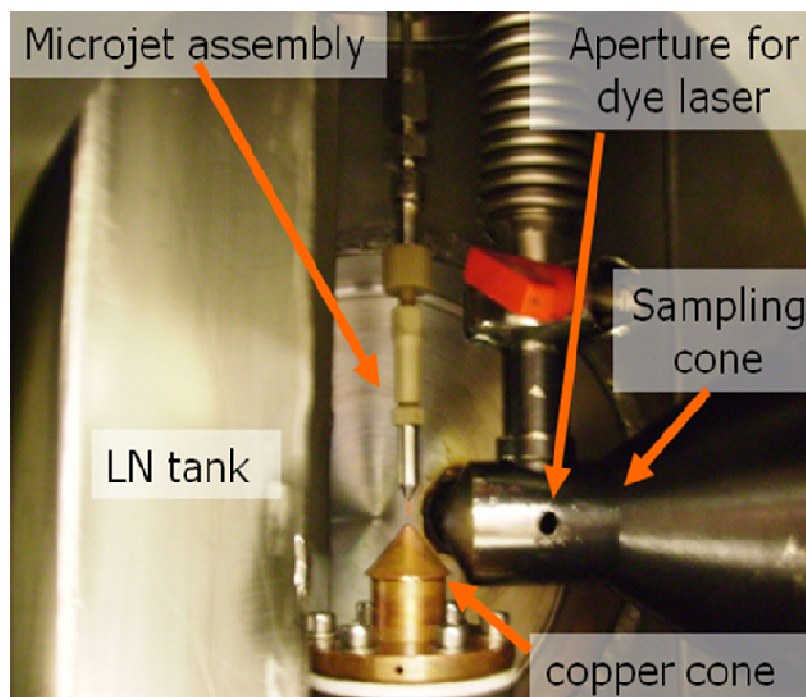
Figure 2.13   Photograph of the main vacuum chamber interior

Figure 2.14 shows the fluorescence collection part of the apparatus in more detail. Any fluorescence produced is collected by a liquid light guide attached to the cone. This assembly consists of a flexible tube, one end of the tube being connected to the top of the chamber through a KF port and the other end is attached to the sampling cone. The vacuum seal between the flexible tube and the cone is provided by a lens coupled with an o-ring and a compressions fitting. The lens has a focal length of 10 mm and a diameter of 10 mm and it is positioned ~ 10 mm of the dye laser beam. LIF is collected and collimated by lens and passes into a liquid light guide (Lumatec). The liquid light guide slides into the tube from top of the vacuum chamber. The overall length of the liquid light guide is 1 m with a core diameter of 8 mm. The recommended transmission range of the light guide is 300 to 650 nm. The far end of the guide is attached to a photomultiplier (Hammamatsu R928) located on the optical bench next to the vacuum system. A cut-off filter can be placed between the PMT and liquid light guide to remove unwanted wavelengths, e.g., scattered laser light.

Figure 2.14   Light collection assembly

Figure 2.15   Optical arrangement

2.2.5   Data acquisition and processing

This subsection describes the electronic equipment and the software involved in the acquisition and the processing of data.
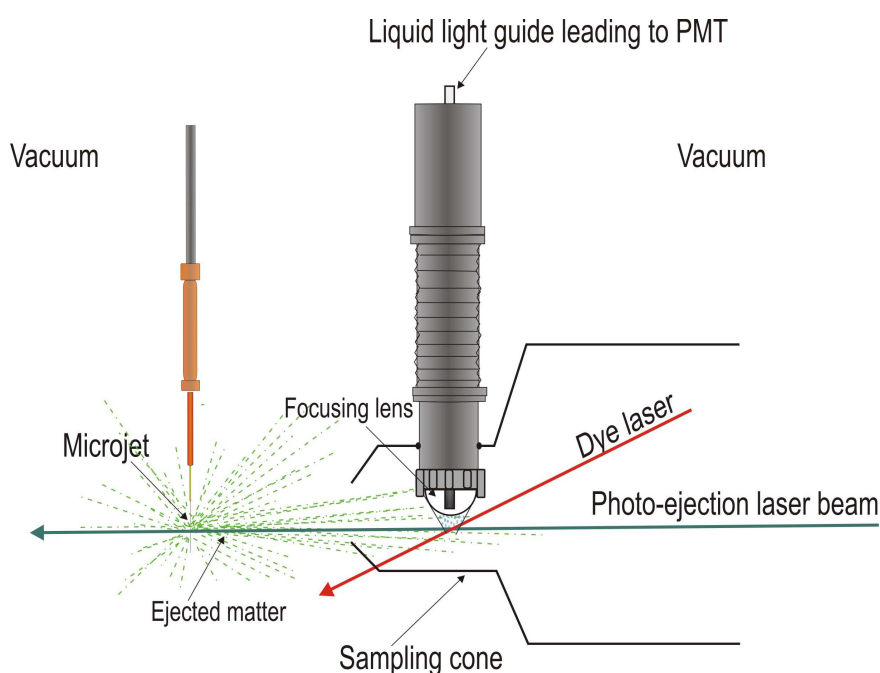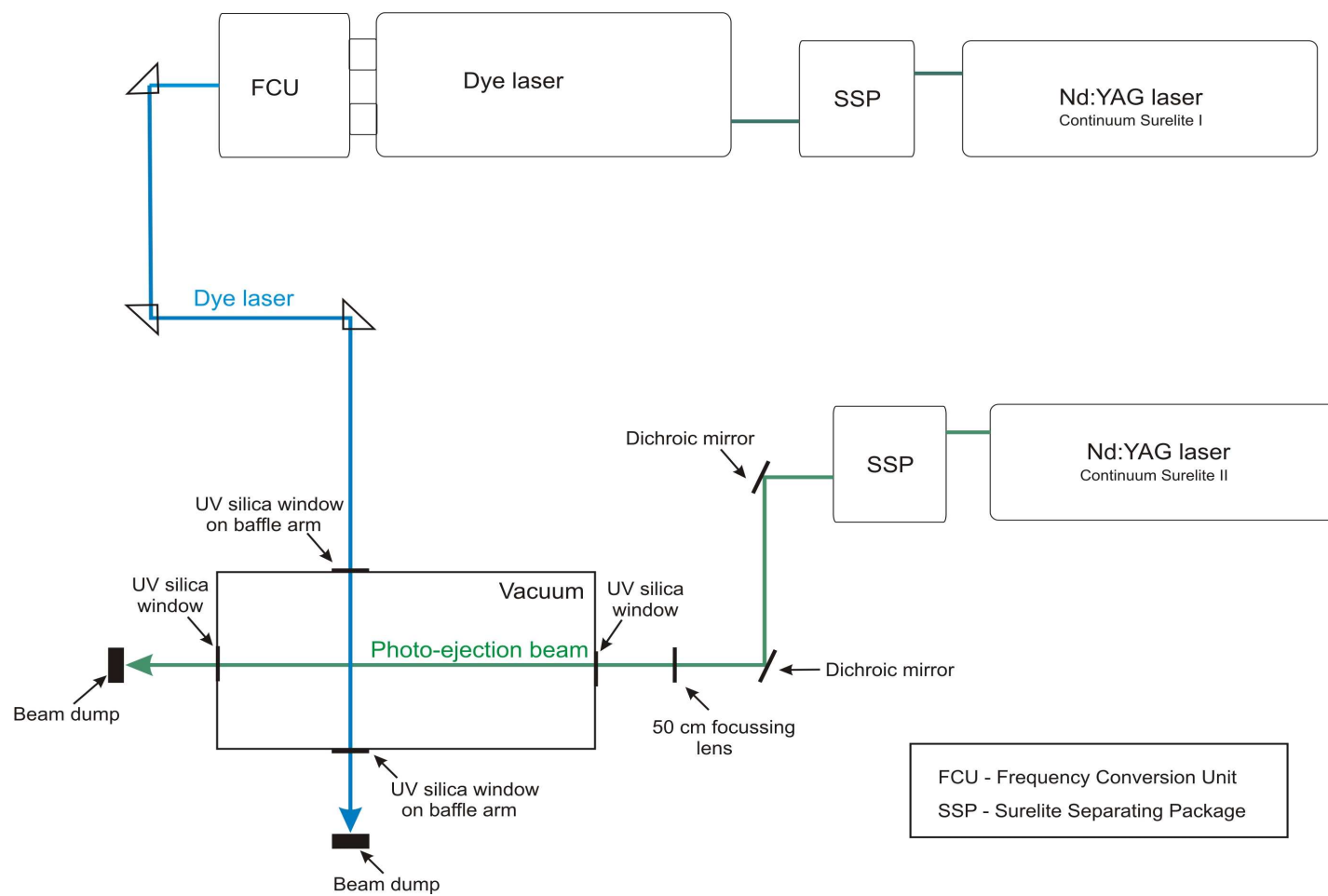
2.2.5.1 Timing of triggering events

Due to the pulsed nature of the experiment, a delay generator (Berkeley Nucleonics Corporation model 555) is employed for synchronization of the lasers. The delay generator allows the triggering of the flashlamps of both Nd:YAG lasers and their respective Q-switches and also correlate the laser jitter. For each cycle, the Nd:YAG laser used for photo-ejection is triggered first, followed by triggering of the Nd:YAG laser that pumps the dye laser. The delay generator allows the delay between the two laser lasers to be varied, to a precision of approximately 1 ns, thus allowing construction of the speed distribution of photo-ejected molecules. As the liquid microjet runs continuously, it does not need to be included in the synchronization process.

2.2.5.2 Data Processing

Figure 2.17 depicts the arrangement of the data acquisition. Signals received by the PMT are first passed to the oscilloscope (Tektronix TDS 5032B). The oscilloscope records, digitises and averages the raw data and then passes it to a built-in computer for processing. The data collection process is controlled by a Labview programme, written mainly by Dr Tom Salter and Dr Adrian Salarou, with contributions from the author. The program controls the wavelength of the dye laser through external control of the proprietary Scanmate software. Specifically, it scans the wavelength of the dye laser by stepping (through software-requested TTL pulses) the grating. Once the signal is captured, a selected part of the signal is defined by a specified "gate". Integration is then performed by the program and the position of the gate can be specified. The final part of the program plots the integrated LIF signal against the dye laser wavelength.

Figure 2.16 shows a flow chart illustrating the main steps in the program. All commands for data collection are specific to each experiment. Before beginning the acquisition of a scan, Labview has to be initialised and several parameters, including wavelength, scan range, wavelength step size and number of shots to be averaged have to be specified. The main program includes a sub-VI (virtual instrument) that can be employed for communication

between the oscilloscope and the built-in computer. The commands for controlling the oscilloscope (i.e., gating for the signal acquisition and averaging) are specified in the sub-VI program.
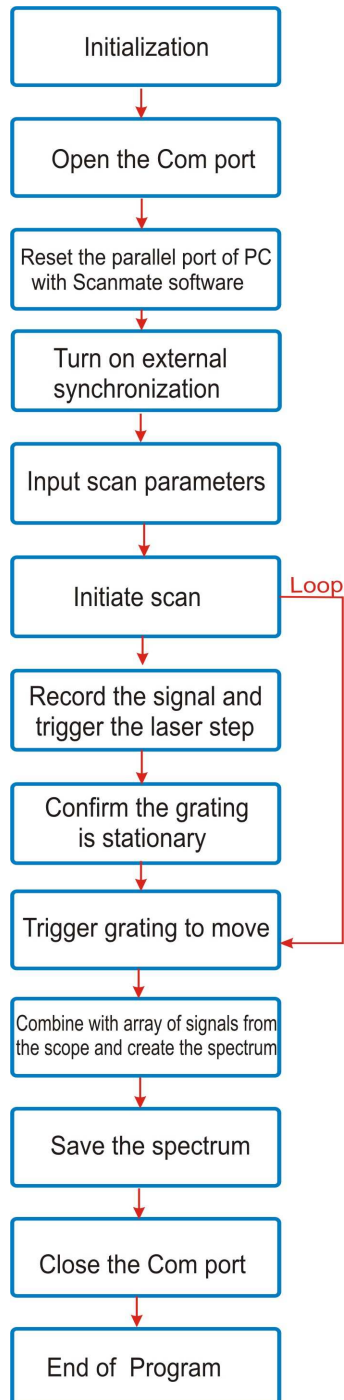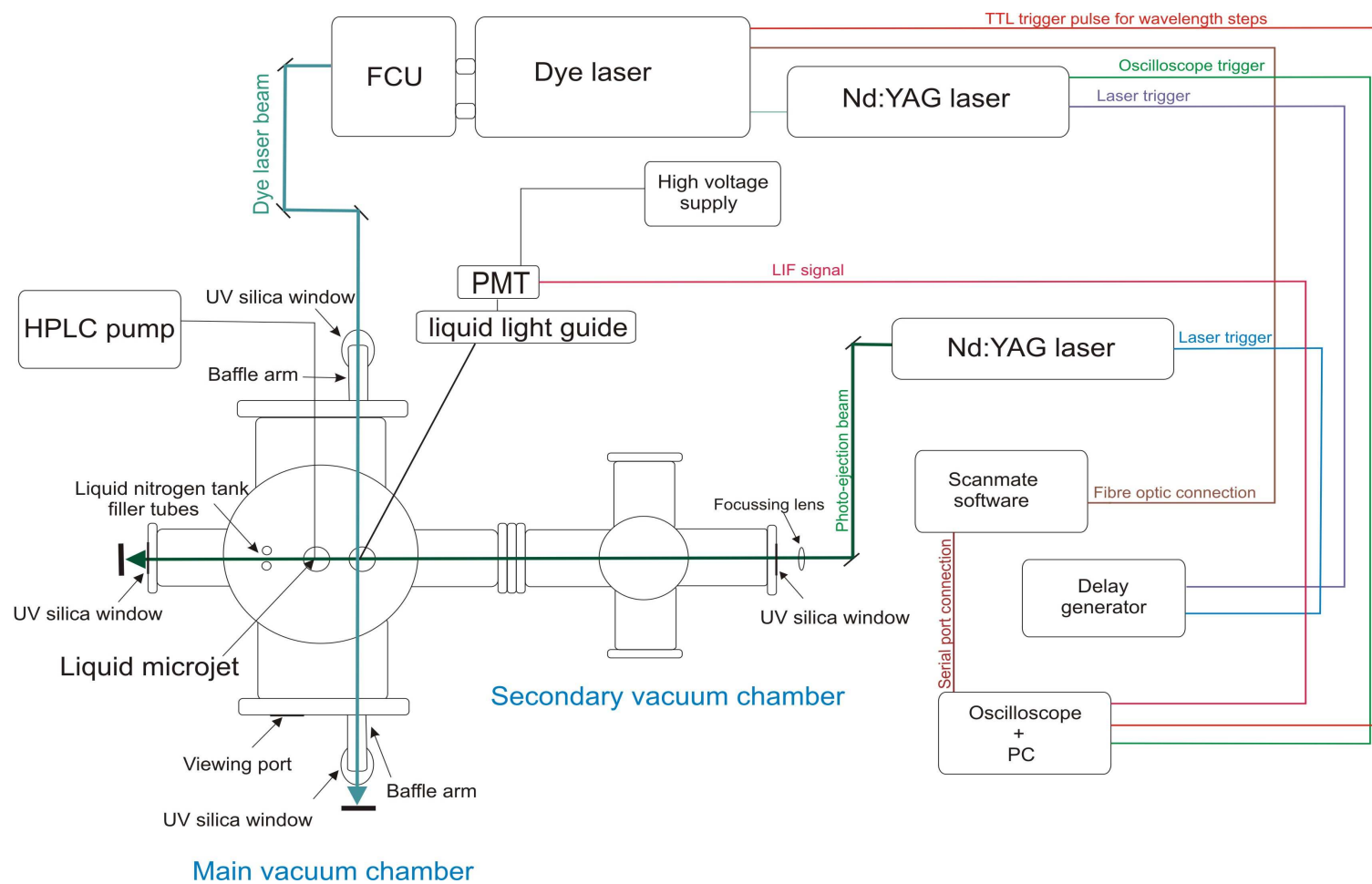

Figure 2.16   Labview data processing chart

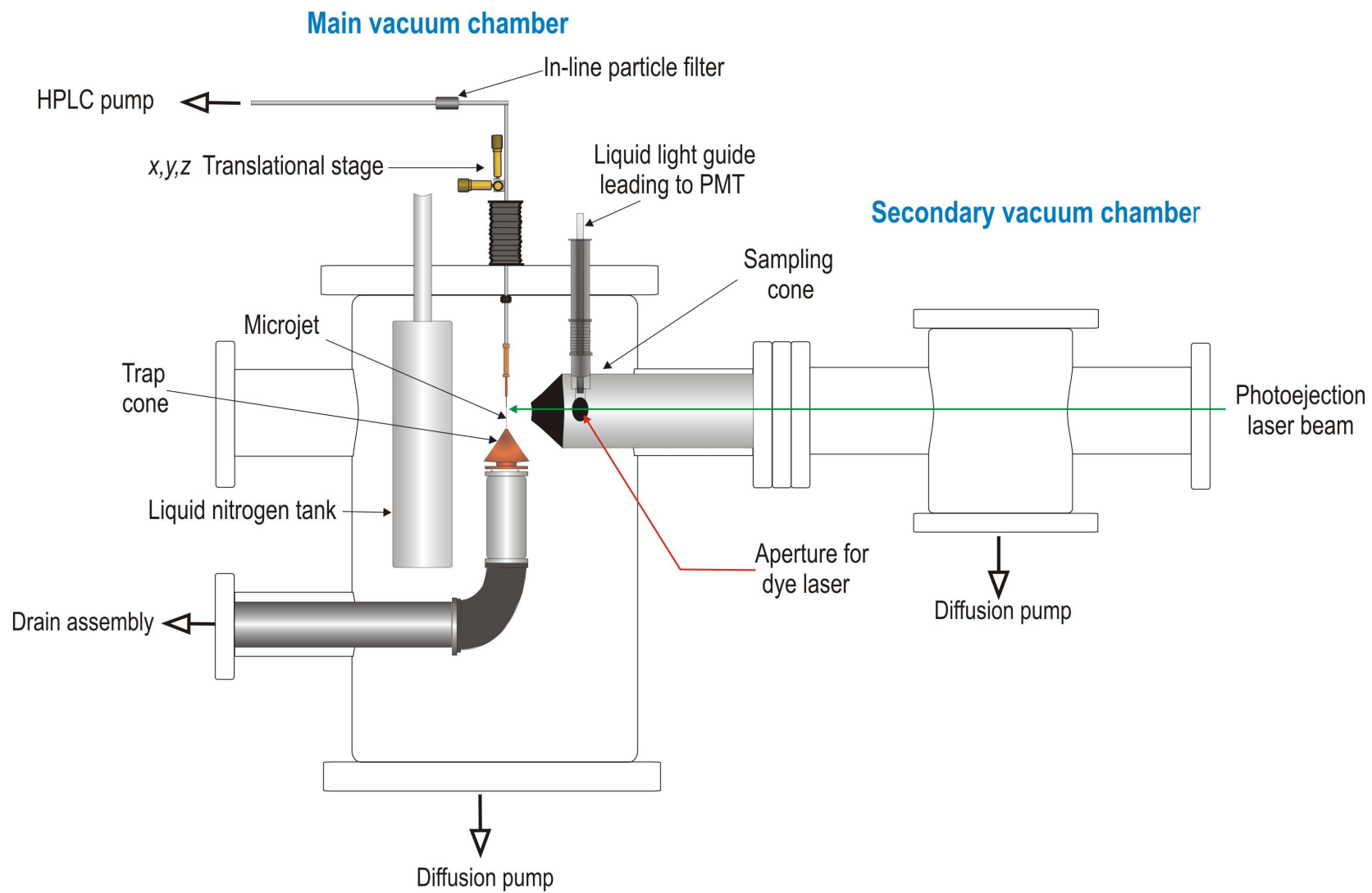**Figure 2.17**   Overall experimental setup including data acquisition component

Figure 2.18   Diagram of the final design of the experimental apparatus

2.2.6 Conclusion

Figure 2.18 shows the final design of the liquid microjet system. This consists of the main vacuum chamber and contains the major components of the experiment: the liquid microjet source, a liquid trap, a light collection assembly and a liquid nitrogen tank.

2.3   Optimization and characterization of the liquid microjet

This section focuses on the experimental determination of the parameters (i.e., stability, diameter of the liquid microjet) relevant to the liquid phase. Firstly, various solvents employed as the liquid phase (subsection 2.3.1) were screened with regard to their stability under vacuum conditions. Secondly, the diameter of the liquid microjet was determined (subsection 2.3.2) to ensure that the microjet is operating in the expected manner.

2.3.1 Stability of the liquid microjet under vacuum

Selected liquids have been screened to determine the most suitable candidate for the microjet. A laminar flow of liquid is a prerequisite to conduct successful microjet experiments and is therefore largely dependent on the selection of the liquid employed (see chapter 1).

Water was initially assessed, not only because of its importance as a liquid phase but also because of its use in several previous liquid microjet studies.[5-8] However, liquid microjets of pure water tested in our instrument have not been proved to be suitable. In particular freezing of the liquid microjet was consistently observed. Due to evaporative cooling the water liquid microjet had a tendency to freeze when reaching the liquid trap (the nozzle-trap distance is ~ 4 mm). Ices rapidly grew from the trap surface and quickly lead to the obstruction of the microjet nozzle. Depending on the liquid mixture, the freezing occur progressively (taking between several minutes and up to an half an hour). As well as ice forming at the surface of the trap, freezing was observed around the edges of the silica capillary, leading to increased blockage of the nozzle aperture (taking a few minutes and up to an hour). Consequently, a liquid water microjet could not be maintained for more than a few minutes, making it unsuitable for our experiment.

It is important to note that some efforts were made to try and solve these problems. One change made was to install a heating element around the liquid trap. However, this solution was found to be inadequate. The heating actually caused an increase of the vapour pressure (from 10^{-5} to 10^{-3} mbar) in the chamber due to the added evaporation of the depositing water.

66

Consequently, with the heated trap alone very poor vacuum conditions were found for the experiment. An alternative solution to avoid freezing was to install a chopper inside the vacuum chamber just above the trap surface to avoid the ice formation by chopping the liquid beam. This method was reported by Kondow *et al.*[9] In our system we could not install a chopper due to the lack of space in our vacuum system.

Another choice for the liquid phase was ethanol. Several groups[9,10] have shown that ethanol is a good liquid phase to use in microjets. This is mainly due to physical properties of ethanol (e.g., viscosity, surface tensions and freezing point) discussed in chapter 1. Therefore, pure ethanol was tested and demonstrated the abilities in term of stability (laminar flow) compare to water and was selected as a medium to form the first stable liquid beam in our experiment. Several ratios (from 5 to 95 % ethanol in water) have been tried to form a microjet. However, ethanol–water mixtures exhibited a non-stable behaviour (such as disintegration followed by freezing of the microjet) and could not be used for the experiment.

Table 2.1 includes list of the several liquids and possible analytes tested during different experiments and where appropriate will be discussed in more detail in following chapter 3.

Table 2.1 The behavior of some liquids in the microjet system

Liquid	Pure (%)	Mixture of analyte/ethanol (v/v)	Stability under vacuum
Water	100	-	Freezing
Ethanol	100	-	Laminar flow
Toluene	-	10:90	Laminar flow
Acetyl acetone	-	15:85	Laminar flow
Benzene	-	10:90	Laminar flow
Aniline	-	10:90	Laminar flow
Benzoic acid	-	10:90	Re-crystallization

2.3.2 Diameter of the liquid microjet

The diameter of the liquid microjet was determined using a diffraction procedure similar to that described by Horimoto and co-workers.[11] The underlying principles of the diffraction analysis are outlined in the next subsection and this is followed by a discussion of results found in the current study.

2.3.2.1 Fraunhofer diffraction

A liquid microjet behaves like a stable liquid filament and exhibits a clear optical diffraction pattern when it is illuminated perpendicularly by a laser.[11] Figure 2.19 shows the experimental arrangement for recording this diffraction pattern. The liquid microjet (of tolune-ethanol mixture 90:10) was intersected with a UV laser (266 nm) beam focused from a distance of 50 cm using a 50 cm focal length lens. The UV laser delivered a typical pulse energy of around 9 mJ.

Two methods, namely a sheet of photosensitive (burn) paper or a CCD camera (Imaging source DMK 21AU04.AS), were used to capture the diffraction pattern image. The diffraction pattern was projected onto a screen positioned at a distance of 0.3525 m ± 0.0005 m from the liquid microjet. In the first method, a sheet of photosensitive (burn) paper attached to the screen was used to the record the diffraction image. In the second method the screen was replaced with CCD camera to capture the image, which was processed by imaging software. The size of the opening aperture of the camera was not large enough by itself to capture the full image. To ensure the capture of the whole image, a focusing lens had to be placed on the path between the diffracted image and the camera. Before the experiment, some safety precautions (for details see subsection 2.3.2.2) had to be followed to protect the CCD camera from damage.

The observed diffraction pattern can be explained in terms of Fraunhofer single slit diffraction[12] if the point of observation is distant in relation to the diameter of the liquid microjet, as is typically the case. Figure 2.20 presents a diagram illustrating Fraunhofer diffraction pattern of a single slit.
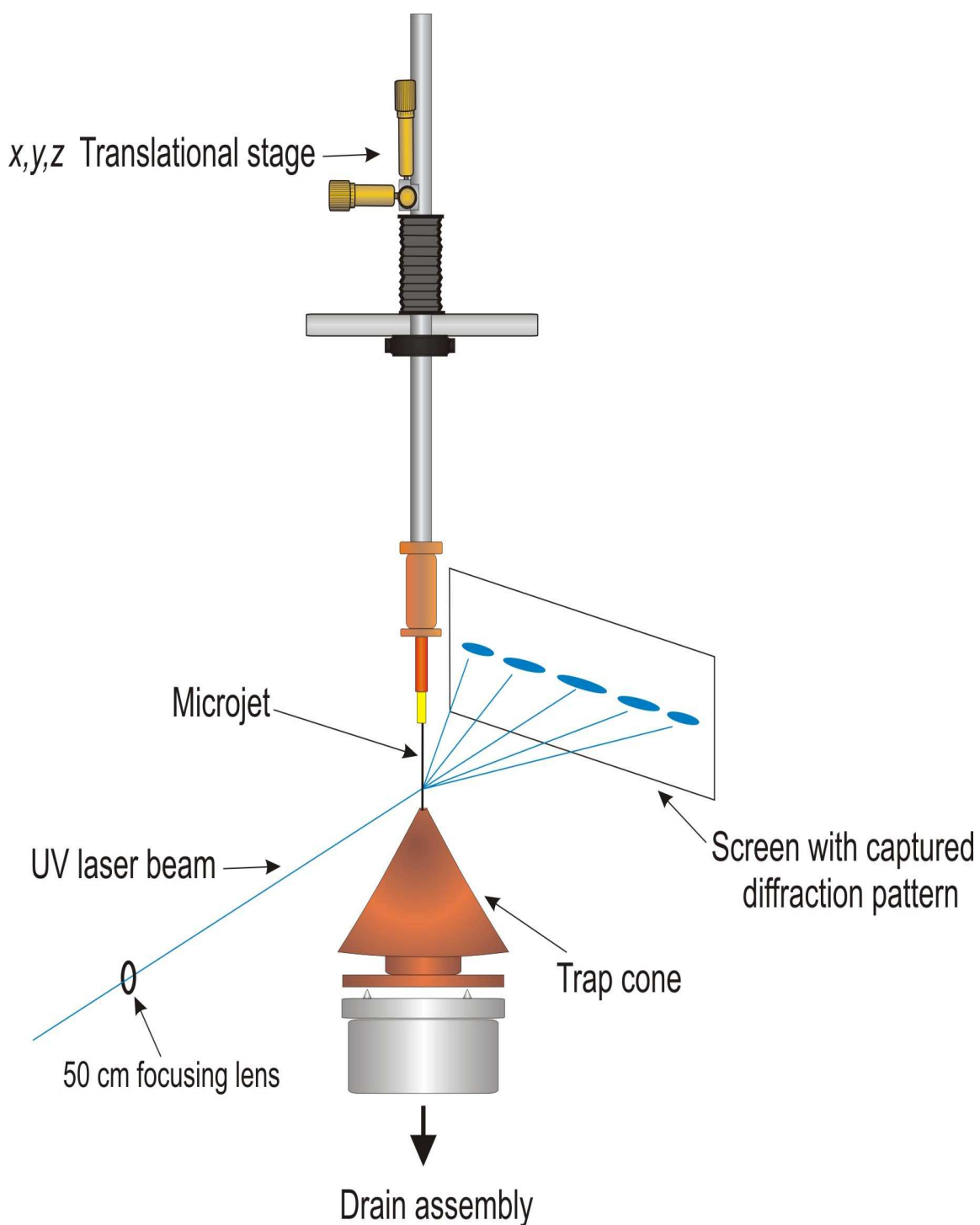
Figure 2.19 Diffraction of the UV laser beam (266 nm)

Screen with captured diffraction pattern
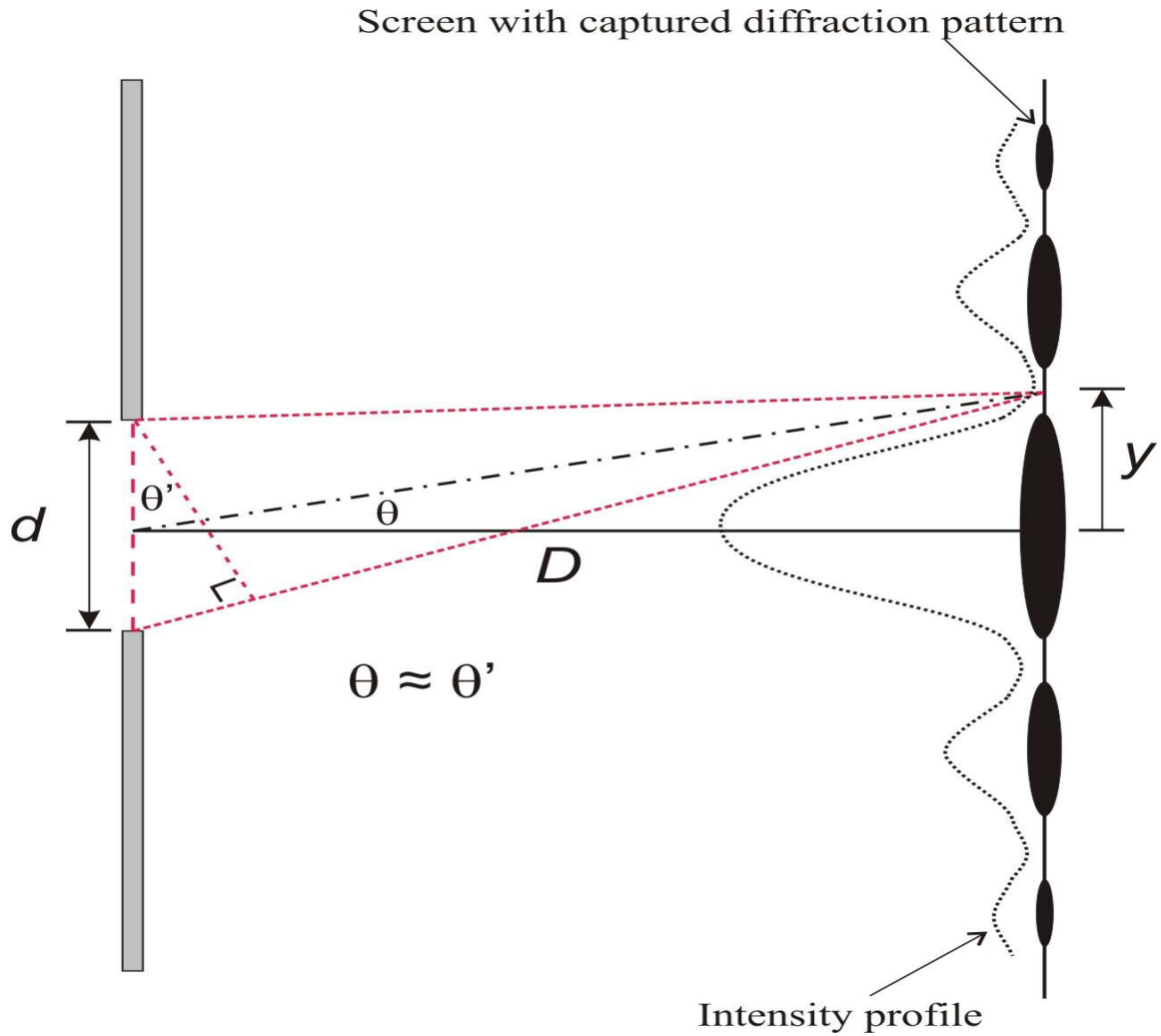
Figure 2.20   Diagram showing Fraunhofer single - slit diffraction

Given observation of the diffraction pattern the diameter, *d*, of the liquid microjet can be determined via equation (1) below:[12]

$$\sin \theta' = \frac{y}{D} = m\lambda / d \tag{1}$$

In the above expression θ' is the diffraction angle, y is half the distance between the centers of the dark regions either side of the central bright region, D is the distance from the liquid microjet to the screen, λ is the laser wavelength, m is the order of diffraction starting from the centre of the screen in either direction (*m* = 1, 2, 3… for the first, second, third order etc..) and *d* is the diameter of the liquid beam.

With the use of the calculated diameter the Fraunhofer intensity profile can be plotted with the use of equations (2) and (3) below:[12]

$$I = I_0 (\sin^2 \beta) / \beta^2 \tag{2}$$

$$\beta = (\pi \cdot d \cdot \sin(\theta)) / \lambda \tag{3}$$

Here I_0 is the intensity of the undiffracted beam and all other terms retain the same definition as above.

2.3.2.2 Determination of the diameter

Figure 2.21 shows the diffraction pattern captured by the CCD camera. When using the CCD camera, protective measures had to be taken to prevent damage by the excessive intensity of the laser beam. For instance, the diffraction centre, which exhibits the laser beam at its highest intensity, was obstructed by a thin piece of metal and a sheet of paper was put in front of the objective in order to prevent the saturation of the camera. Consequently the quality of the image obtained was greatly affected as some diffracted light was also blocked, causing problems for analysis of the image.
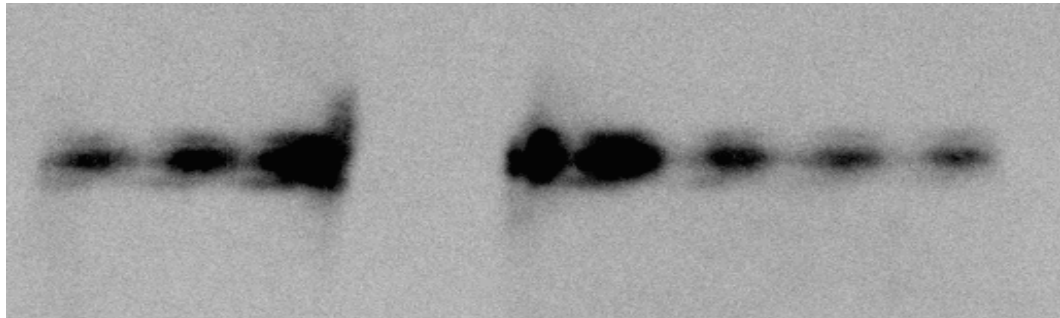
Figure 2.21   Optical diffraction pattern by the liquid beam captured by CCD camera

The alternative method of projecting and capturing the diffraction pattern was to employ a sheet of photosensitive (burn) paper. This proved to be a simpler way of determining the spot displacement (*y*) and was therefore the better choice for calculation of the liquid beam diameter: several orders of the diffraction were then clearly observed (Figure 2.22). Pencil marks on the burn paper show the approximation position of the diffraction minimum.
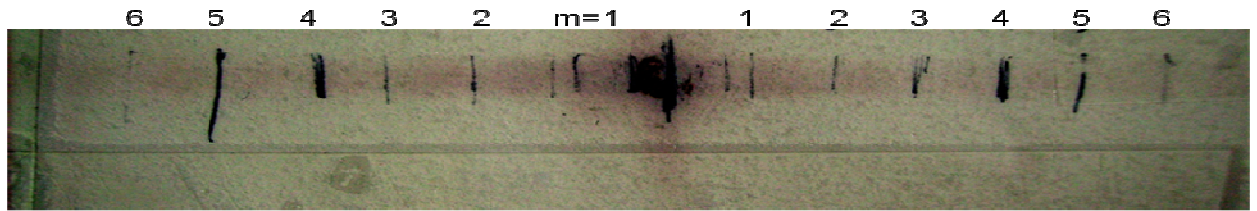
Figure 2.22   Liquid microjet laser diffraction pattern captured onto a sheet of burn paper

From the diffraction pattern the value of y was measured for six orders of diffraction and used in equation (1). The values calculated for the liquid microjet diameter are listed in Table 2.2. The calculations gave a value for the diameter of the liquid beam to be 21.0 ± 0.6 μm, where the error margin represents one standard deviation. This value is close to that of the manufacturer's claim for the inside diameter of the fused silica capillary, 25 μm. The difference between the two values can be explained by evaporation of the liquid microjet as it proceeds through the vacuum chamber to the point of intersection with the laser beam, i.e., we would expect the measured diameter to be less than the ID of the capillary tube.

Table 2.2 Measured and calculated values from the diffraction pattern in Figure 2.22

m	y /cm	d / μm *
1	0.5	20.4
2	0.95	20.2
3	1.35	21.3
4	1.75	21.9
5	2.25	21.3
6	2.70	21.3

* Calculated using $D = 36.05$ cm and $\lambda = 266$ nm
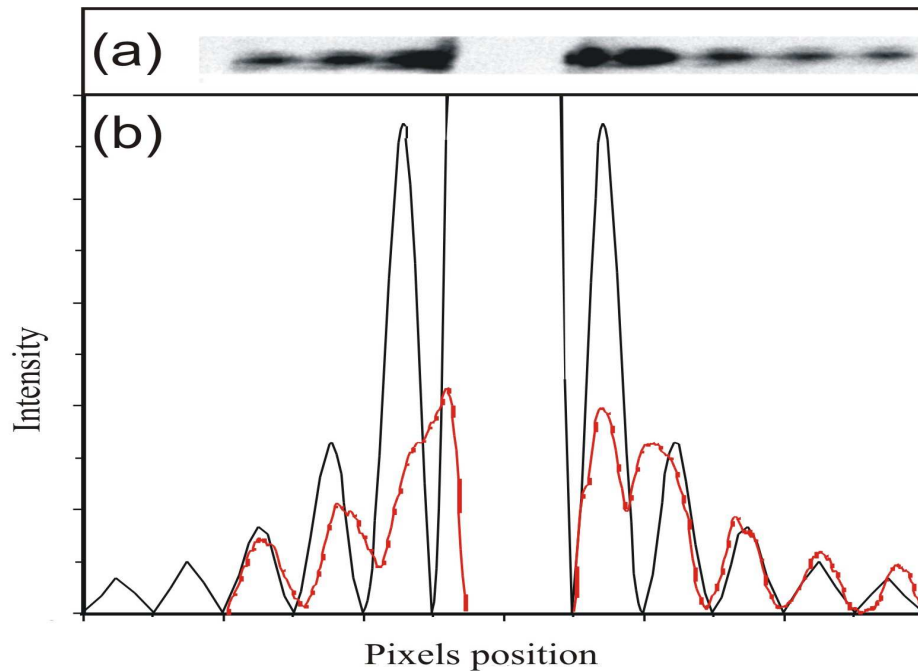
Figure 2.23   (a) Optical diffraction pattern captured by CCD camera and (b) intensity
distributions. The red line corresponds to the intensity distribution determined
from the CCD image while the black line is the intensity distribution predicted
on the basis of Fraunhofer diffraction assuming a liquid microjet of 21 μm

Figure 2.23 shows a comparison of the intensity profile predicted for Fraunhofer
diffraction, obtained from application of equations (2) and (3), with the intensity distribution
of the diffracted light captured by the CCD camera. The intensity distribution of the camera
image was produced by imaging software (Image J) which allowed the illuminated pixel
intensity to be plotted against its position, as represented by the solid red line in Figure 2.23.

The comparison of the calculated Fraunhofer intensity distribution to that captured by
CCD camera (see Figure 2.23), shows a near match to experimental near the wings. It does
less well as the position of the undiffracted beam is approached (the centre of the image).
However, nearest the centre the agreement is much worse. In part, this is due to the use of the
beam-stop to stop the undiffracted light from reaching the CCD. In addition, the intensity
profile may have been affected by saturation of the CCD pixel for the strongest interference
fringes. Nevertheless, the intensity profile behaves roughly as expected and supports the
reliability of the calculated diameter of the liquid microjet.

2.4 References

(1) Holstein, W. L.; Hayes, L. J.; Robinson, E. M. C.; Laurence, G. S.; Buntine, M. A. *J. Phys. Chem. B* **1999**, *103*, 3035.

(2) Charvat, A.; Lugovoj, E.; Faubel, M.; Abel, B. *Rev. Sci. Instrum.* **2004**, *75*, 1209.

(3) Ellis, A.; Feher, M.; Wright, T. *Electronic and photoelectron spectroscopy*; Cambridge University Press, 2005.

(4) Telle, H. H.; Urena, A. G.; Donovan, R. J. *Laser Chemistry: spectroscopy, dynamics and applications*; John Wiley & Sons Ltd, 2007.

(5) Faubel, M.; Schlemmer, S.; Toennies, J. P. *Z Phys D Atom Mol Cl* **1988**, *10*, 269.

(6) Wilson, K. R.; Tobin, J. G.; Ankudinov, A. L.; Rehr, J. J.; Saykally, R. J. *Phys. Rev. Lett* **2000**, *85*, 4289

(7) Wilson, K. R.; Rude, B. S.; Smith, J.; Cappa, C.; Co, D. T.; Schaller, R. D.; Larsson, M.; Catalano, T.; Saykally, R. J. *Rev. Sci. Instrum.* **2004**, *75*, 725.

(8) Holstein, W.; Buntine, M. *Chemistry in Australia* **2001**, *68*, 28.

(9) Kondow, T.; Mafune, F. *Annu. Rew. Phys. Chem.* **2000**, *51*, 731.

(10) Maselli, O. J.; Gascooke, J. R.; Lawrance, W. D.; Buntine, M. A. *J. Phys. Chem. C* **2009**, *113*, 637.

(11) Horimoto, N.; Kohno, J.; Mafune, F.; Kondow, T. *Chem. Phys. Lett.* **2000**, *318*, 536.

(12) Hecht, E. *Optics*; Addison-Wesley Publishing Company, 1987.

Chapter 3

Demonstration
experiments

3.1 Introduction

This chapter summarizes the demonstration experiments carried out on the liquid microjet apparatus. In the first part of this chapter aromatics compounds (*i.e.*, aniline, toluene, benzene) were studied using the liquid microjet system and LIF spectroscopy. The second part of the chapter describes a series of photodissociation experiments on benzoic acid and acetyl acetone.

3.2 Aromatics

3.2.1 Aniline

Aniline was initially selected as a typical aromatic molecule due to a characteristic electronic transition easily observable by Laser induced fluorescence (LIF) spectroscopy. The electronic transition $S_1(^1B_2) \leftarrow S_0(^1A_1)$ in aniline is strongly allowed, with transitions involving totally symmetric vibrations appearing dominantly in both the absorption and the excitation spectra.[1,2]

3.2.1.1 Experimental setup for the glass cell

Before carrying out liquid microjet experiments on aniline the room temperature gas phase LIF spectrum of aniline was investigated. Prior to the experiment, aniline was purified by distillation before being placed into a glass cell (see Figure 3.1). The aniline was then irradiated by UV radiation (tunable dye laser) between 295.0 - 330.0 nm. The fluorescence signal was collected by a fiber optic cable attached to a spectrograph/monochromator (Princeton Instruments).
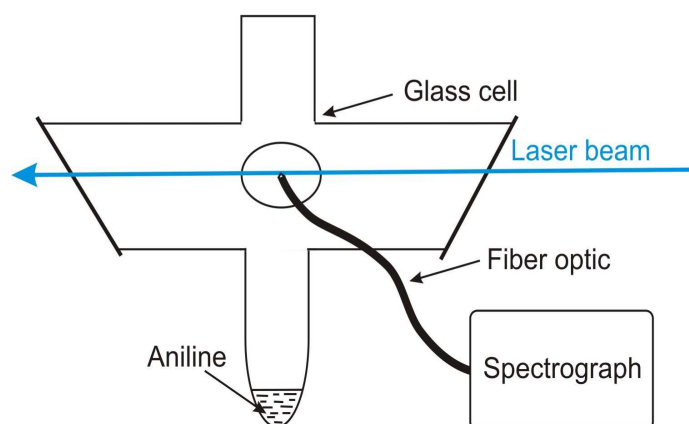
Figure 3.1   Schematic drawing of the experimental setup

3.2.1.2 Discussion

The LIF spectrum for the aniline vapour in the glass cell can be seen in Figure 3.2. The spectra shows a sharp peak at 298 nm followed by a broader peak from 300 to 350 nm. Consequently, the aniline was subjected liquid microjet experiment. The aniline/ethanol solution (15:85 v/v) exhibited a stable behavior in a form of liquid microjet under vacuum conditions. However, after the series of the experiment no fluorescence signal from the liquid microjet was observed. A possible explanation could be that the oxidation of the aniline/ethanol mixture under the liquid microjet conditions could trigger a polymerization reaction that would prevent further experimental applications.
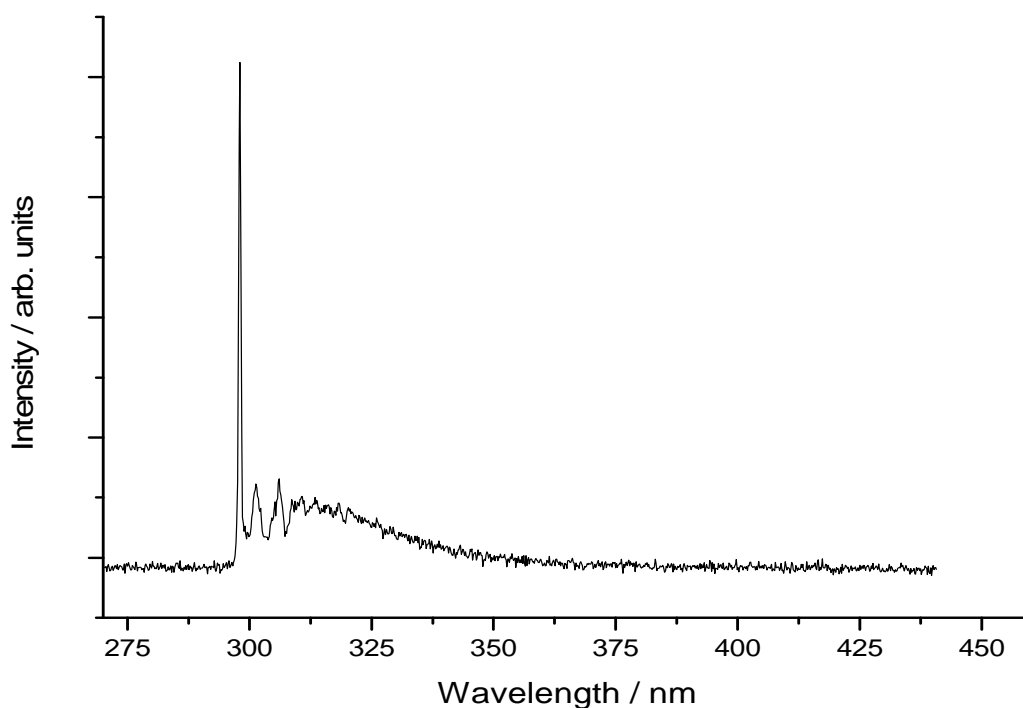
Figure 3.2   LIF spectra of aniline vapour in the glass cell

3.2.2   Toluene

To gain information on the ablation mechanism, toluene molecules ejected into the gas phase are detected by time-resolved laser-induced fluorescence (LIF) spectroscopy to determine their velocity distribution. This initial examination of the photo-ejection mechanism was intended to confirm the validity of the pump-probe methodology for exploring liquid microjets described in the previous chapters.

Laser ablation involves a sequence of steps, namely the laser excitation by absorbing molecules, the transfer of energy from the excited molecules into internal and translational modes of the material, and ultimately the ejection of the molecules.[3,4] A thorough understanding of each of these elementary steps in laser ablation is essential for the characterization of the velocity and angular distribution of the ejected individual molecules or clusters.

Toluene has been chosen in this initial investigation for two reasons: (i) it has a strong LIF spectrum in the gas phase that is readily accessible via standard dye laser excitation and (ii) it can form a stable liquid microjet once mixed with a suitable liquid. The laser ablation mechanism of toluene from solid surfaces under vacuum or from the liquid in air has been the subject of a number of recent studies.[5-10] In spite of liquids being ideal systems for studying laser ablation, due mainly to their physical properties, this experiment is the first laser ablation study of a liquid toluene surface carried out under vacuum conditions. It therefore has the potential to provide insight into the dynamics of molecules ejected into the gas phase without the presence of a surrounding gas atmosphere, which would provide a colliding mass that would quench much of the translational motion. The findings obtained here can also be compared with previous studies of laser ablation of solid toluene that have been carried out in vacuum.

Most of the experimental conditions employed for the laser photo-ejection experiment have been detailed in experimental chapter 2. The results obtained and a discussion of the experimental finding will be given in following subsections.

3.2.2.1 Experimental parameters

3.2.2.1.1   Choice of the liquid phase

Toluene was considered as a good candidate for testing molecular photo-ejection from a liquid surface, not least because it can be readily detected by LIF spectroscopy of the S_1-S_0 transition. A series of experiments, in which the proportion of toluene in ethanol was gradually increased from 2-100 % v/v solutions, were conducted. Each mixture was tested for ~90 minutes at a flow rate of 0.25 ml/min in order to determine the stability of the liquid microjet over a reasonable period of time under a high vacuum. It was found that using a 100% v/v solution of toluene led to instabilities in the microjet resulting in the formation of droplets. The experiment displaying the most stable conditions under high vacuum, while also

having the maximum amount of toluene was observed with a 90:10 v/v solution of toluene/ethanol. Toluene was used as supplied by the vendor (laboratory reagent grade, > 99%) without further purification.

3.2.2.1.2   *Experimental setup*

A solution of toluene/ethanol (90:10 v/v) was introduced as a liquid microjet into the main vacuum chamber at a flow rate of 0.25 ml/min. With the microjet flowing the chamber pressure was typically $\sim 8 \times 10^{-5}$ mbar. After flowing a distance of ~ 0.2 cm downstream of the nozzle aperture, the liquid microjet was then intersected with a focused UV (266 nm) laser beam. 266 nm is coincident with the S_1-S_0 transition of toluene, *i.e.,* resonant absorption is possible. This may lead to more rapid dissipation of heat into the liquid than would be the case for non-resonant laser ablation, thus assisting the photo-ejection process.

The pulse energy of the UV laser beam was varied between 2 and 9 mJ. At lower pulse energies the LIF signal of the ejected toluene molecules was extremely weak. Consequently, the UV laser beam at the highest pulse energy (9 mJ/pulse) was employed to photoeject the toluene molecules for the remaing experiments. The molecules ejected along the same direction as the incoming photo-ejection laser beam were collimated by the sampling cone (aperture diameter of ~ 0.4 cm and placed 1 cm from the liquid microjet (see schematic drawing in Figure 3.3). At a distance of 3.5 ± 0.05 cm from the liquid microjet the toluene molecules were irradiated by UV radiation from a frequency-doubled dye laser at 266.45 nm (80 μJ/pulse) and were observed by LIF excitation spectroscopy of the S_1-S_0 transition. The fluorescence was collected by a liquid light guide and detected by a photomultiplier tube (typical voltage ~ 800 V). The UV laser beam was focused to a spot size of approximately 100 μm at the microjet, giving a fluence of approximately 100 J cm^{-2}, which is more than three orders of magnitude above the threshold fluence identified for laser ablation of toluene.[10] The delay between the initial photo-ejection process and the detection by LIF was varied using a delay generator. Delay times, ranging from 5-500 μs, were employed in order to measure the velocity distribution of the ejected toluene molecules. At each delay time, the fluorescence signal was gated, integrated and averaged for 200 laser shots.
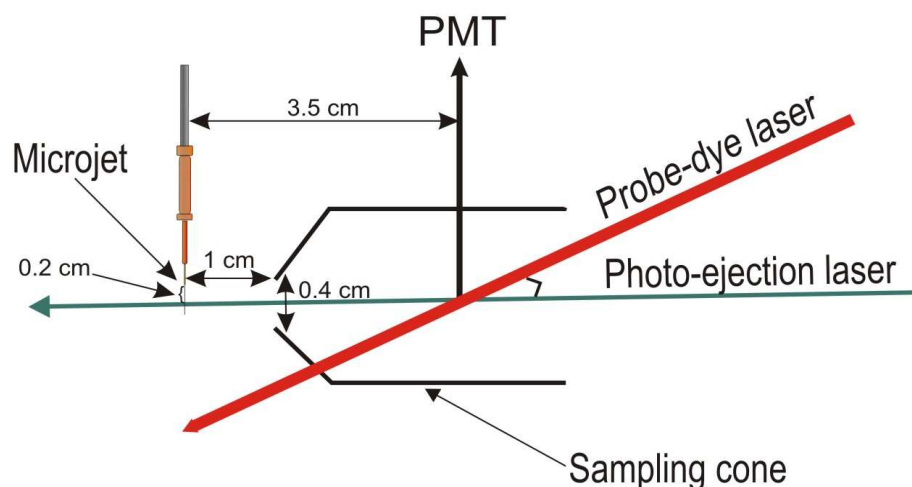
Figure 3.3   Schematic drawing of experimental setup

3.2.2.2 Results

3.2.2.2.1   Toluene spectra

In the 1971, Cvitas and Hollas reported the first S_1-S_0 spectrum of toluene ($C_6H_5CH_3$) with partial rotation resolution. The S_1-S_0 spectrum of toluene has a sharp contour with features characteristic of strongly asymmetric top. This made the 0-0 band of the toluene the most suitable system for the partial rotational analysis. Cvitas and Hollas obtained a room-temperature ultraviolet absorption spectrum of the origin band of toluene, and analyzed their results assuming free internal-rotation of the methyl group.[11]

Figure 3.4 shows the LIF excitation spectrum of toluene photoejected from the liquid microjet surface. The spectrum consists of an asymmetric 0-0 band with a clear band head and strong red degradation that corresponds to a ground state vibration.[12] The shape of the spectrum is comparable with results presented by Cvitas and Hollas. Due to several limitations, such as the resolution the dye laser, the temperature of the ejected toluene, and congestion from internal rotor transitions, it was not possible to analyse the rotational contour to determine the rotational temperature of the ejected toluene molecules.
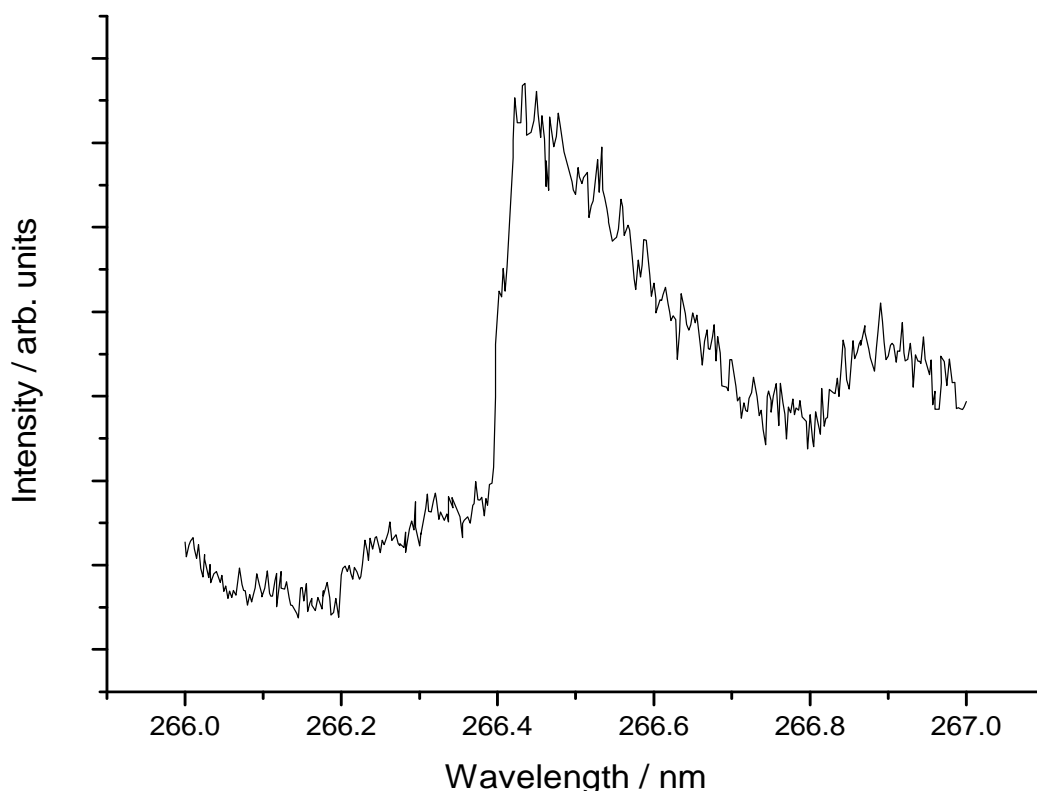
Figure 3.4   Typical LIF excitation spectrum of toluene near 266 nm at 50 μs laser delay

3.2.2.2.2   Time-of-flight profile

The time-of-flight distribution (Figure 3.5) shows two discernible features. The most striking is a sharp and relatively intense peak with a maximum at a pump-probe delay of 58 μs. This is followed by a second, broader 'hump' that peaks at roughly 200 μs. The background signal due to thermally evaporating toluene, which is not dependent on the pump-probe delay, was subtracted from the time-dependent toluene LIF signal to yield the plot shown in Figure 3.5. Notice also that the small decline in signal at the very start of the plot this represents residual (declining) signal from scattered 266 nm pump radiation and should be ignored.

The maximum of the fast component corresponds to a toluene velocity of 620 m s^{-1}, while that of the slower component is at 190 m s^{-1}. However, it is necessary to be careful when interpreting the feature due to slower molecules, since the combination of a downward velocity component from the liquid microjet and the relatively slow velocity in the orthogonal

direction means that particularly slow molecules will struggle to get through the 0.4 cm diameter aperture that leads to the probe laser beam.

Given the known flow rate of the liquid and the diameter of the microjet, we estimate that this cut-off occurs beyond 200 μs. Thus the first 200 μs of the time-of-flight profile is not biased by the size of the aperture, but all data points thereafter are unreliable.
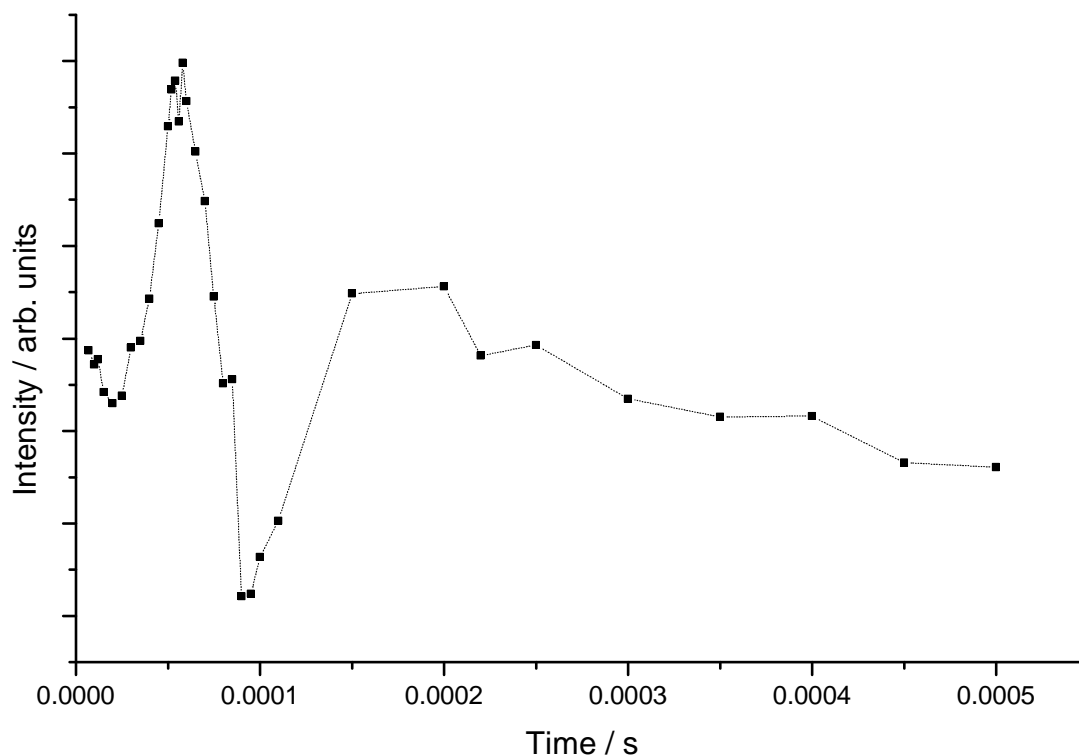
Figure 3.5 Flight time distribution of molecules obtained by 266.45 nm irradiation of a liquid microjet of a toluene/ethanol liquid microjet (each pair of points are joined by dashed line to help to visualize main features in the in the profile)

3.2.2.2.3   Data analysis

The flight time data, they were further processed to obtain translational temperature of the ejected molecules. The time flight distribution plot below (Figure 3.6) shows an intense peak (between 7 to 100 μs), corresponding to a fast component.
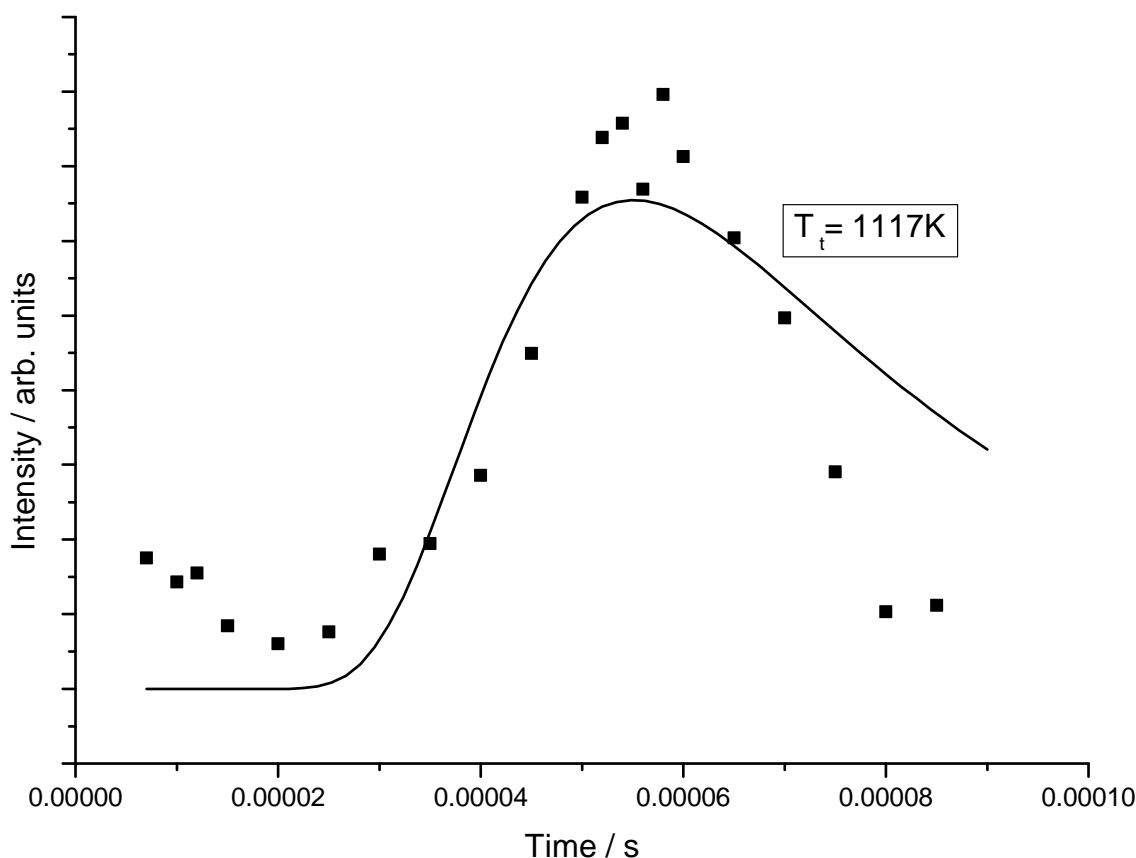
Figure 3.6 Time of the flight distributions of toluene molecules ejected from the liquid microjet (points) and the best fit Maxwellian distributions (solid line))

The ejection of large neutral clusters from liquid microjet surfaces can be expressed by a Maxwellian distribution.[13-15] The Maxwellian distribution is given by the function $f(t)$ in equation (1):

$$f(t) = A\left(\frac{r^4}{t^4}\right)\exp\left[-\frac{m \cdot r^2}{2\ k\ t^2\ T}\right]$$

(1)

where A is a scaling factor, m is the mass of an individual molecule, r is the flight path length, k is the Boltzmann constant, T is the translational temperature and t is the time flight of the molecules. Equation (1) was put in the Origin program (version 7) and a non-linear curve fit carried out. The solid curve in Figure 3.6 shows the Maxwellian distributions fit based on equation (1).

From the fitting process the fast components were found to have translational temperature of 1117 K ± 3.54. The corresponding most probable speed, mean speed and root mean square speed were 620 m s^{-1}, 668 m s^{-1} and 693 m s^{-1} for the fast molecules and 190 m s^{-1}, 214 m s^{-1} and 233 m s^{-1} for slow molecules respectively.

3.2.2.2.4   *Discussion*

The ablation process depends on several laser parameters: the fluence, pulse length, and wavelength. Ultraviolet light tends to yield a higher proportion of ions, whereas infrared radiation leads to higher kinetic energies of the released particles.[16] Different processes appear with increasing laser fluences, starting with the release of neutral particles at low laser fluences (< 0.5 J cm^{-2}), closely followed by the threshold for ion formation. At higher fluences, Coulomb explosion[17] are observed and finally a hot plasma develops.[16] An access to the dynamics of the laser ablated plume is given by the analysis of the velocity distribution of the released particles. A column explosion is a process in which a molecule moving with high velocity strikes a solid and the electrons that bond the molecule are torn off rapidly in violent collisions with the electrons of the solid; as a result, the molecule is transformed into a cluster of charged atomic constituents that then separate under the influence of their mutual Coulomb repulsion.

Previous studies of laser-induced ejection were reported by Kondow *et al*.[15] They investigated the laser ablation mechanism of a liquid beam of water under irradiation by an intense pulsed IR laser. The water molecules were liberated into the gas phase as water clusters $(H_2O)_n$, which undergo unimolecular dissociation before arriving to the detector (a Daly multiplier). The flight-time distribution indicates that neutral clusters are exhibiting fast and slow components, ejected from the surface and interior regions of the liquid beam, respectively. Clusters ejected from the surface region were reported to suffer fewer collisions than those from the interior of the liquid microjet and as a result exhibited lower internal energies which consequently yielded lower translational temperatures.

The flight time distributions obtained in this study are consistent with the ejection mechanism described by Kondow *et al*.[15] for IR excitation and clearly show that two processes with characteristic velocities (668 m/s for the fast component and 214 m/s for the slow component) are occurring. The first is indicative of a process by which molecules at the surface region are being rapidly heated upon UV irradiation, which leads to the ejection of

molecules with a super thermal velocity (668 m s^{-1}). The second process can be described by an ejection mechanism in which molecules are gradually ejected from the inside region of the liquid beam with a thermal velocity (214 m s^{-1}) over a period of several tens of microseconds to several hundreds of microseconds after the UV irradiation. This ejection mechanism can be rationalised by considering that the molecules ejected from the surface region will suffer far fewer collisions with any ambient gas (or liquid phase molecules) than those from the interior of the microjet and will therefore experience greater velocities.

The translational temperatures obtained from the best fit Maxwellian plots show that the faster molecules exhibit a high translational temperature (1117 K). The liquid microjet employed consisted of a 90:10 v/v toluene/ethanol solution. Unlike previous work by Buntine[18] and Kondow,[15] in which the solvent transfers heat into the solute upon IR-irradiation, the temperatures obtained in this study are consistent with a process by which molecules ejected from the inside of the liquid beam experience a cooling effect by the liquid following UV irradiation.

As the flight time distribution of the toluene molecules ejected from the liquid microjet could not be investigated further, due to problems with the equipment (such as probe dye laser) and time constraints, the flight time distribution obtained may not be representative of all the ejection processes occurring at the liquid surface.

Other studies on the laser ablation of toluene have been reported by Niino and co-workers.[5,8] Their results suggest that toluene molecules are ejected from the solid surface during laser ablation with high kinetic energies. They report on the investigation of the plume propagation of the ablated products of toluene solid film at 180 K in vacuum. A spontaneous photoemission of the plume was detected at the laser fluence *ca*. 1.0. J cm^{-2}. The velocity at the centre of the plum was *ca*. 12.5 km s^{-1}, which is at a much greater velocity that was observed in our experiment.[5] Mashure and co-workers have also observed the supersonic ejection of a plume from a liquid surface in UV laser ablation of pure toluene in the ambient condition.[19]

3.2.3   Benzene

Similar experiments to that of the UV excitation of toluene have been initiated with benzene with a view to gain information about the population of internal quantum states and to determine the internal energy distribution of molecules liberated from liquid microjet. The study of benzene presents several advantages over that of toluene: its spectroscopy is well characterized and there is no added complication in analyzing its rotational structure contour from the methyl rotor structure.

Benzene has been studied by various methodologies (e.g. liquid microjet technique[18,20] or jet cooled[21]). Buntine *et al.* report results on benzene evaporating from water-ethanol solution into vacuum using liquid microjet methodology combined with laser spectroscopy (REMPI). Used spectroscopy technique allows quantifying the rotational and vibrational energy content of molecules evaporating from a liquid surface. The UV spectrum of the benzene $6^1_0 \, S_1 \leftarrow S_0$ vibration transition of benzene is located at 259 nm. Benzene is a good candidate with which to determine the internal energy distribution of molecules liberated from liquid microjet because its spectroscopy is well characterized.[18,20,21]

3.2.3.1 Experimental setup

Experimental arrangement was described in detail in a previous subsection (Figure 3.3). A benzene/ethanol (10:90) v/v mixture was found to form a stable liquid microjet under vacuum conditions.

A solution of benzene/ethanol (10:90) v/v was introduced as a liquid beam into the main vacuum chamber at a flow rate of 0.25 ml/min, Travelling a distance of ~ 0.2 cm downstream of the nozzle aperture, the liquid microjet was then intersected with a UV laser beam (photo-ejection laser) of 266 nm (~9 mJ/pulse). The benzene molecules evaporated from the liquid microjet and were irradiated by UV radiation (probe-dye laser) in a range between 258.5 – 259.0 nm. Benzene was used as supplied by the vendor (99,0 %) without further purification.

3.2.3.2 Discussion

Figure 3.7 shows the spectrum of the benzene spontaneously evaporated from a water-ethanol liquid microjet recorded by Buntine *et al.*[20] This is compared with rotational contour from vapour phase benzene at room temperature. The spectrum derived from the microjet in the lower half of Figure 3.7 was recorded with the UV laser beam set at a distance of 300 μm

from the liquid filament and 1 mm downstream of the nozzle orifice. Comparison with the room-temperature spectrum in the upper part of the figure reveals a considerably colder rotational energy distribution from the microjet evaporation than found at room temperature. Overlaid on each spectrum is the best-fit spectral simulation. The simulated spectral contours, displayed as dashed lines in Figure 3.7, are convoluted with Gaussian of $0.3.cm^{-1}$ (fwhm) to account for the laser bandwidth. Simulation of the gas-cell spectrum in Figure 3.7 (a) yields a best-fit rotational temperatures of 295 ± 6 K, where the uncertainty represents one standard error. In contrast Figure 3.7 (b) represent spectrum of benzene evaporated from liquid microjet with rotational temperature of 206 ± 4 K. Here, the error in the measurement represents three times the standard error of the mean (3σ).[20]

(a) Room temperature gas cell

(b) Evaporation from liquid microjet

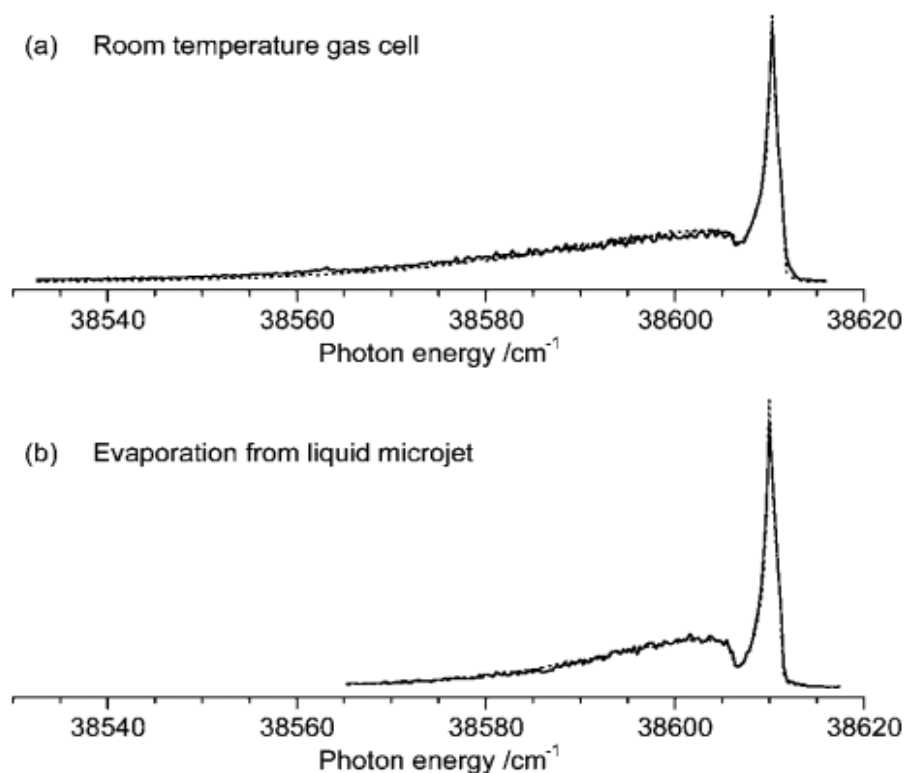**Figure 3.7** 1+1 resonance-enhanced multiphoton ionization (REMPI) spectra of the $S_1 – S_0$ 6^1_0 vibronic transition of benzene (a) under room temperature gas cell conditions and (b) benzene evaporated from the surface of a H_2O/EtOH liquid microjet (Overlaid on each spectrum is a dashed line representing the best-fit spectral simulation from the 6^1_0 transition, assuming a Boltzmann distribution of rotational states)

Using the same experimental setup (see subsection 3.2.2.1.2), we have recorded the LIF spectrum. The S_1-S_0 transition of benzene thermally evaporated from the liquid microjet was observed by laser induced fluorescence spectroscopy (Figure 3.7). The spectrum shows the S_1-S_0 6^1_0 band envelope of benzene. However, the analysis and the interpretation of the resulting spectrum requires more experimental work to be carry out in the future.
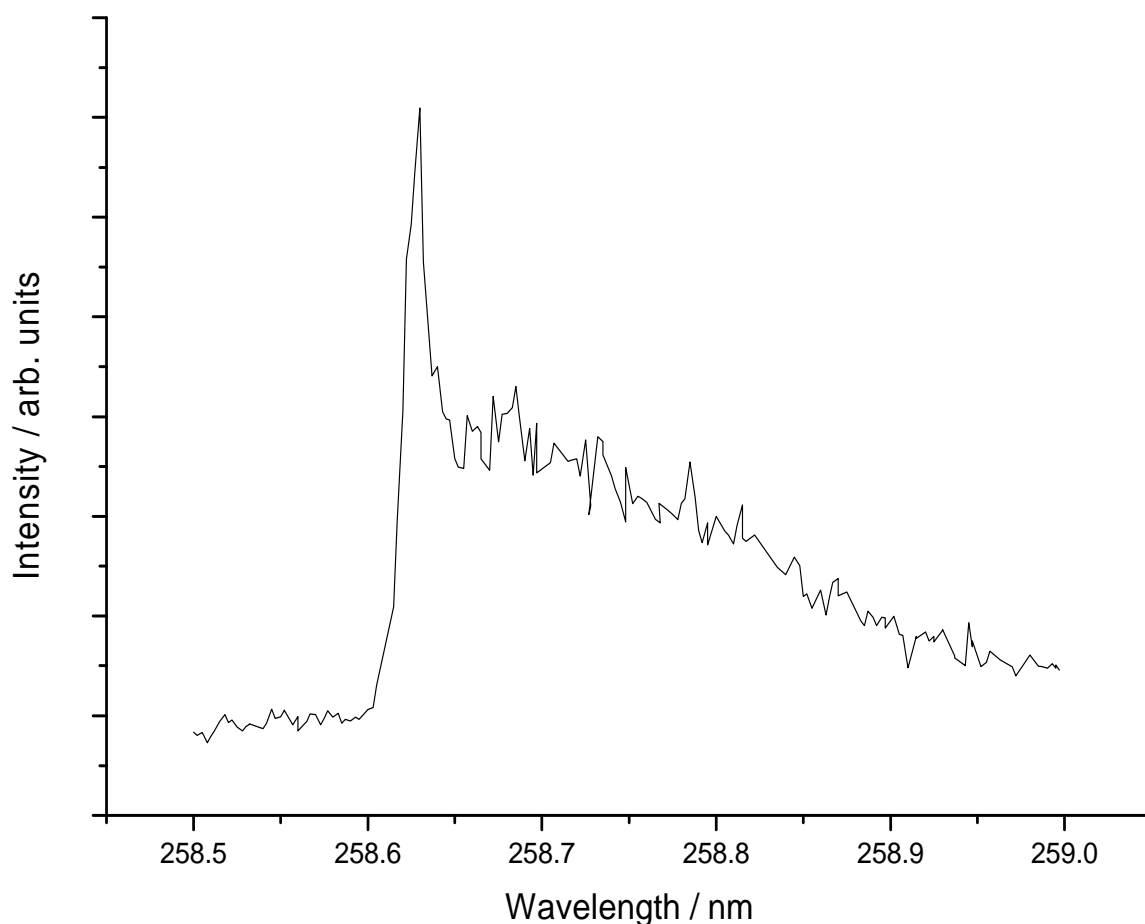

Figure 3.8   LIF spectrum of the benzene molecules evaporated from the microjet surface

3.3 OH formation

In experiments concerning photodissociation products, benzoic acid and acetyl acetone were chosen due to their ability to generate OH photofragments upon absorbing UV radiation of 266 nm. Measurement of the energy distribution of ejected hydroxyl photofragments could potentially provide important information on the surface photodissociation dynamics through determination of the quantum state resolved OH velocity distribution. These observations could be compared to results of the photodissociation dynamics of (*e.g.,* acetyl acetone) in the gas phase. Details of the experiments will be given in the following subsections.

3.3.1   Benzoic acid

Benzoic acid(s) was dissolved in ethanol to give 5 and 10 % v/v solutions. When the 10 % solution was introduced into the source chamber under high vacuum, benzoic acid recrystallised causing the microjet to become blocked, and clogging of the chromatography tubing which greatly affected the performance of the HPLC pump. The 5 % concentration was found to be more stable, but clogging of the chromatography tubing was observed after frequent use. It was found necessary to flush the system with a fresh supply of ethanol after the benzoic acid/ethanol solutions were used in order to prevent the solid from recrystallising in the tubing over night. As a result of the recrystallising issue, benzoic acid was not considered as suitable choice for the liquid microjet formation.

3.3.2   Acetyl acetone

The aim of this study was to generate OH photofragments (radicals) by photodissociation of acetyl acetone (AcAc) on or near the surface of the liquid using the liquid microjet technique combined with LIF spectroscopy.

Acetyl acetone exists predominantly in an enolic form in the gas phase (see schematic Figure 3.9 below).[22] This has been attributed to the formation of relatively strong intermolecular hydrogen bonds. In the current study we have used proton NMR spectroscopy to confirm the presence of the enolic form in our liquid sample of AcAc. The NMR spectra shows evidence of that both tautomeric (enolic and ketonic) forms in the liquid phase.
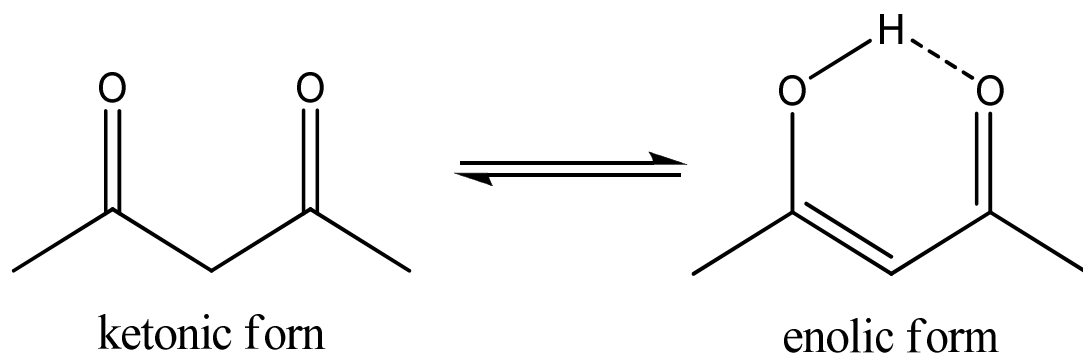
Figure 3.9   Schematic drawing of the keto and enol form of acetyle acetone

Upadhyaya *et al.* have published a number of papers on the investigation and detection of OH photofragments.[23-25] In their studies, they explored the photodissociation dynamics of AcAc in the gas phase at room temperature using a laser pump-probe approach.[26] The nascent distribution of the primary photofragment OH was measured with LIF spectroscopy at 266 nm, 248 nm and 193 nm. The OH photofragment was found to be vibrationally cold and shows essentially a Boltzmann distribution of rotational states. The rotational energy imparted into an OH fragment is calculated to be 1.9, 2.5, and 2.2 kcal/mol at 266, 248 and 193 nm respectively. The average translational energy partitioned into the photofragment pairs in the center-of-mass co-ordinate is found to be 16.0±4.0, 17.3±4.2 and 19.2±4.7 kcal/mol at 266, 248, and 193 nm, respectively.[26]

Due to the photodissociation dynamics being carried out in the condensed phase in the current work, the contribution from the solvent has to be taken into account as it is likely to affect the ability of acetyl acetone to produce OH radicals. In order to generate hydroxyl photofragments, the OH would have to gain enough kinetic energy to escape from the solvent cage if generated below the liquid surface. Those OH radicals formed with insufficient kinetic energy may recombine, with any excess energy in the newly-formed bond being removed by collisions with solvent molecules. The LIF signals for the OH photofragments should be detectable under our condition (see appendix). If the excited species is present near the surface region, it is expected that bond cleavage will be followed by direct ejection of OH radicals into the gas phase. The OH radicals originating from deep within the liquid beam will most likely recombine due to the surrounding solvent cage, with the energy dissipated as heat.

3.3.2.1 Choice of the liquid phase (acetyl acetone)

The acetyl acetone was chosen to form a liquid microjet as it is a liquid at room temperature with a vapour pressure of 8 mbar. AcAc was tested with ethanol solutions of 10-30% under vacuum conditions. At high concentrations (30:70) of acetyl acetone/ethanol, the liquid microjet was unstable and ice formation was observed on the copper cone. To overcome this, a less concentrated (15:85) v/v solution was used, which exhibited a stable liquid microjet at vacuum chamber pressures of ~6 × 10^{-5} mbar. This mixture of AcAc/ethanol (15:85) was therefore used in all subsequent experiments. Acetyl acetone was used as supplied by the vendor (Across Organic, 99 + %) without further purification.

3.3.2.2 Experiment setup

The experimental set up employed for the photodissociation experiments on acetyl acetone (AcAc) is depicted in Figure 3.3. AcAc employed in the experiment was used after several freeze-pump-thaw cycles. A solution of AcAc/ethanol (15:85) v/v, kept under an argon atmosphere (to prevent contact with oxygen), was introduced into the main vacuum chamber as a liquid microjet with a diameter of ~ 20 μm. After travelling a distance of 0.2 cm from the nozzle exit the liquid microjet was intersected by a UV laser beam of wavelength 266 nm (9 mJ/pulse) to photolyze the acetyl acetone molecules and thus to generate OH photofragments. Any OH photoproducts generated on photolysis were collimated by a 0.4 cm aperture placed at a distance of 1 cm from the liquid microjet. At a distance of 3.50 ± 0.05 cm from the liquid microjet attempts were made to probe for OH radicals using a second UV dye laser (120 μJ/pulse). This second UV laser was operated in the wavelength region 307.5 – 308.5 nm in order to excite the $A^2\Sigma \leftarrow X2\Pi$ (0-0) transition of OH. A band pass filter (λ = 280 nm) was placed between the liquid light guide and the PMT to cut off the scattered light from the photolysis and probe lasers. The residual light reaching the PMT was gated, integrated and averaged for 50 laser shots with a wavelength step size of 0.001 nm.

3.3.2.3 Experimental observations and conclusion

In searching for the OH fluorescence signal the pump-probe laser delay was varied between 10-150 μs. However, despite considerable effort no fluorescence signal was observed that could be attributed to OH photofragments.

A number of hypotheses can be considered to explain these results. The amount of ethanol within the microjet was bigger than that of acetyl acetone; therefore acetyl acetone could be

more abundant in the inside regions of the liquid microjet and OH radicals produced could be failing to escape from the solvent cage. Furthermore, increasing the proportion of acetyl acetone present in the liquid microjet might lead to an increase in the amount of excited acetyl acetone species present near the surface, i.e. there may be a bias for ethanol to reside at the surface in the more dilute mixtures.

Due to problems with equipment and time constraints further improvements to the study of OH radicals could not be achieved. However, the approach outlined in this study shows the potential future use of the liquid microjet methodology in the study of photodissociation reactions.

3.3.3   Appendix: predicted detection sensitivity in the liquid microjet pump-probe experiment

This section is intended to illustrate the expected detection sensitivity of the proposed experiments to show that photofragments, such as OH ejected from acetylacetone, is potentially detectable. We start by calculating the number of molecules in the surface layer. Consider a microjet with a diameter of 20 μm in which a 2 mm segment is illuminated. This corresponds to a surface area 6.28 x 10^{-8} m^2. If we assume that a single molecule has a surface area of 4×10^{-20} m^2, then this corresponds to ~ 2×10^{12} molecules in the illuminated surface area. Of these, in a reasonably dilute solution (1 M) this gives rise to 5×10^{10} *solute* molecules at the surface.

Now suppose that all the solute molecules undergo photodissociation by the pump laser pulse. The number of photofragments entering the detection region will then be limited by two factors:

(i)   Losses due to recombination (or some other process) at the surface or in the bulk.

(ii)   Geometric selection by the aperture placed in front detection region.

We expect the effect of (i) to be modest at worst because in the examples chosen a relatively large translational energy release is imparted to the fragments on photodissociation. It is conceivable that the proportion of photofragments released into the gas phase may easily exceed 50% and it is unlikely in any of the cases selected to fall below 10%.

The geometric effect due to the aperture is under our control. If we select a large aperture placed close to the microjet, then the proportion of the photofragment molecules will pass through the aperture but our ability to measure the velocity distribution with decent precision

will be tarnished. A compromise will be adopted, most probably allowing ~ 5% transmission. Thus taking a worst-case scenario for both (i) and (ii), we will be able to detect 0.5% of the photofragment molecules. However, even that gives rise to 3×10^8 molecules passing through aperture. Even allowing for the range of velocity distributions likely to be seen (which means we see only one velocity slice at any instant in time), the strong LIF signal for the chosen photofragments (OH) should make them readily detectable.

There is one further assumption that needs to be justified, namely that all solute molecules will undergo photodissociation in a single laser shot. The probability of photon absorption is given by σF where σ is the absorption cross section and F is the photon flux. At 266 nm one mJ of laser light corresponds to ~ 10^{15} photons. Now if we use a lens to focus that down to a diameter of 20 μm, but retaining a length approximately of 2 mm, then the photons flux incident on the liquid microjet is 1.77×10^{22} photons m^{-2} pulse^{-1}. We want an absorption probability of unity, and to achieve this minimum absorption the cross section must be 6×10^{-23} m$^2 = 6 \times 10^{-21}$ cm^2.

Of course implicit in the above is the assumption that we have a near 100% quantum yield for the desired process.

3.4   References

(1) Kerstel, E. R. T.; Becucci, M.; Pietraperzia, G.; Consalvo, D.; Castellucci, E. *J. Mol. Spectrosc.* **1996**, *177*, 74.

(2) Yamanouchi, K.; Isogai, S.; Tsuchiya, S. *Chem. Phys.* **1987**, *116*, 123.

(3) Zhigilei, L. V.; Garrisona, B. J. *Appl. Phys. Lett.* **1997**, *71*, 551.

(4) Zhigilei, L. V.; Kodali, P. B. S.; Garrison, B. J. *J. Phys. Chem. B* **1998**, *102*, 2845.

(5) Niino, H.; Kawaguchia, Y.; Satoa, T.; Narazakia, A.; Gumpenbergera, T.; Kurosakia, R. *Appl. Surf. Sci.* **2005**, *252*, 4387.

(6) Niino, H.; Yasuia, Y.; Dinga, X.; Narazakia, A.; Satoa, T.; Kawaguchia, Y.; Yabe, A. *J. Photochem. Photobiol., A* **2003**, *158*, 179.

(7) Ding, X.; Kawaguchi, Y.; Sato, T.; Narazaki, A.; Kurosaki, R.; Niino, H. *J. Photochem. Photobiol., A* **2004**, *166*, 129.

(8) Kawaguchi, Y.; Ding, X.; Narazaki, A.; Sato, S.; Niino, H. *Appl. Phys. A* **2005**, *80*, 275.

(9) Hatanaka, K.; Itoh, T.; Asahi, T.; Ichinose, N.; Kawanishi, S.; Sasuga, T.; Fukumura, H.; Masuhara, H. *J. Phys. Chem. A* **1999**, *103*, 11257.

(10) Tsuboi, Y.; Fukumura, H.; Masuhara, H. *Appl. Phys. Lett.* **1994**, *64*, 2745.

(11) Cvitas, T.; Hollas, J. M. *Mol. Phys.* **1971**, *20*, 645.

(12) Scott, D. W.; Messererly, J. F.; Todd, S. S.; Hassenlopp, I. A.; Douslin, D. R.; McCullough, J. P. *J. Chem. Phys* **1962**, *37*, 867.

(13) Zimmermann, F. M.; Ho, W. *J. Chem. Phys* **1994**, *100*, 7700.

(14) Zimmermann, F. M.; Ho, W. *Surf. Sci. Rep.* **1995**, *22*, 127.

(15) Kohno, J.; Mafune, F.; Kondow, T. *J. Phys. Chem. A* **2004**, *108*, 971.

(16) Maul, J.; Karpuk, S.; Huber, G. *Phys. Rev. B* **2005**, *71*, 045428.

(17) Stoian, R.; Ashkenasi, D.; Rosenfeld, A.; Campbell, E. E. B. *Phys. Rev. B* **2000**, *62*, 13167

(18) Maselli, O. J.; Gascooke, J. R.; Kobelt, S. L.; Metha, G. F.; Buntine, M. A. *Aust. J. Chem.* **2006**, *59*, 104.

(19) Tsuboi, Y.; Hatanaka, K.; Fukumura, H.; Masuhara, H. *J. Phys. Chem.* **1994**, *98*, 11237.

(20) Maselli, O. J.; Gascooke, J. R.; Lawrance, W. D.; Buntine, M. A. *J. Phys. Chem. C* **2009**, *113*, 637.

(21) Okruss, M.; Müller, R.; Hesea, A. *J. Mol. Spectrosc.* **1999**, *193*, 293.

(22) Caminati, W.; Grabow, J. U. *J. Am. Chem. Soc.* **2006**, *128*, 854.

(23) Kumar, A.; Upadhyaya, H. P.; Naik, P. D.; Maity, D. K.; Mittal, J. P. *J. Phys. Chem. A* **2002**, *106*, 11847.

(24) Dhanya, S.; Kumar, A.; Upadhyaya, H. P.; Naik, P. D.; Saini, R. D. *J. Phys. Chem. A* **2004**, *108*, 7646.

(25) Naik, P. D.; Upadhyaya, H. P.; Kumar, A.; Sapre, A. V.; Mittal, J. P. *Chem. Phys. Lett.* **2001**, *340*, 116.

(26) Upadhyaya, H. P.; Kumar, A.; Naik, P. D. *J. Chem. Phys* **2003**, *118*.

Chapter 4

Conclusions

4   Overall conclusions

A new instrument has been designed and constructed for studying the dynamics of photochemical reactions at or near the surface of a liquid. The experimental conditions have been optimized to allow the continuously flow of the liquid phase to be submitted to a UV laser to cause the photoejection of molecules and fragments of within the liquid phase.

The diameter of the liquid beam has been determined from the observed diffraction pattern produced when the liquid microjet is being intersected by the UV laser light. The diameter of the liquid microjet has been confirmed to be 20 μm and shows that liquid microjet suffers significant evaporation at distance from the pinhole of the nozzle exit.

The ejection processes of molecules by the irradiation of a UV laser onto the liquid microjet have been studied for an ethanol-toluene solution by measuring the flight-time distributions produced at different delay times after the pulsed UV-irradiation. The time-of-flight distribution shows two groups of molecules, namely a sub-set of fast moving molecules originating from or near the liquid surface and a second group of slower, hotter molecules which are assumed to originate from within the liquid interior. From the Maxwellian distribution fitting process the fast components were found to have translational temperature 1117 K. The corresponding most probable speed, mean speed and root mean square speed were 620 m s^{-1}, 668 m s^{-1} and 693 m s^{-1} for the fast molecules and 190 m s^{-1}, 214 m s^{-1} and 233 m s^{-1} for slow molecules respectively.

The UV excitation experiments of benzene have been initiated with a view to gain information about the population of internal quantum states and to determine the internal energy distribution of molecules liberated from liquid microjet. The benzene that was thermally evaporated from the liquid microjet was examined by using LIF spectroscopy. However, the current analysis and the interpretation of the resulting LIF spectra has shown that more experimental work needs to be carry out in the future.

Finally, the use of a liquid microjet methodology for the photodissociation dynamics of an aqueous solution of acetyl acetone has been studied, yielding only, so far, modest results. However, significant progress has been obtained and more results are expected from the initial effort discussed in this thesis.

Experimental results showed that liquid microjet methodology, when combined with LIF spectroscopy, is capable of providing information on the photo- and thermal- ejection

processes occurring at liquid surfaces. This methodology can be extended to new liquid system and potentially allow the access photodissociation dynamics at the gas-liquid interface.